Joint Antenna Technical Group
Test Results

April 15, 2005

Prepared By:	Organization
A.J. Beasley (editor)	JAO
J. Baars	ESO
D. Emerson	NRAO
R. Hills	MRAO
L. King	NRAO
F. Koch	ESO
R. Lucas	IRAM
J. Mangum	NRAO
B. Nikolic	NRAO
F. Schwab	NRAO
R. Sramek	NRAO
K. Wirenstrand	ESO
D.P. Woody	OVRO

Table of Contents

EXECUTIVE SUMMARY

During late 2004 and early 2005 the Joint Antenna Technical Group (JATG) has reanalyzed existing data and conducted a supplementary test program on the two prototype antennas at the ALMA Test Facility to clarify issues raised in 2004 about their ability to meet the ALMA antenna technical specifications. Performance data from the prototype antennas will be used to assess the production antenna vendor bids submitted to the project in mid 2004.

The tests included:

- New radio holographic measurement and setting of the main reflector of both prototype antennas;
- New optical photogrammetry of both prototypes;
- Radiometric Out-Of-Focus beam mapping and beam cuts on the Vertex prototype;
- Optical pointing tests on the AEC prototype;
- Laser quadrant detector measurements on Vertex;
- Fast-switching tests to examine surface stability under accelerations encountered during normal operations;
- Examination of the need for cabin thermal regulation of the Vertex cabin structure ("on – off" tests).

Limits on structural deformations that would limit the scientific performance of the production antennas were derived from the tests and cross-compared between the different techniques. These include: astigmatism of the main reflector, non-homologous deformation of the reflector surface due to gravity; temperature effects; and wind and gravity deformation of the antenna backup structure. In many cases the performance of the antenna prototypes was compared to the vendor finite-element models to examine the accuracy of the antenna engineering models.

Based on all available data and the ATF testing done by the AEG and the JATG, it is the consensus view of the JATG that both prototype antennas meet the ALMA antenna specifications under direct consideration (surface accuracy at all elevations, all-sky absolute pointing performance) under the environmental conditions encountered during the testing, and that the production antennas based on either design can also be expected to meet these specifications.

1 Introduction

The Atacama Large Millimeter Array (ALMA) is an international astronomy facility. ALMA is an equal partnership between Europe and North America, in cooperation with the Republic of Chile, and is funded in North America by the US National Science Foundation (NSF) in cooperation with the National Research Council of Canada (NRC), and in Europe by the European Southern Observatory (ESO) and Spain.

ALMA construction and operations are led on behalf of North America by the National Radio Astronomy Observatory (NRAO), which is managed by Associated Universities Inc. (AUI), and on behalf of Europe by ESO. In this role NRAO and ESO are referred to as the Executives. The ALMA funding organizations have created a Joint ALMA Office (JAO) to lead project design and construction, including coordination of the NRAO & ESO activities.

The baseline ALMA project consists of sixty-four 12-m diameter telescopes observing at millimeter and submillimeter wavelengths at the 5000-m Chajnantor site in Region II of northern Chile. A subset of the primary technical specifications for the antennas is shown in Table 1.1. In this table, "*SCI-90.00.00.00-0100-00*" and similar references originate in *ALMA Scientific Specifications & Requirements* (EDM document ALMA-90.00.00.00-001-A- SPE, draft A), "*Antenna Bid TS*" refers to the production antenna technical specifications document (ALMA-34.00.00.00-006-A-SPE), "*BLA*" indicates this item was specified in the ALMA Bilateral Agreement between the National Science Foundation and ESO establishing the ALMA project, and "*Tech Req.*" refers to technical requirements indicated in *ALMA System Technical Requirements* (document ALMA-80.04.00.00-005-A-SPE). Other derivative and independent requirements and specifications for the antennas can be found in these documents.

Parameter	**Value**	**Reference**
Number of antennas	64	SCI-90.00.00.00-0100-00
Diameter	12 m	SCI-90.00.00.00-0100-00
Surface Accuracy	25 microns (goal 20um)	SCI-90.00.00.00-0110-00 + BLA
Forward efficiency	0.95	SCI-90.00.00.00-0120-00
Aperture Efficiency at 30 GHz	75%	SCI-90.00.00.00-0140-00
Aperture Efficiency at 675 GHz	45%	Tech Req. 130
Geometric Blockage	<3%	SCI-90.00.00.00-0150-00
Offset pointing	0.6" RSS over 2° radius	SCI-90.00.00.00-0260-00 + Antenna Bid TS
Fast switching	1.5 deg/1.5 s, settle to peak pointing error <3"	Antenna Bid TS + BLA
Non-repeatable absolute pointing	2" RSS	Antenna Bid TS
Delay Error from Structure	(a) rms, non-repeatable, drift, over 300sec <13 fsec.	Tech Req. 151/152

	(b) rms deviation from 10 sec average, short term <38 fsec	
Repeatable pointing error (measured, corrected)	1.5 arcmin	Antenna Bid TS
Nonrepeatable errors (wind, temperature diff/changes, servo & drive errors, others…)	Minimize	Antenna Bid TS
Calibration of pointing model	Once per month	Antenna Bid TS
On the fly requirements TP	0.5 deg/s, turn around 1', settle 0.8s, continue, 2" accuracy	Antenna Bid TS

Table 1.1 - Subset of ALMA Antenna Technical Specifications

During 2003 and 2004 the ALMA Antenna Evaluation Group (AEG) evaluated two prototype antennas built to ascertain whether or not the ALMA antenna specifications could be met – one from Vertex/RSI (hereafter Vertex) and one from Alcatel-EIE-Costamasgna (AEC). These antennas are situated at the ALMA Test Facility (ATF), at the Very Large Array site near Socorro, New Mexico. In parallel, in December 2003 a Call for Tender (CFT/ESO)/Request for Quotation (RFQ/AUI) was distributed to industry for the production run of ALMA antennas. The production antenna Technical Specifications and Statement of Work were jointly prepared, in part based on the understanding and experience available from the prototype antennas at that time (December 2003)

A preliminary executive summary of the AEG findings was available in late May 2004. At the same time, a team of astronomy community experts was formed to evaluate the production antenna bids (received April 2004) – the Joint Technical Evaluation Team (JTET). The JTET evaluation of the technical and managerial aspects of the production antenna bids took place in May-June of 2004. The JTET did not initially incorporate the findings from the draft AEG summary. After the first round of JTET analysis & reporting was completed, a subset of the JTET (JTETII) was reconvened to reexamine their conclusions after having access to the draft AEG report, and an addendum to the JTET report was produced.

During their analysis of the technical aspects of the production antenna bids, the JTET raised specific concerns about some of the production antenna designs and their ability to meet the demanding ALMA specifications; access to the AEG draft Executive summary by the JTETII did not remove these concerns for those bids derivative from the prototype antennas. In response to this situation, the Executives and the JAO requested further input from another technical review group – the Antenna Technical Working Group (ATWG) – which was specifically charged to: (a) investigate specific technical questions relevant to

whether the proposed designs could be expected to fulfill the ALMA technical specifications; (b) determine the level of remaining technical risk associated with the production antenna bids; and (c) to suggest specific modifications to the designs to address any issues they identified. The specific technical issues identified to the ATWG were:

- Will the antenna designs maintain the ALMA surface accuracy specifications over all elevation ranges?
- To what extent can the metrology systems improve the pointing performance?
- Comment on maintainability and life-cycle costs associated with the designs,
- Any other issues the ATWG felt relevant.

The ATWG report was delivered to the Executives on Sept 29th 2004. The report identified the following concerns for the Vertex antenna, based on the production bid information and measurements of the ATF Vertex prototype antenna (quoted):

- "The photogrammetry measurements on the prototype telescope indicate that the focal length change as a function of elevation is about 1.5 times larger than predicted by the FEM. The opto-mechanical data shows a larger and more complex deviation from the FEM, but these results may be due to unexpectedly large deformations in the mount supporting the laser transmitter. The gravitational deformations represent 8% of the RSS in a total surface error budget of 22 μm. If the error components due to gravity and wind (included because a weaker BUS would also deflect more in the wind - the wind deflections represent 15% of the RSS) are scaled up by a factor 1.5 and the telescope surface is effectively set at the rigging angle, either by measurements at that angle or using a corrected FEM to extrapolate from measurements at low elevations, then the projected peak RMS surface error would be 24 μm. Under these assumptions the antenna would still meet the specification. If, however, the BUS does have deformations that differ from those predicted by the FEM, these are likely to have a non-homologous form, in which case the residual errors would scale by a larger factor than that seen in the change in the focal length. The evidence for excess deformations is not yet compelling, but we regard it as sufficiently strong for this area to be regarded as a high risk at present. Additional measurements are required to settle this issue. We also have a concern that, with no temperature regulation in the walls of the receiver cabin, the gradients may be larger than assumed and that this would cause excess deformations in the dish."

- "The proposed metrology system has not been extensively tested. We believe that it is based on sound principles that should work satisfactorily, although its performance has not yet been proven. The measured offset pointing performance of the prototype telescope was good. The measured servo tracking error is however significantly larger than predicted. With the metrology system in operation, the predicted nighttime offset pointing error has an RSS of 0.595", leaving no margin for the increased servo tracking error. The risk of not meeting the offset pointing

requirements occurs in the tightest configurations when wind turbulence may dramatically increase the variability of the wind forces on short timescales. Overall this presents a small risk to the project."

At this time some concerns about the stiffness of the Backup Structure (BUS) of the Vertex prototype antenna were expressed. Differences between the Finite-Element Model (FEM) predictions for the antenna structural performance and the measured data available to the ATWG were detected, but not accurately quantified.

For the Alenia design (based on engineering studies and derivative from the AEC prototype antenna design):

- "There is no evidence that the FEM for the AEC prototype is incorrect. For the Alenia telescope of very similar design and with a projected net surface error budget of 19 μm, the gravitational and wind deformation components in the surface error budget that would be affected by FEM errors represent 7% of the RSS (root square sum) errors. The risk of the telescope not meeting the RMS surface specification of 25 μm because of gravitational deformations is therefore low, but the Alenia FEM still needs to be verified by measuring the elevation dependent deformations of the first production antenna."

- "The proposed metrology system is untested and has potential flaws associated with using tiltmeters at the ends of the yoke arms, even to correct for thermal deformations. If the proposed metrology system fails to work satisfactorily, then an alternate method will be required to correct for the wind effects and a robust thermal correction algorithm, probably based upon the temperature sensors, will need to be developed. This represents a significant risk until a suitable system is devised. The main case in which uncorrected offset pointing errors are likely to be a problem is when there are high winds and the antennas are closely packed."

During this period there were interactions occurring between the prototype antenna manufacturers and the Executives to investigate these issues.

At the ALMA Management Advisory Committee meeting in Florence in early October 2004 the two Executive management teams met to discuss these findings. During that meeting it was decided to continue testing of the prototype antennas in the hopes of addressing the technical issues raised rapidly (a contract signing date of December 15th 2004 was under consideration). Previously the antenna testing had been carried out by the AEG and the Executives semi-independently; during this meeting it was decided that the JAO would oversee and coordinate all further prototype antenna testing. The ATWG was reconvened (ATWGII) and requested to report any additional findings or conclusions in early November 2004.

During October and early November 2004 additional tests of the ATF antenna prototypes were carried out, including:

- New quadrant detector measurements, using an improved laser mount ;
- A symmetric deflection test on the Vertex prototype antenna;
- Additional photogrammetry data taken by Vertex in Sept/Oct 2004 as part of their own investigations of the BUS issue were made available to the group;

The ATWGII report was presented to ALMA management on the 17th of November 2004; the report states (quote):

- "The gravitational deformation of the VertexRSI antenna was a major concern of the ATWG. At the time of the original report the information was insufficient to determine whether the antenna met the demanding ALMA surface specifications; in particular there were indications that the FEM provided by Vertex did not accurately predict the deformations. The new measurements were intended to give a more accurate comparison between the prototype deformations and the VertexRSI FEM. Our conclusion is that the photogrammetry and quadrant detector measurements indicate that the BUS deformations are as much as 1.3 times larger than predicted by the FEM. This is based on several analyses that are not yet complete and it still remains to verify the all of the corrections and algorithms are correct. Nevertheless it is also true that a significant nonhomologous astigmatic deformation is detected. This astigmatism is not predicted by the FEM and indicates the difficulty of arriving at a correction to the non-homologous gravity contribution to the surface error budget. Following the methodology of the first ATWG report we have scaled the gravity component from the Vertex error budget by 1.5 to incorporate these non-homologous effects for both the gravity and wind. This is the same correction as we had in the first report and gives a net surface RMS of 24.5 microns. The photogrammetry data has also been analyzed to obtain an estimate of the upper limit to the non-homologous gravitational deformations by using the consistency between different maps as a measure of the photogrammetry measurement errors. This estimated upper limit is 12.5 microns assuming that the panel setting can be fully optimized to minimize the effects of these errors. This estimate also assumes that there are no systematic effects in the photogrammetry that would give different answers depending upon where and when the photographs are taken. Replacing the VertexRSI gravity deformation component of 6.2 microns with this upper limit and applying the global scaling factor of 1.3 to the wind deformations yields an estimated surface RMS of 25.1 microns. It is worth noting that all indications are that the tightening of bolts on the antenna improved the gravitational performance of the telescope. The photogrammetry from 2004, old quadrant detector data and the out-of-focus holography maps taken early in 2004 all indicate larger gravitational deformations than are seen now. The following concern expressed in the original summary still remains. We also have a concern that, with no temperature regulation in the walls of the receiver cabin, the gradients may be larger than assumed and that this would cause excess deformations in the dish."

Regarding the issues raised about Alenia, the report states:

- "The new calculations from Alenia indicate that the revised metrology system should work. We support their new approach and it should be possible to retire or mitigate the risk soon after the first article is delivered."

Analysis of the prototype antenna datasets continued after the submission of the ATWGII report. In early December 2004 a meeting was held between the Executives and the JAO at Dulles airport to discuss the technical and contractual situation associated with the production antenna bids (it should be noted that in parallel to these technical evaluations a process to review and evaluate the contractual aspects of the bids was underway in both Executives). During this meeting it was decided to repeat a subset of the measurements on the prototype antennas in order to provide high signal-to-noise data on which firm conclusions about the technical capabilities of the prototype antennas (and derivative productions antenna designs) could be made. The group formed to do this was the Joint Antenna Technical Group (JATG), involving all internal and external people and resources that could be made available for the effort.

1.1 ALMA Joint Antenna Technical Group

In early December 2004 the ALMA JATG devised a testing program to produce high-quality datasets which would: (a) assess prototype performance against the ALMA antenna specifications; (b) address specific issues or concerns that have been raised about the prototypes based on the results of ALMA AEG, JTET and ATWG measurements and analyses; (c) have a high probability of successful execution, providing directly relevant data. The measurements tests are listed in Table 1.2; during the course of the testing program some responsibilities shifted, and schedule delays have occurred (in most cases due to weather), but in most cases the tests have been carried out successfully. In addition to the measurement program, analyses of existing data sources was continued (these are listed in Table 1.3). Regular telecons were held during December, January and February 2005 to assess progress and to plan additional tests based on the incoming results. One test added was a 10-day (~100,000 cycle) Fast-Switching test, proposed to examine surface stability in standard operating conditions.

This report is divided into subsections authored by the individuals responsible for the test execution and result analysis.

Test	Antenna	Available	Duration	Responsible	Comment	Issue
All-sky pointing	Alcatel	Dec 20th?	5 days	Mangum, Lucas, Wirenstrand, Wallace	Post-acceptance	**Examine AEG PF after realignment**
Holography(1)	Both	Dec 17th	24 days	Mangum, Lucas	5 deg elevation. Reset surfaces based on results?	**Evaluate current surfaces at low elevation. Search for NHD.**
Holography(2)	Vertex	Dec 17th	2 days	Mangum, Lucas	Cabin thermal control on/off; decision to proceed after thermal data evaluation	**Examine effects of lack of cabin thermal control in production design**
Photogrammetry	Both	Jan 12th	3 days	GSI & Schwab, Hills & Schwab	Range of elevations (6)	**Estimate surface performance at different elevations**
Thermal Behavior of Cabin	Vertex	Dec 6th	Ongoing	Gasho, Emerson	Ongoing measurements; data evaluated for H(2)	**Same as Holography (2)**
Out of Focus (OOF) Beam Maps	Both	Jan 1st	20+ days?	Mangum, Lucas, Hills	Will use nutator	**Estimate surface performance at different elevations**
Orthogonal Beam Cuts	Vertex	Jan 1st	5 days?	Mangum, Lucas, Emerson		**Estimate astigmatism**
Fast-switching test	Both	Feb 20th	10 days	Stanghellini, Sramek		**Examine surface stability**
			59 days			

Table 1.2 – Test plan

Data	Antenna	Responsible	Comment	Issue
Quadrant Detector	Vertex	Woody, King	Approaching convergence? Still inconsistent with QD focus estimate	**QD vs. FEM predictions re: BUS stiffness**
Photogrammetry	Vertex	Hills, Schwab	Existing data sets analyzed; other datasets possibly available (Alcatel, APEX?)	**Estimate surface performance at different elevations; focus as function of elevation**
Accelerometer **(did not occur; no data produced)**	Vertex	Snel, Woody	Simultaneous optical pointing & accelerometer data; may require further testing	**Examine 0.6 deg offset pointing performance; servo loop tuning issue**
Existing OOF data/ simulations	Vertex	Hills		**Estimate surface performance at different elevations; pursue changes in Vertex surface with time**

Table 1.3

2 JATG Results

2.1 Holography (J. Mangum, R. Lucas, N. Emerson, J. Meadows)

2.1.1 Summary

This report summarizes the holography measurements made 2004/12/17-2005/02/11. Figure 2.1.1 shows a comparison of the final AEC and VertexRSI surface measurements. A comparison with the photogrammetry measurements made 2004/10 and 2005/01 is also made. For the chronology of surface measurement, setting, and related activities on both prototypes antennas, see Gasho (2004) and Stanghellini (2005).

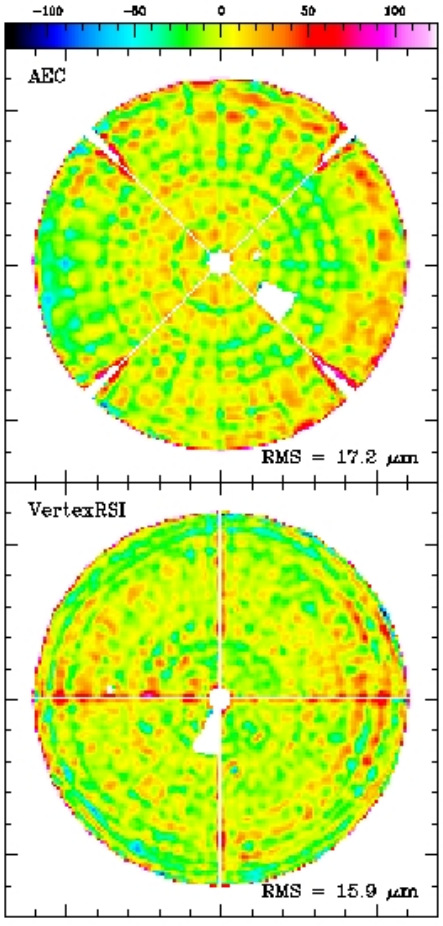

Figure 2.1.1: Comparison between the final February 2005 AEC (top) and VertexRSI (bottom) holographic surface measurement maps. ***Note that this figure uses a nearfield correction referenced to the midplane of the antenna aperture.*** **The -12 db taper weighted RMS values for each measurement are indicated.**

Note that throughout this report all quoted surface RMS values, unless otherwise indicated, refer to a nearfield correction referenced to the midplane of the aperture. This is **not** the nearfield correction reference used in the AEG holography analysis.

2.1.2 VertexRSI

2.1.2.1 Winter 2004/2005 Holography Measurements

For the Winter 2004/2005 VertexRSI holography measurements:

- Holography measurements were made in exactly the same way as for May-July 2003.
- A total of 78 maps were made, of which
  - Pre-Adjustment:
    - With the receiver cabin cooling system active, eleven maps were acquired, four of which were of sufficient quality to derive surface RMS values. With several known bad panels included, surface RMS values were in the range 31-38μm.
    - With the receiver cabin cooling system deactivated, sixteen maps were acquired, eleven of which were of sufficient quality to derive surface RMS values. With several known bad panels included, surface RMS values were in the range 33-38μm.
    - Surface structure is very consistent from map-to-map.
  - Post-Adjustment I:
    - Seven maps were made immediately following surface adjustment on 2004/12/28-29. Due to poor weather conditions, none of these maps are of sufficient quality, but all yield surface RMS values, with several known bad panels included, of < 18μm.
    - A problem with the holography system transmitter was discovered and fixed, solving the problems which resulted from the low signal power at the DSP inputs to the holography receiver. Eight more holography measurements were made, all of good quality. Derived surface RMS values, with several known bad panels included, are in the range 13-15μm.
    - Panels 8-53 and 8-54 were purposely offset by +100 μm (toward the prime focus). Five more maps were made with predictable results.
  - Post-Adjustment II:
    - On 2005/01/18 Robert Lucas realized that the reference point chosen for the nearfield correction to all of our nearfield holography measurements was not appropriately chosen. All holography measurement analyses to-date had been carried out using the intersection of the azimuth and elevation axes as the reference point for the rather large nearfield correction. A more

appropriate choice would have been to reference the nearfield correction to the midplane of the aperture. This change leads to a spherical aberration-like structure in the surface measurements which has been "adjusted-into" the surface by the holography measurements. This spherical aberration-like structure is apparent in the photogrammetry and OOF measurements.

- An adjustment of the surface was made on 2005/02/04 to remove the nearfield reference spherical aberration and to readjust panels 8-53 and 8-54. Due to poor weather conditions, an additional adjustment of the panels in rings 7 and 8 was required on 2005/02/09. Continued poor weather conditions (rain/snow) resulted in the collection of only four good measurements following surface adjustment. All of these maps yield derived surface RMS values, with several known bad panels included, in the range 16-17μm.

2.1.2.2 Pre-Adjustment Comparison to AEG Measurements

Figure 2.1.2 shows a comparison of July 2003 and December 2004 holography maps. This comparison shows:

- Good correlation between known deformation structures (warped and "nicked" panels and signal compression ringing) measured in May-July 2003 and December 2004.
- The known surface defects confirm the three-dimensional orientation of these measurements.
- Note that deformations on the edges of the maps are not well measured due to the limitations listed elsewhere in this document.
- The primary focus derived in July 2003 (Final map; $\Delta(X,Y,Z)$ = (0.37, 1.71, 0.77) mm) and that derived from these new (December 2004) measurements (Map used to set surface; $\Delta(X,Y,Z)$ = (0.51, 1.28, 0.36) mm) shows at most a 0.5 mm difference, which is within the tolerances of the mounting of the holography receiver.

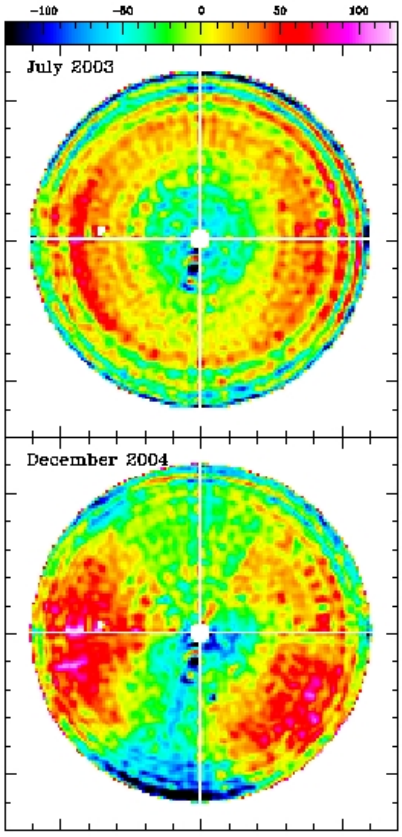

Figure 2.1.2: Comparison between the July 2003 and December 2004 VertexRSI holography measurements. Note that this analysis represents a reinterpretation of the July 2003 measurements which utilizes a more appropriate reference point for the nearfield correction. The map in the top panel (July 2003) was made after all surface setting was complete and had a weighted RMS of 18μm or 30μm for nearfield reference at the azimuth/elevation axis intersection or aperture midplane, respectively. The December 2004 map is typical and has an RMS of 33-36μm. Note that for all displays in this report the amplitude scale is given as the "surface error" as viewed from the prime focus prespective. Therefore, positive is a "bump" and negative is a "hole".

2.1.2.2.1 Correlation With Loose Bolts

Figure 2.1.3 shows a typical pre-adjustment December 2004 holography measurement with the locations of the loose bolts indicated. Note that Figure 2.1.3 suggests that:

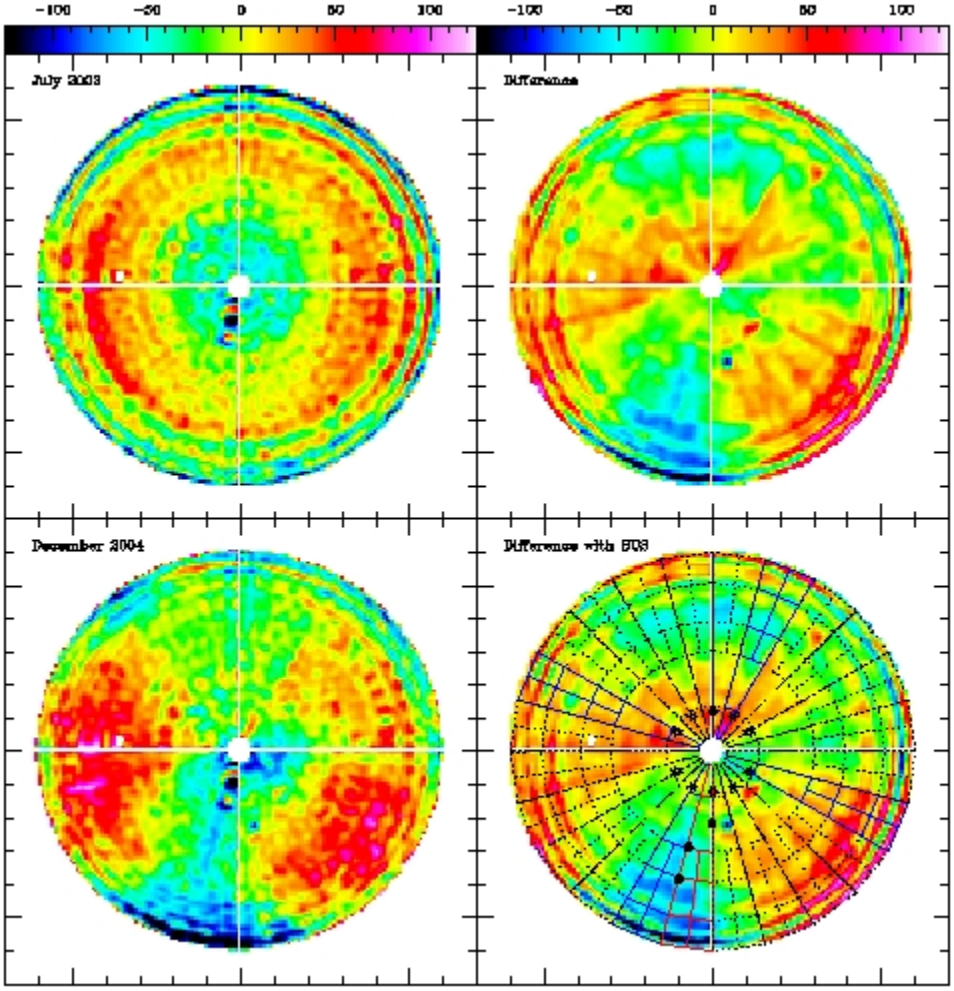

Figure 2.1.3: Comparison between the July 2003 and December 2004 VertexRSI holography measurements. Note that this analysis represents a reinterpretation of the July 2003 measurements which utilizes a more appropriate reference point for the nearfield correction. The top-right panel shows the difference between the December 2004 and July 2003 holography measurements, while the bottom-right panel shows this difference with BUS sector outline and loose bolt locations indicated. In the bottom-right panel, stars indicate turnbuckle bolt locations, filled-circles indicate loose hoop segment locations, blue BUS sectors indicate those whose central hub connections were loose, and red BUS sector indicates the BUS sector with loose hoop segment bolts.

- The region at “6:30" on the surface, which shows the largest deviations from the best-fit paraboloid, is also the region which had all four types of loose bolts (Invar ring setup, central hub, hoop connection, and turnbuckle).

- The panel boundary regions between rings 7 and 8 are regions which were not well characterized during the May-July 2003 measurements. This was due to two effects:
  - A suspected signal saturation effect which produced a low-level “ripple" pattern on the outer rings of the antenna (see AEG report on holography for details).
  - Poor amplitude sensitivity at the edges of the reflector, due to an improperly large taper of the holography receiver signal feeds. This poor surface edge sensitivity, coupled with atmospherically-induced phase instabilities which are near-field corrected, lead to an additional “ripple" component which is strongest near the edges of the reflector (see Figure 2.1.4).

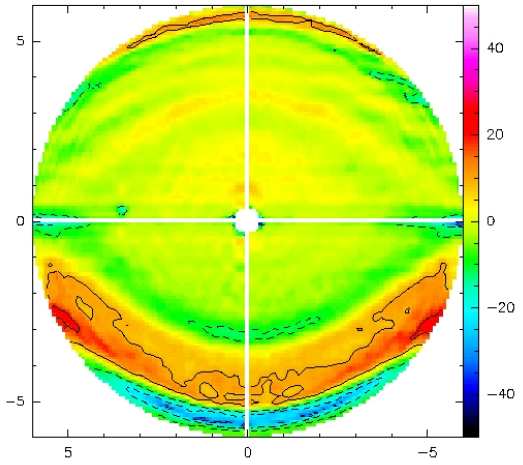

Figure 2.1.4: The effect of high-frequency phase noise on holography measurements. Phase calibration during holography measurements does a pretty good job of removing the low-frequency phase noise, but some higher-frequency noise is left over. Shown is the difference between two calibration solutions which used solution intervals of 0.5 and 0.02 hours to calibrate a map whose phase stability was rather poor (due to poor weather conditions). A residual phase noise of characteristic time scale of say 0.5 hour will be seen as a set of horizontal stripes in the holography beam map, and as a horizontal stripe in the phase map far away from the center. These stripes in the raw phase map are distorted by the near field correction process into the features seen in many of the holography maps in this report.

- All of the loose bolts were tightened when the antenna was at the zenith position. This could suggest that, since nearly all of the bolts were tightened when the antenna was at zenith, a downward “sag" was frozen-in to the upper and lower portions of the surface during this bolt tightening.

2.1.2.2.2 Holography Measurements Following Surface Adjustment

Holographic measurements following the overall surface adjustment were made starting on 2004/12/29. Due to poor weather conditions, site power problems, and the continuing problems with low signal power at the holography receiver, useable measurements were not obtained until 2005/01/08.

On 2005/01/18 Robert Lucas realized that the reference point chosen for the nearfield correction to all of our nearfield holography measurements was not appropriately chosen. All holography measurement analyses to-date had been carried out using the intersection of the azimuth and elevation axes as the reference point for the rather large nearfield correction. A more appropriate choice would have been to reference the nearfield correction to the midplane of the aperture. This change leads to a spherical aberration-like structure in the surface measurements which has been “adjusted-into" the surface by the holography measurements.

An adjustment of the surface was made on 2005/02/04 to remove the nearfield reference spherical aberration and to readjust panels 8-53 and 8-54. Due to poor weather conditions, an additional adjustment of the panels in rings 7 and 8 was required on 2005/02/09. Continued poor weather conditions (rain/snow) resulted in the collection of only four good measurements following surface adjustment. All of these maps yield derived surface RMS values, with several known bad panels included, in the range 16-17μm.

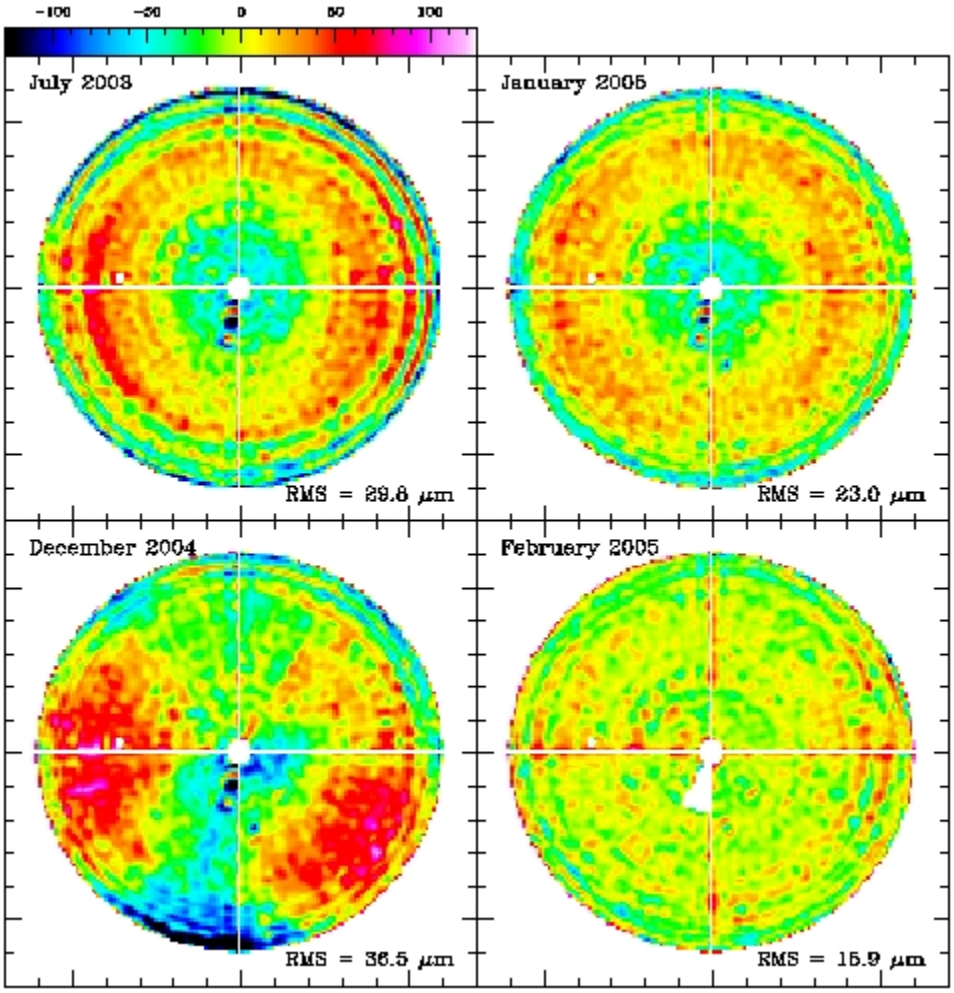

Figure 2.1.5: Comparison between the AEG (July 2003), before-adjustment (December 2004), after-initial-adjustment (January 2005), and final-adjustment (February 2005) VertexRSI holography measurements. Weighted RMS values are shown for each map.

Figure 2.1.5 shows a compendium of surface error maps for the VertexRSI antenna. All useable measurements made following surface adjustment show very consistent structure.

2.1.2.3 Comparison to Photogrammetry

Photogrammetry measurements of the VertexRSI antenna were made in October 2004 and January 2005. Figure 2.1.6 compares these photogrammetry measurements with their associated holography measurements. One sees some correlation.

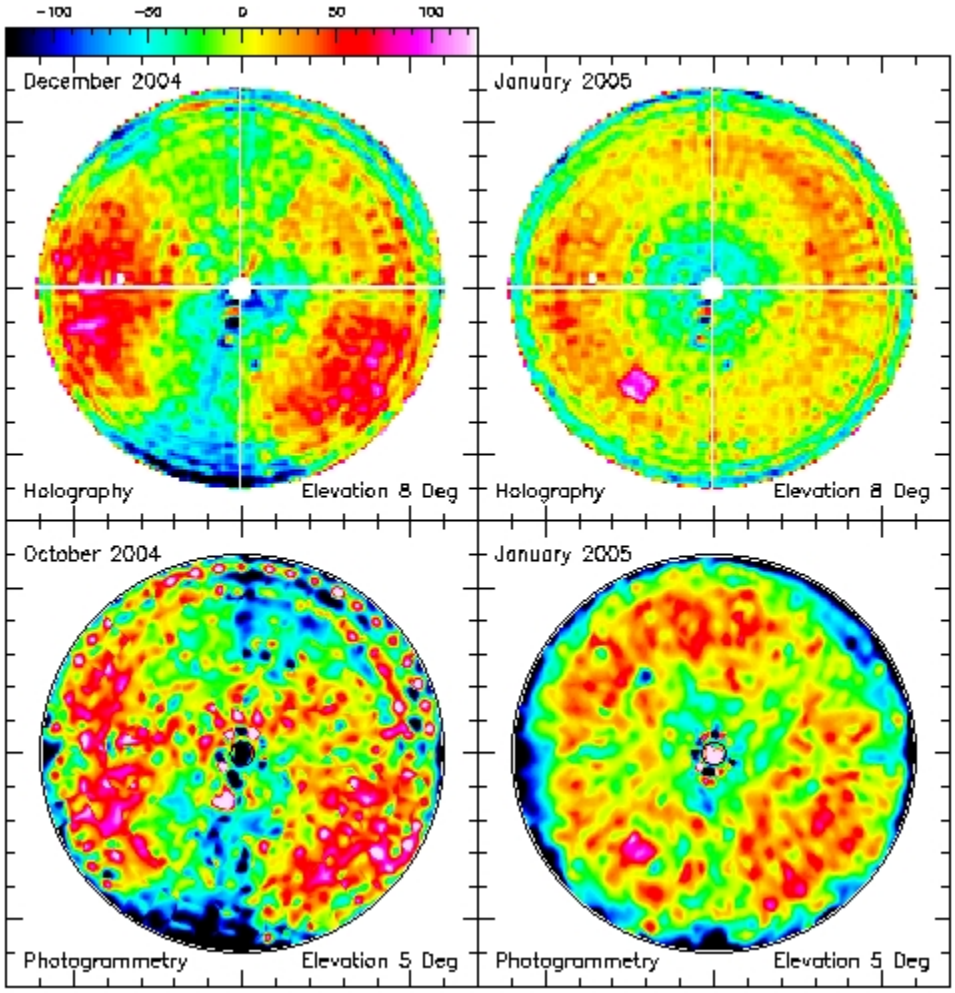

Figure 2.1.6: Comparison between the October 2004 "Run 4'' photogrammetry, the December 2004 holography, the January 2005 photogrammetry, and the January 2005 holography measurements. Note that this comparison uses the normal deflection definition for the Z-coordinate.

2.1.3 AEC

2.1.3.1 January 2005 Holography Measurements

For the Winter 2005 AEC holography measurements:

- Holography measurements were made in exactly the same way as for January-February 2004.
- A total of 17 good maps were made:
  - Pre-Adjustment:

- Seven maps before panel setting. Two of the these maps were of sufficient quality to derive surface RMS values, with several known bad panels included, which are in the range 19-21μm (before donut aberration removal).
- Surface structure is very consistent from map-to-map.

o Post-Adjustment I:
- 2 maps were made immediately following surface adjustment on 2005/01/26. Surface RMS values of 18μm measured.
- A second-order analysis software error in the application of the nearfield correction was discovered, which resulted in a small residual spherical error over the surface. Even though this error was small, a minor resetting was done to remove this software artifact.

o Post-Adjustment II:
- 8 maps were made immediately following surface adjustment on 2005/01/27.
- Seven good maps made. Surface RMS values in the range 16--18μm derived.
- Surface structure is very consistent from map-to-map.

A comparison of the pre-adjustment holography results on the AEC antenna with those made during the February 2004 holography campaign (Figure 2.1.7) show some significant differences:

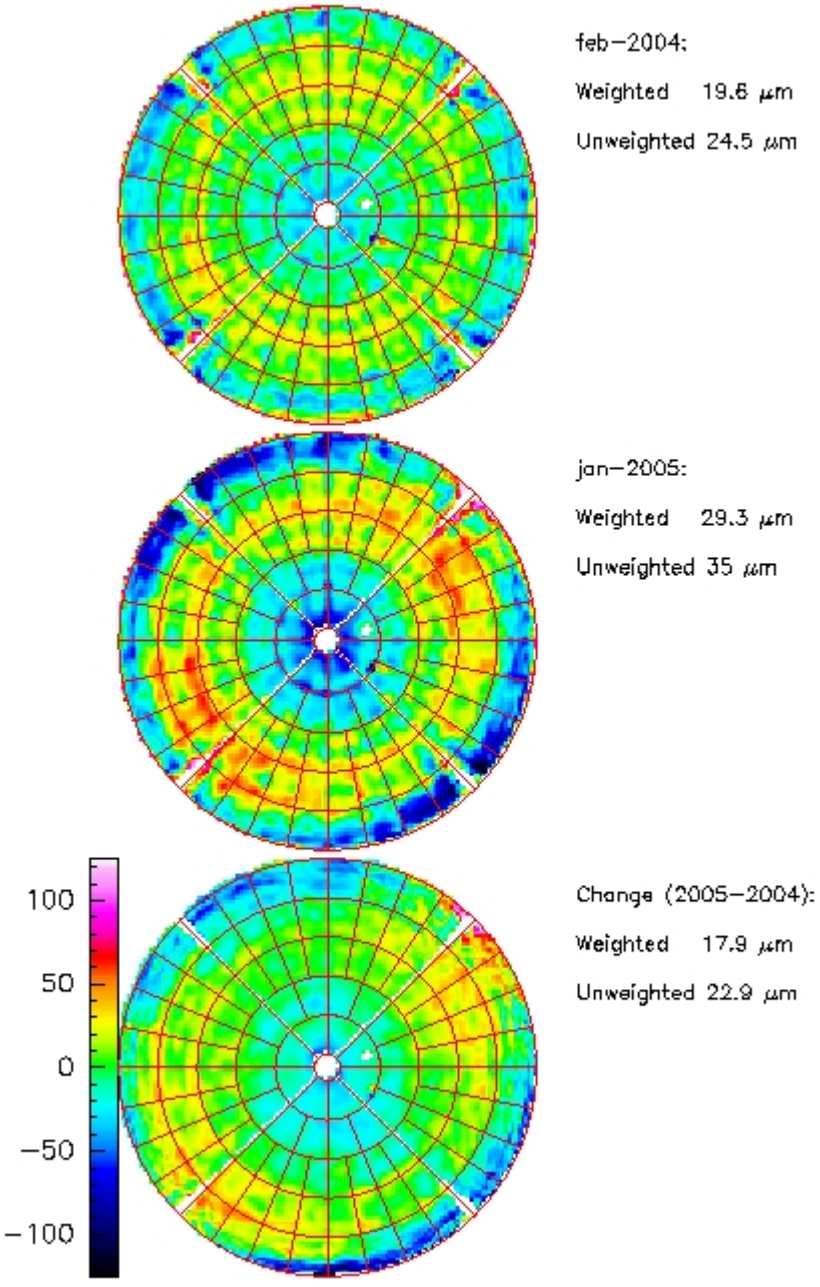

Figure 2.1.7: Comparison between the February 2004 (top), January 2005 (middle) and the difference between these 2005 and 2004 holography measurements (bottom) using a nearfield correction referenced to the midplane of the antenna aperture. The unweighted and -12 db taper weighted RMS values for each measurement are indicated.

- The primary focus derived in February 2004 (Final map; $\Delta(X,Y,Z) = (1.07, -5.26, 1.10)$ mm) and that derived from these new (January 2005) measurements (Map used to set surface; $\Delta(X,Y,Z) = (4.42, 1.53, 0.63)$ mm) shows some significant differences. The -5 mm offset in Y, in addition to a -10 mm offset in Z which was also noted in the 2004 AEC holography and radiometry measurements, was ultimately traced to a misaligned apex. The apex was realigned in May 2004 (see Stanghellini (2005)). The relative X and Y shifts of approximately +3 and +7 mm, respectively, observed in these new holography measurements could be due to:
    - A misalignment of the holography signal feed. Note that the signal feed for the holography receiver when mounted on the AEC antenna is not mounted rigidly to the apex structure (in contrast to the rigid mounting of the holography receiver on the VertexRSI antenna).
    - A further misalignment of the apex structure.

- There is clearly a change in the surface RMS between the two periods at the level of 17 μm RMS, with a residual signature of astigmatism at 45 degrees position angle.
- In a sense this confirms the recent photogrammetry results (See Hills (2005); however with a much better sensitivity.

One is tempted to link this change to the re-adjustment of the focus in May 2004 (see Stanghellini (2005)). This re-adjustment, required as the antenna could not be focussed on the radiometry receiver, involved a displacement of the feet of the quadripod legs (the quadripod was moved sideways and the bolts retightened).

2.1.3.2 Paraboloidal Reference (Donut) Correction and Surface Setting

Based on the holography measurements made on 2005/01/23, and using the redefined reference paraboloid for the near field correction to these measurements, the AEC surface was reset. Unfortunately at this stage the distance to the transmitter had not been consistently reduced by 3.1 m in the data reduction software for the AEC antenna as needed by the change of reference plane. This software oversight was fixed and a second setting of approximately half of the panels was made. Figure 2.1.8 shows this new measurement.

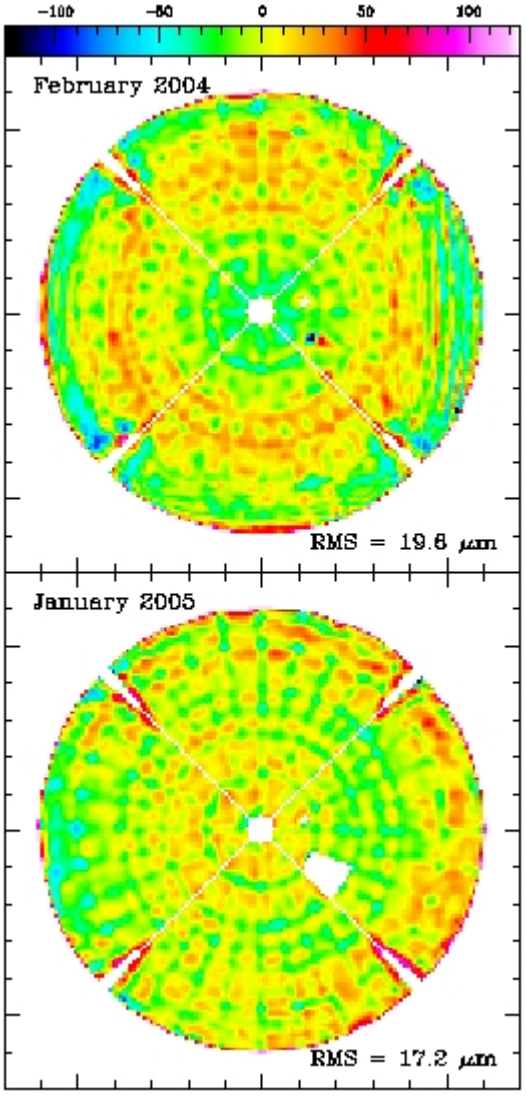

Figure 2.1.8: Comparison between the February 2004 (top) and final January 2005 (bottom) using a nearfield correction referenced to the midplane of the antenna aperture. The -12 db taper weighted RMS values for each measurement are indicated.

Note also that the AEC subcontractor Microgate fixed the internal timing error which was causing a low-level position jitter in the holography measurements just prior to the last of these new (post surface setting) measurements.

2.1.3.3 Comparison to Photogrammetry

Photogrammetry measurements of the AEC antenna were made in January 2005. Figure 2.1.9 compares these photogrammetry measurements with their associated holography measurements. One sees some correlation.

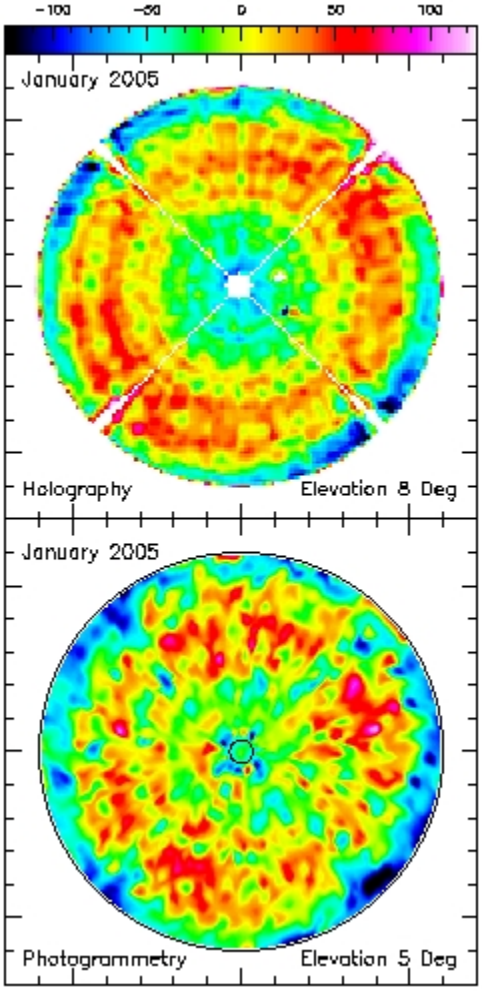

Figure 2.1.9: Comparison between the January 2005 photogrammetry and holography measurements. Note that this comparison uses the normal deflection definition for the Z-coordinate.

2.1.4 Bibliography

- Gasho, V. L., "VertexRSI Surface Measurement Chronology and Events Possibly Influencing Surface Setting" (2004/12/03)
- Stanghellini, S., "Alcatel-EIE Antenna Surface Measurement Chronology" (2005/01/10).
- Hills, R. & Schwab, F. Photogrammetry report, this document.

2.2 Quadrant Detector (Woody/King/Koch)

2.2.1 Background

A direct measurement of the gravitational distortion of the reflector provides a method for evaluating the accuracy of the FEM of the antenna structure. Quadrant detectors, QD, provide a simple method for measuring the changes in the structure that are accurate to a few microns over distances of several meters. A quadrant detector system consisting of a laser mounted at the vertex of the primary was use to measure the lateral shift of the target mounted at eight points around the rim of the primary as a function of elevation. A critical aspect of this measurement is the stability of the laser and its mount at the vertex. The first QD measurements in the spring of 2004 indicated that there were problems with the laser mount and it was not possible to verify that the gravitational deformations were consistent with the surface error budget. The laser mount was improved substantially and an additional set of eight target positions around the edge of the central hub was used to evaluate the laser and its mount. A complete set of measurements was obtained on the Vertex antenna by the IPT and AEG in October 2004 after Vertex tightened the bolts in the BUS. This report analyzes these measurements in comparison to the FEM of the reflector provided by Vertex.

The AEC antenna is very stiff and the predicted gravitational deformations and are a small part of the surface error budget. The QD deflections measured on the AEC antenna were small enough to not raise any concerns about the FEM, although a detailed comparison with the FEM was not made.

2.2.2 Measurements of the Vertex Antenna

The antenna IPT and AEG groups performed the QD measurements. These groups also provided preliminary analysis of the data, including evaluation of the laser mount deformation using the measurements of the inner target positions. This work in described in the following documents:

"VertexRSI ALMA Antenna Prototype Backup Structure Reflection Measurements Results of Data Analysis," By Angel Otárola, November 15, 2004 (Draft) Data gathered by: Engineers Nicholas Emerson (NRAO), Pascal Martinez (ESO) and Dr. Jinquan Cheng (NRAO).

"Vertex Antenna BUS Behaviour Measurements," Oct 25th 2004 – Nov 5th 2004 ALMA-00.00.00.00-000-A-TTT Version: Draft 7 Status: (Draft, Pending, Approved, Released, or Obsolete) 2004-11-02 by Pascal Martinez.

"Mechanical Measurements of the ALMA Prototype Antennas Path Lengths, thermal Behaviour, Azimuth Bearing, and Gravity Induced Deformations", Albert Greve (IRAM) and Jeff Mangum (NRAO) December 1, 2004.

"Deflection Measurements of the VertexRSI BUS," A. Greve, 15 Sept. 2004.

These reports provide useful descriptions of the measurement set up and other details of the tests that were performed. Much of the QD displacement data is summarized in tables in the above reports. The raw "chart recorder" plots of the QD readings vs. time and elevation were provided for all of the targets. The data that was not directly reported in table form in the above reports was estimated by eye from these charts.

The measurements were of high quality and accurately followed simple Hooke's law deformations, i.e. the individual deflections are accurately fit by A+B*cos(el)+C*sin(el). The data are presented as deflections relative to readings at 5 deg elevation to be consistent with other analyses and reports. The noise in the QD data is a few microns for each target reading and is sufficient to measure the small gravitational deformations required to meet the RMS surface specifications.

The measurements of the inner hub targets provided a measure of the laser mount gravitational sag and tilt. After the measurements on the antenna were made, the gravitational tilting of the laser within its commercial housing was measured. The tilt is 0.5+-0.5 micro-radians for 1 G change. This produces a negligible 3 micron effect at the rim of the reflector.

2.2.3 Vertex Finite Element Model (FEM)

Vertex provided the dx, dy, dz surface node deformations for gravity with the telescope pointed at the zenith and horizon in a spreadsheet. Figure 2.2.1 shows a side view of the surface deformations in going from 0 to 90 deg elevation predicted by the FEM. The reference plane is the inner hub where the Quadrant detector laser is mounted. A significant aspect of this distortion is that reflector rim remains very accurately in a plane and is characterized by a simple axial displacement and a 28.2 arcsec tilt of the rim relative to the central hub.

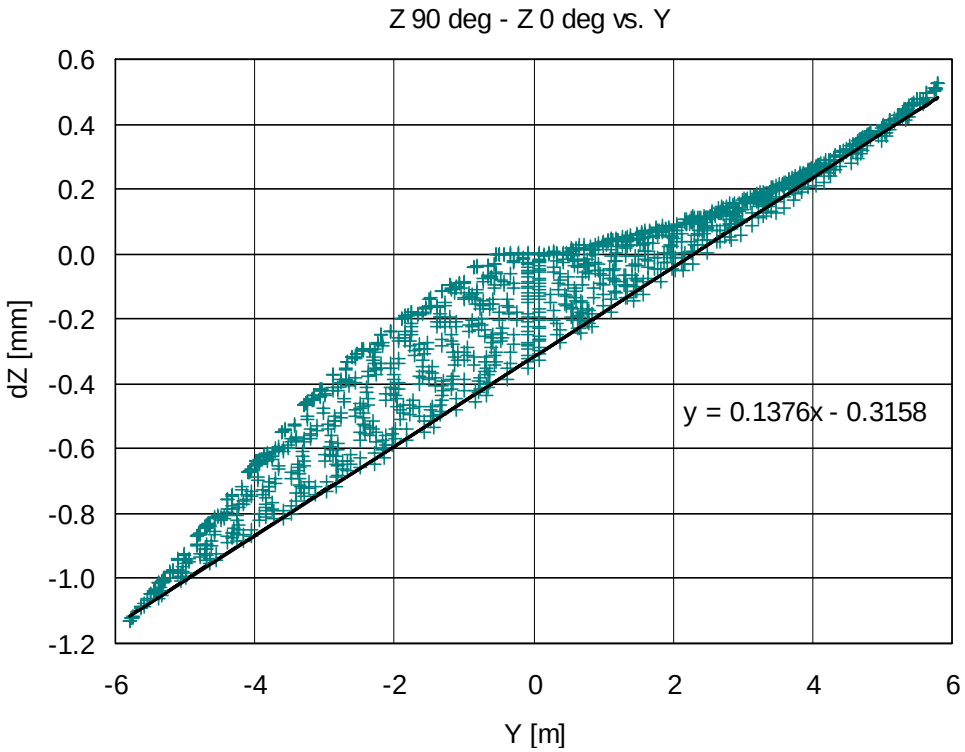

Fig. 2.2.1. FEM of the Vertex reflector surface gravity deflections at 90 deg minus those at 0 deg elevation. The axial deflections are plotted in side view looking along the elevation axis vs. y. The bottom edge of the reflector is at positive y. The data in referenced to the central hub where the quadrant detector laser is mounted. The best fit plane to the rim nodes is shown as a solid line.

Conveniently, Vertex also calculated the motion of the eight nominal rim points relative to the central hub in terms of cos(el) and sin(el) Hooke's law coefficients. These are given in the Vertex spreadsheet titled "gravity-displacement-data-121203-ALL.xls". Our own analysis of the full FEM of the surface nodes gave essentially the same results for the deflection of the rim relative to the central hub.

The FEM results are used to predict the change in the target position that would be seen by the laser beam mounted on the Vertex hub, including the radial and lateral shifts as well as the shift along the optical axis direction. The geometry of the mounting of the QD laser and targets makes the measurements sensitive to radial motion of the rim as well as the axial motion and it is important to include these geometry effects in comparing the FEM to the QD data.

The feedlegs obscured the four cardinal rim positions and the targets were mounted ~2 degrees away from the nominal nodes tracked in the FEM. A Fourier interpolation with eight terms was used to derive FEM calculations for positions of the targets. This

interpolation made a significant improvement in the quality of the fit between the measurements and the FEM although the targets were only ~2 deg away from the nominal positions.

2.2.4 Analysis of the Vertex Quadrant Detector Measurements

The basic analysis method is to compare the QD measurements to the FEM of the antenna provided by Vertex. The central hub QD measurements can be used to calibrate laser mount sag and tilting as a function of elevation. Figure 2.2.2 shows the quality of the fit to these measurements. The fitted values for the tilt and sag of the laser mount are in good agreement with Franz Koch's FEA calculations of the laser mount deformations. Correction has been applied to the QD data to account for the bending of the targets. The peak error is less than 4 microns and the RMS error is 1.7 microns. The residuals follow smooth curves indicating that there are systematic deviations at the level of a few microns not fit by this simple two parameter model of the laser mount relative the central hub targets. The noise on the measurements is less then one micron.

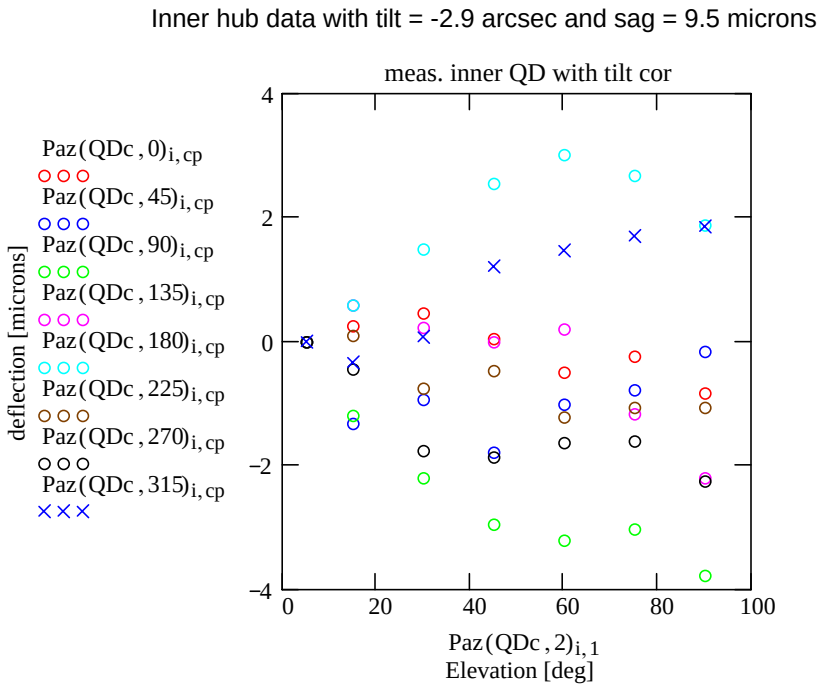

Fig. 2.2.2. QD measurements of the central hub targets after fitting to a simple model of the laser mount with gravitational tilt and sag terms. The QD measurements are shown as points with different colors for each azimuth orientation around the rim referenced from the top of the rim (when looking at the horizon) and increasing clockwise around the rim when looking from the prime focus. The measurements are referenced to 5 deg elevation. The fitted tilt is –2.9 arcsec and the sag is 9.5 microns.

Figures 2.2.3 and 2.2.4 compare the axial rim measurements corrected for the laser mount tilt and sag determined from the central hub calibration to the FEM. Hooke's law deflections have sine and cosine terms resulting in different curve shapes depending upon the ratio of these terms. It is important to compare the deflections over the full elevation range in evaluating the accuracy of the FEM. Although the form of the measured deflections agree well with the FEM, it is clear that the some of the parameters need to be adjusted to improve the fit. The QD measurements and FEM calculations in fig. 2.2.4 are accurately fit by a cos(az) curve indicating that the dominate effect at the rim is a simple tilting of the rim plane.

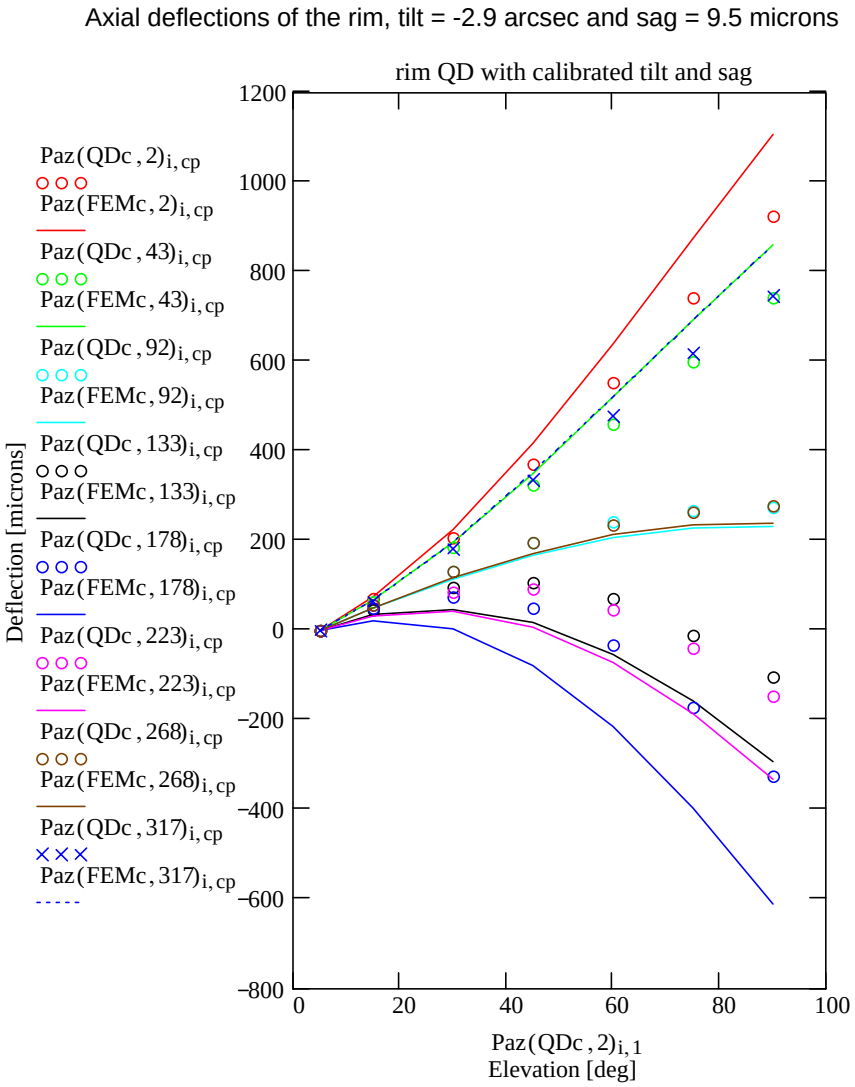

Fig. 2.2.3. QD measurements and FEM of axial rim deflections relative to the central hub vs. elevation. The central hub calibration of the laser mount from fig. 2.2.2 has been applied. The color code is the same as for fig. 2.2.2. The FEM calculations are shown as

solid lines with color matching the corresponding QD data. The plotted deflections are the readings from the QD target so that positive values actually indicate at shift in the QD target away from the prime focus.

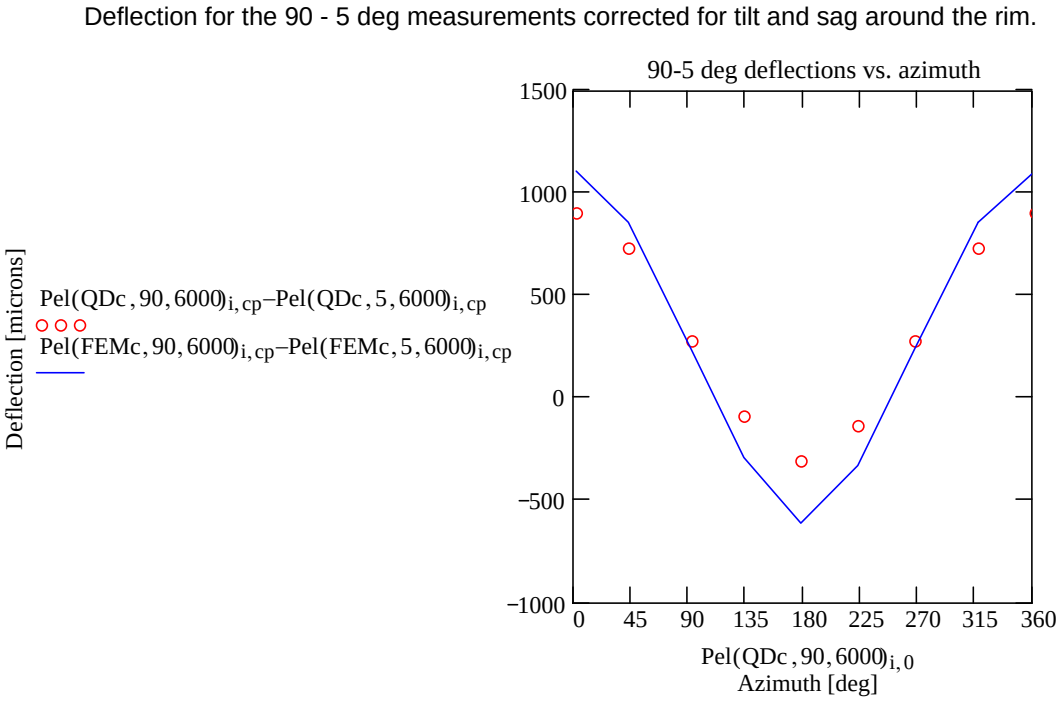

Fig. 2.2.4. Plot of the axial rim deflections at 90 deg minus those at 5 deg vs. azimuth around the rim. The central hub calibration of the laser mount from fig. 2.2.2 has been applied. The QD measurements are shown as circles while the FEM is show a solid line.

It is tempting to try to improve the fit by simply scaling the FEM deflections. The measured deflections in fig. 2.2.4 are actually less than the FEM predictions and you have to assume that the structure is ~20% stronger than predicted to improve the fit with just this parameter. Even then the fit is not particularly good.

The approach taken in this report is to include fit parameters for the laser mount sag, sin(el), and tilt, cos(el), as well as a parameter for scaling the FEM. Fitting for the tilt allows for inaccuracies in the FEM for the tilt of the central hub relative to the rim. An additional parameter for rotation about the optical axis is also included to aid in fitting the lateral displacements measured by the QD targets. Figure 2.2.1 shows that the distortions near the vertex of the primary where the laser is mounted are complicated and small errors in this part of the structure will give disproportionately large QD errors at the rim. In this approach, the central hub targets simply become added measurement points to be fit along with the rim measurements. The QD system also measures the lateral displacement of the target and this data is included in the analysis to help constrain the

fitting parameters. Hence there are 32 measurements at each of six elevations (all measurements are referenced to 5 deg elevation) to be fit by four parameters.

Figures 2.2.5 to 2.2.8 show the best fit results. The fit is excellent and is approaching the limit of the noise in the rim deflections. The residual from the fit to all of the data, including the lateral displacements, is 20 microns RMS. The RMS of surface displacements over the full elevation range is 11 microns while the rim and central hub surface errors (corrected for the optical ray geometry) for the 90 deg minus 5 deg data is 16 microns. The RMS is dominated by the axial deflections of the bottom lip, but there is no reason to suspect that this data is inaccurate. The noise in the rim measurements is estimated to be ~5 microns from the scatter in the individual curves in fig. 2.2.6. This noise includes various time dependent changes in the structure caused by the wind and temperature. Correcting for this noise and dividing by two to account for an optimal tuning of the surface setting leaves an **upper limit of the deviation from the predicted gravitational distortion of 8 microns at the extremes of the elevation range after scaling the FEM by 1.16.** This an upper limit because it only includes the measurements at the extreme rim of the reflector where the deformations are expected to be the largest and at the central hub where the deformations are complex and represents a small fraction of the collecting area. A representative number for the whole surface is difficult to determine but could be as much as a factor of two smaller.

Figure 2.2.8 shows the relationship between the FEM and QD measurements. The FEM was scaled by 1.16 and the rim nodes for the FEM and the quadrant detector data were fit to planes. This shows the deviation in the relative tilt of the central hub and rim for the FEM and QD targets. The FEM shows curling at the top and bottom edges that is twice as large as that seen by the QD. A detailed comparison of the rim data is shown in fig. 2.2.9. The lowest order non-homologous distortion is astigmatism. The FEM predicts astigmatism around the rim for the 90 deg – 5 deg deflections with a peak-to-peak amplitude of 25 microns with the peaks at 7 and 187 deg azimuth from top. This astigmatism is dominated by the localized curl at the bottom edge. . The QD measurements show a marginal astigmatism with a peak-to-peak amplitude of ~10 microns with the peaks at 47 and 227 deg.

Fit results for sag=9.8um, tilt=-17.4arcsec and FEM scaling=1.16

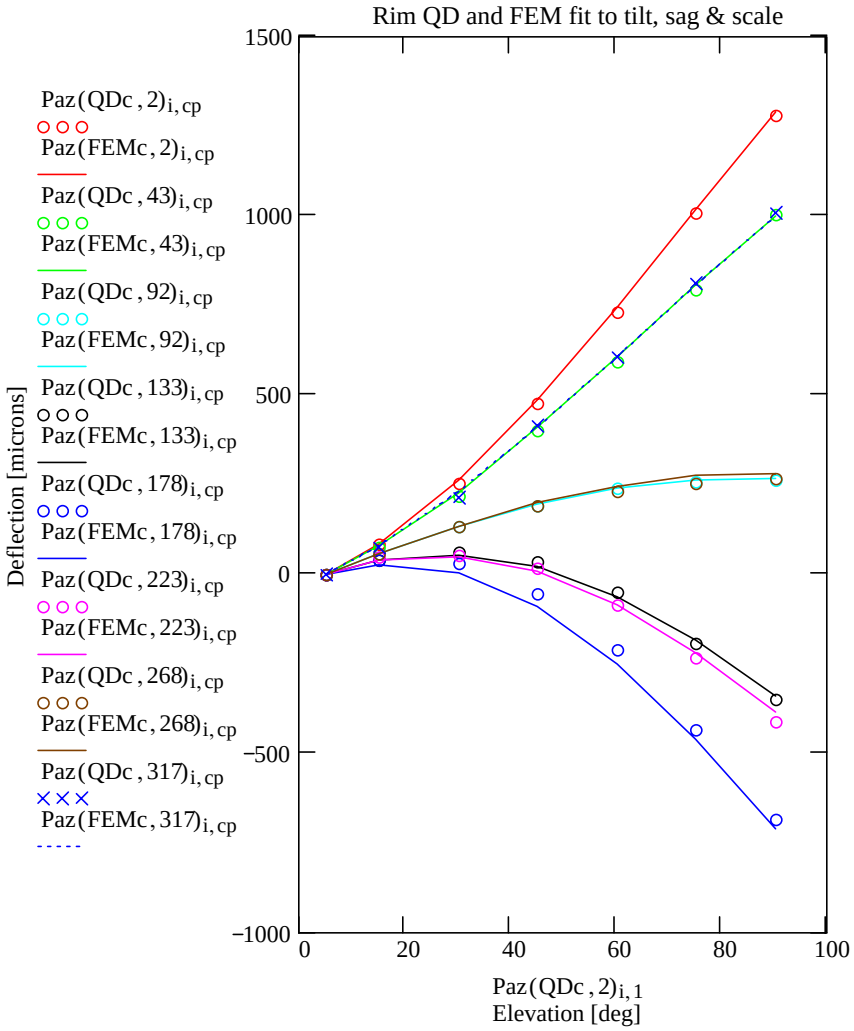

Fig. 2.2.5. Best fit results for QD measurements and FEM. The format is the same as fig. 2.2.3. The fitted parameters are sag = 8.3 microns, tilt = -14.9*cos(el) + 2.1*sin(el) arcsec, and FEM scaling = 1.15. The residual RMS is 9.5 microns for all of the data, including the lateral displacements not shown here.

Fit results for sag=9.8um, tilt=-17.4arcsec and FEM scaling=1.16

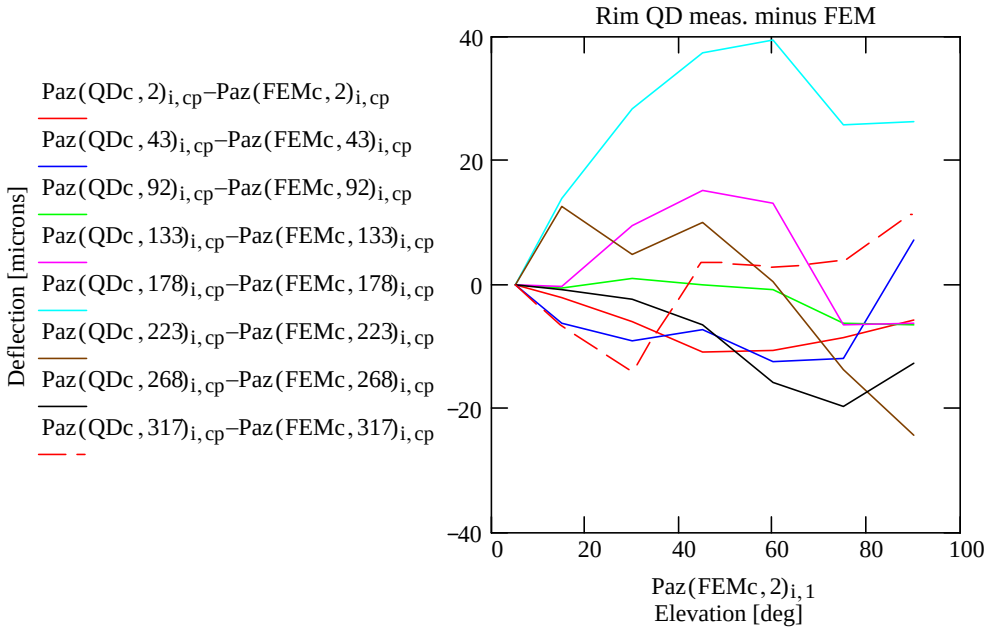

Fig. 2.2.6. Residuals from fit shown in fig. 2.2.5.

Fit results for sag=9.8um, tilt=-17.4arcsec and FEM scaling=1.16

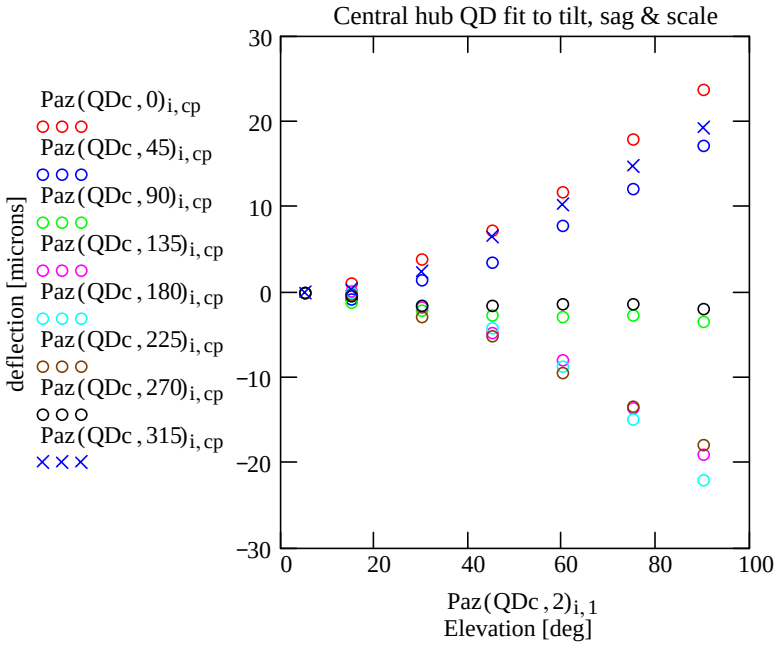

Fig. 2.2.7. Best fit results for central hub.

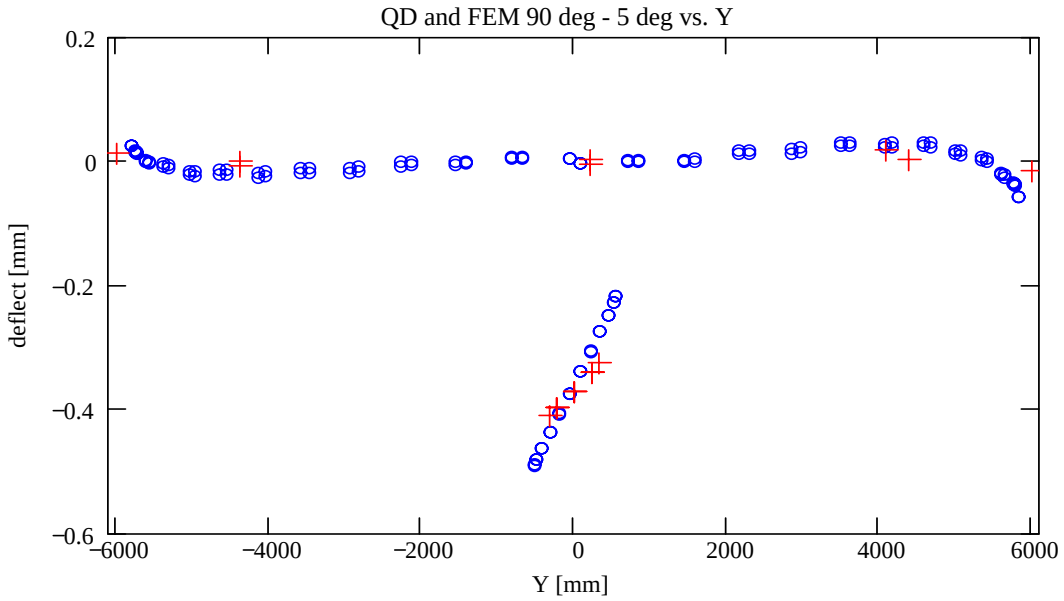

Fig. 2.2.8. FEM node and QD target displacements after fitting a plane to the rim data. The FEM nodes are shown as blue o's and the QD measurements are shown as red +'s. Note that the FEM hub nodes are at a radius of 544 mm while the QD targets were at a radius of 330 mm.

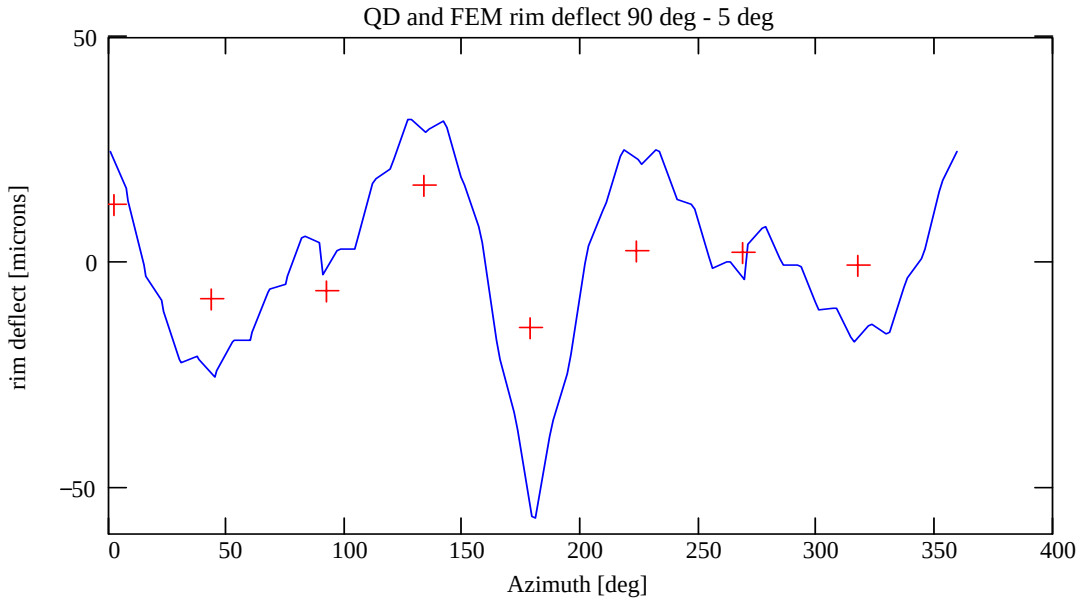

Fig. 2.2.9. Deviations of the rim deflections from a plane. The FEM rim data is plotted as a blue line while the QD measurements are shown as red +s.

2.3 Focus Length vs. Elevation (Schwab/Hills)

2.3.1 Introduction

The focal length dependence on elevation and temperature, of each of the ALMA prototype antennas, is described in this report. These data are derived from photogrammetric measurements.

Three photogrammetric measurement campaigns have been conducted on the VertexRSI prototype antenna:

- The first campaign, of Nov. 4–8, 2002, was commissioned by the antenna manufacturer. Its primary purpose was to achieve the initial, rough panel setting accuracy which was specified by the prototype contract, and to verify that the specification was met over the full range of elevation coverage. The total focal length excursion observed over the 5° to 90° elevation range in these data is ~1.4 mm.

- The measurement campaign of Sept. 29–Oct. 1, 2004, again was commissioned by the manufacturer. These measurements, intended to investigate the elevation dependence of focal length, were preceded by and evidently motivated by a series of back-up structure (BUS) adjustments, including bolt re-torquing and adjustment of radial tensioners. Some of the adjustments were made during the period between the Sept. 29 and Oct. 1 photogrammetry runs. The total variation in focal length over the 5° to 90° range observed in these data is ~1.3 mm.

- The final campaign, of Jan.17–19, 2005, was carried out under auspices of the JATG in order to investigate concerns which arose out of the analyses, by myself and Prof. Hills, of the Sept.–Oct. 2004 data. The specific concerns were: (i) a curious pattern, resembling classical astigmatism, in the 2-D residuals of the least-squares fits of paraboloidal surfaces to the 2004 data; and (ii) excess variation in the best-fit paraboloid (BFP) focal length, with respect to the finite-element model (FEM) analysis of the back-up structure. Here, a smaller total variation in focal length vs. elevation is observed (1.15 mm to 1.23 mm), and a strong correlation with temperature is evident. Fitting for both an elevation dependence and a linear dependence on temperature, the coefficient of the sin(elevation) term is further reduced, to ~1.0–1.1 mm.

The data sets taken prior to Jan. 2005 are deficient in the following respects: The times at which the measurements at the various elevations were taken have not been accurately reported, though partial information does exist. Temperatures from the sensors in the back-up structure were not —to our knowledge— recorded in either of the two previous campaigns. Neither are there air-temperature measurements available from the ATF

weather station (though some VLA weather station data do exist for these time periods). Too few measurements were taken to obtain statistically significant estimates of the simultaneous dependence of focal length on temperature and elevation (and more especially so, in the cases for which we have no time and temperature information).

For our Jan. 2005 campaign, complete weather station and BUS sensor data were recorded, and we believe that the overall integrity of the photogrammetry measurements is significantly better. More photogrammetry runs were done than in previous campaigns, so that now it is possible to look in detail at the temperature dependence of BFP focal length simultaneously with the elevation dependence. We find a strong correlation between BFP focal length and both measured air temperature (ρ=0.982±0.014) and mean BUS temperature (ρ=0.967±0.029). Statistically significant estimates now can be made of the simultaneous dependence of focal length on temperature and sin(elevation). The derived temperature coefficients are in rough agreement with radiometric measurements. And when temperature is included in the fit, the coefficient of the sin(elevation) term is reduced to ~1.0 mm. Thus, the Jan. 2005 data appear to be in substantial agreement with the FEM prediction of BUS deflection.

However, this picture is still a bit confused if one looks back at the Sept./Oct. 2004 photogrammetry data: There is a partial log of the times of nine of the photogrammetry runs for Oct. 1, taken at 5° and 90° (twice each), and at five intermediate elevations. In addition, air temperature measurements are available (but only from the VLA weather station). Here the χ^2 value for the focal length fit is not significantly reduced by including a temperature coefficient. A possible explanation is the fact that the HVAC system was shut off during the Sept./Oct. photogrammetry runs.

Photogrammetric measurements of the AEC antenna also were acquired in Jan. 2005. Here, the results are not at all startling: The total focal length variation with elevation is small, as expected. The sin(elevation) dependence is reasonably well behaved, and there appears to be little temperature dependence. The coefficient of the sin(elevation) term is ~0.25–0.3 mm.

2.3.2 Results from the Jan. 17-19 2005, photogrammetry

As described in more detail in another section of this report, the main reflector surfaces of the AEC and Vertex prototypes each were targeted with 1080 retroreflective adhesive film targets arranged in similar patterns on the two antennas, each with a relatively uniform areal density (1079 on AEC antenna; one was missed due to the optical telescope aperture). Estimates of the Cartesian (x, y, z)-coordinate locations of the 1080 targets were the basic end-product of the photogrammetric reduction that was performed on each run by the contractor (GSI, Inc., of Melbourne, FL).

With each data set we solved, by least-squares regression, for the paraboloidal surface that best matches the measured target coordinates. Our nominal target locations on the surface are specified in a right-handed Cartesian coordinate system with origin at the vertex of the design paraboloid and axis orientation conventions the same as those of the FEM. We solved for six parameters: best-fit focal length f; three translational parameters (x_0,y_0,z_0); and two rotation angles (θ_x,θ_y), about the x- and y-axes, respectively. We solved by minimizing the sum of squared z-residuals. In most cases we performed two least-squares regressions: one which was unweighted, and another with the data points weighted in proportion to an assumed 12 dB illumination taper (of parabolic shape, rather than Gaussian).

Table A1 (see Section 2.3.6) gives a summary of the Jan. 2005 focal length fits for the Vertex antenna. Included in the last two columns are the standard errors of the fitted focal lengths (these are merely formal error estimates, based on the normal distribution theory, assuming zero-mean, independent, identically distributed errors in the measured coordinates). On the first night there were eight photogrammetry runs, which occurred in the antenna elevation sequence 90°, 5°, 90°, 60°, 45°, 30°, 15°, 5°. The night's first run commenced shortly after 19:00 local time Jan. 17 (which would be 0200 UT, Jan.18). Photogrammetry runs the first night typically took around 20–40 minutes. The third night's runs were all taken at 90° elevation; these typically were of shorter duration, say 10 minutes. Column 3 of the table gives the approximate midpoint, in time, of each run. Data from longer runs may show glitches if temperatures are falling rapidly. Once or twice, a run had to be interrupted in the middle to replace a depleted battery pack for the camera or the strobe. The photogrammetry contractor has promised to provide a CD-ROM database which will include full information, such as the time at which each photograph was taken. The ATF weather station and monitor data acquisition system was operating during each of the January photogrammetry sessions. Column 5 of the table shows the measured air temperature at the ATF weather station. Column 6 gives the mean of the temperatures measured by the BUS temperature sensors (sensors 62–85).

Table A2 shows the corresponding summary data for the AEC antenna, which was measured on the second and third nights. We've included in this table only the measured air temperature at the weather station. If we understand correctly, the only temperature data recorded for the AEC data are for lower parts of the structure than the BUS. On Night 2 there were nine photogrammetry runs on the AEC antenna, which occurred in the sequence 90°, 5°, 90°, 60°, 45°, 30°, 15°, 5°, 90°. On Night 3 there were eight runs at 90° elevation, as with the Vertex antenna.

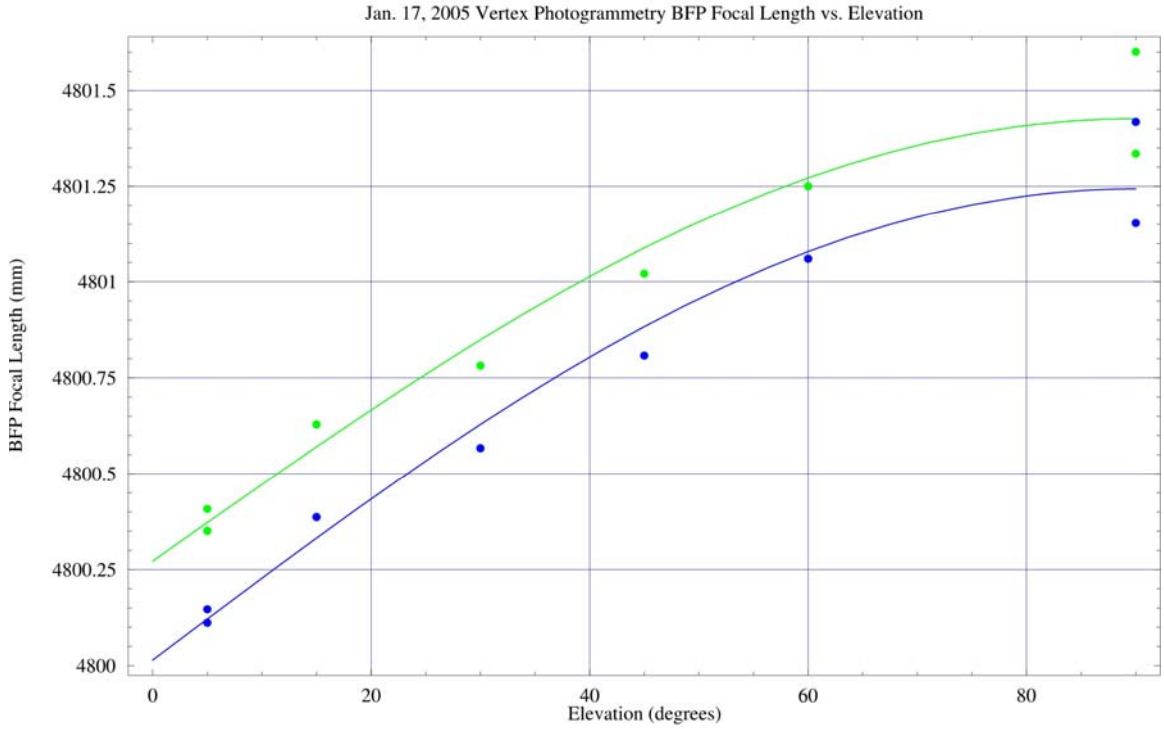

Figure 2.3.1. This figure shows the BFP focal length vs. elevation curves for the Vertex photogrammetry runs of Jan. 17, 2005, together with the best-fitting sin(elevation) regression curves. The results for the illumination-taper weighted fits are shown in Blue; the unweighted fits, in Green.

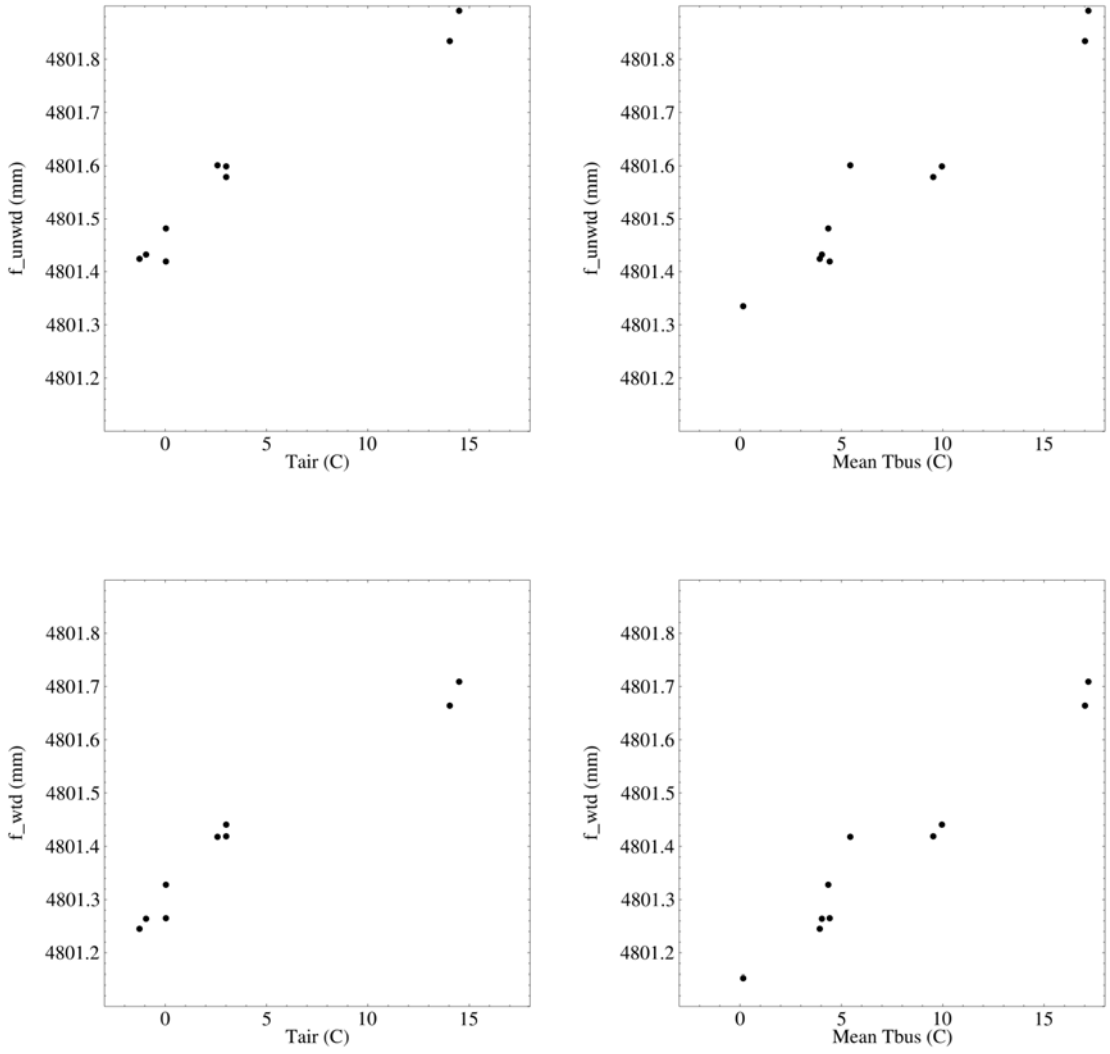

Figure 2.3.2. Scatterplots of BFP focal length vs. temperature for all the Jan.2005 Vertex photogrammetry runs at 90° elevation. There were ten runs at 90°: two on Night 1 and eight on Night 3. Top left shows f_{unwtd} versus T_{air} ; top right, f_{unwtd} versus T_{BUS}; bottom left, f_{wtd} versus T_{air}; and bottom right, f_{wtd} versus T_{BUS}. The corresponding sample correlation coefficients are ρ=0.982, 0.967, 0.982, and 0.974.

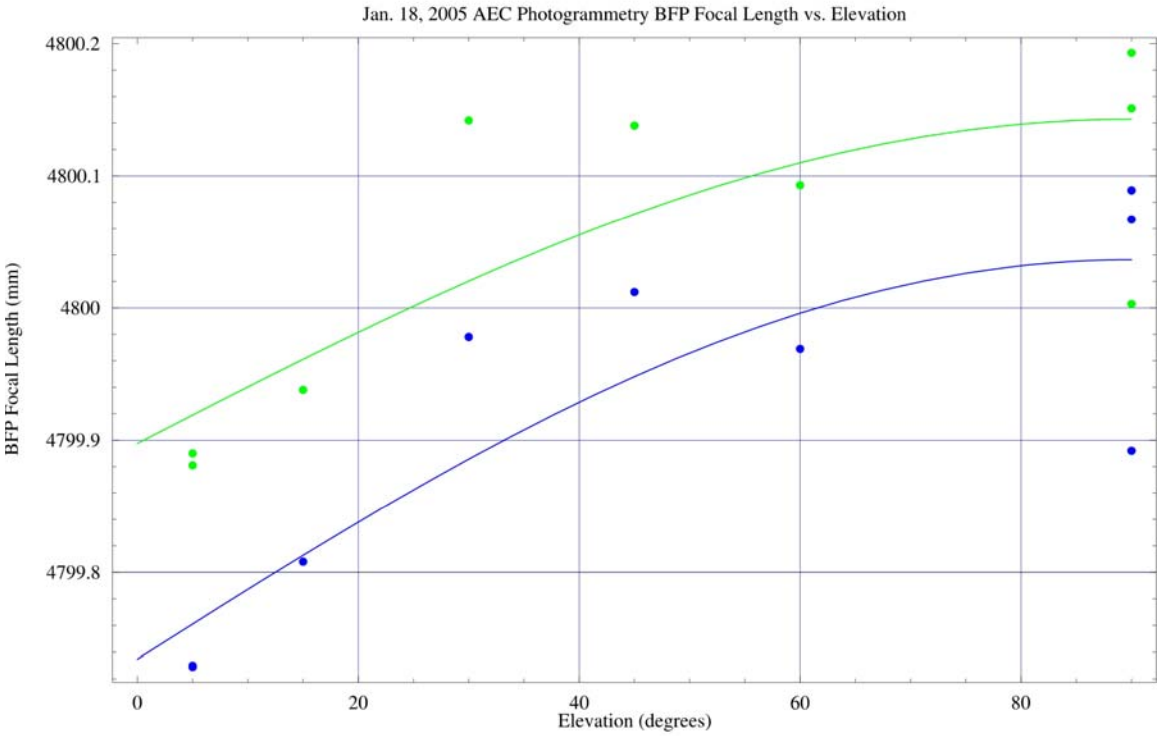

Figure 2.3.3. This figure shows the BFP focal length vs. elevation curves for the AEC photogrammetry runs of Jan.18, 2005, together with the best-fitting sin(elevation) regression curves. The results for the illumination-taper weighted fits are shown in Blue; the unweighted fits, in Green.

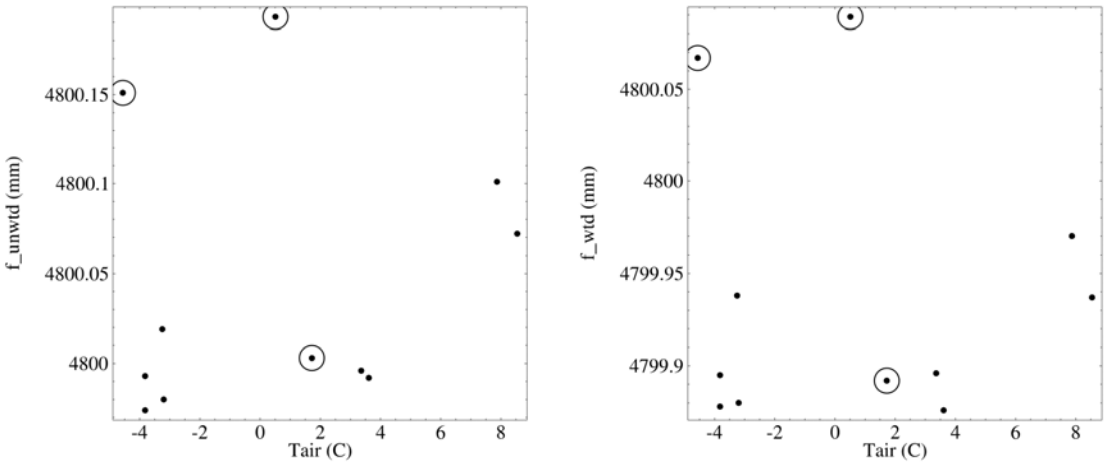

Figure 2.3.4. Scatterplots of BFP focal length vs. temperature for all the Jan.2005 AEC antenna photogrammetry runs at 90° elevation. There were eleven runs at 90°: three on Night 2 and eight on Night 3. *(Left panel)* f_{unwtd} versus T_{air}; *(Right panel)* f_{wtd} versus T_{air}. The corresponding sample correlation coefficients are ρ=0.172 and –0.034. The circled points are runs APG1-90, APG2-90, and APG3-90 of Night 2; two of these are apparent outliers.

Figure 2.3.1 shows the focal length vs. elevation curves for the Vertex photogrammetry data from Night 1, together with the best-fitting sin(elevation) regression curves. For the unweighted BFP case, the best-fit curve is

$$f_{unwtd} = 4800.272(\pm 0.062)+1.154(\pm 0.092)\sin(\text{elevation}), \qquad (1)$$

and the r.m.s. of the fit is 0.082 mm. For the weighted case the best fit is

$$f_{wtd} = 4800.014(\pm 0.061)+1.229(\pm 0.091)\sin(\text{elevation}), \qquad (2)$$

with an r.m.s. of 0.081 mm. The total focal length excursion between elevations 5° and 90° is 1-sin5°≈ 0.913 times the coefficient of the sin(elevation) term, or 1.05 mm and 1.12 mm, respectively, for the two fits.

Figure 2.3.2 shows scatterplots of BFP focal length vs. air temperature T_{air}, and vs. mean BUS temperature T_{BUS}, for all the Vertex runs at 90° elevation (two from Night 1, and eight from Night 3). The BFP focal lengths clearly are strongly correlated with temperature. For the unweighted case, we calculate a correlation coefficient of ρ=0.982±0.014 for *f* vs. T_{air}; and ρ=0.967±0.029 for *f* vs. T_{BUS}. For the illumination-taper

weighted BFP calculation, we find correlation coefficients of ρ=0.982±0.013 for *f* vs. T_{air}, and ρ=0.974±0.023 for *f* vs. T_{BUS}. For the error estimates on the correlation coefficients we used the so-called "jackknife" method of von Mises, Quenouille, and Tukey; we also included the jackknife correction for bias (See Bradley Efron, *The Jackknife, the Bootstrap, and Other Resampling Plans*, CBMS—NSF Regional Conf. Ser. Appl. Math. 38, SIAM, Philadelphia, 1982.).

Now, if we fit all of the Jan. 2005 Vertex data for both a sin(elevation) dependence and a linear dependence on temperature we find —first in the unweighted BFP case vs. air temperature— the result

$$f_{unwtd} = 4800.462(\pm 0.031) + 0.028(\pm 0.002)T_{air} + 1.011(\pm 0.038)\sin(\text{elevation}); \qquad (3)$$

the r.m.s. residual of the fit is 0.042 mm. Including the temperature dependence clearly reduces a lot of the excess variance that was seen in the fit that included only a sin(elevation) term. For the weighted BFP case we get

$$f_{wtd} = 4800.200(\pm 0.032) + 0.028(\pm 0.002)T_{air} + 1.103(\pm 0.038)\sin(\text{elevation}), \qquad (4)$$

and an r.m.s. residual of 0.043 mm. The total focal length excursions between 5° and 90° are 0.923 mm and 1.007 mm, respectively, for these two fits.

For the regression on T_{BUS} and sin(elevation), we get

$$f_{unwtd} = 4800.330(\pm 0.031) + 0030(\pm 0.002)T_{BUS} + 1.008(\pm 0.043)\sin(\text{elevation}), \qquad (5)$$

an r.m.s. of 0.048 mm; and

$$f_{wtd} = 4800.068(\pm 0.028) + 0.030(\pm 0.002)T_{BUS} + 1.097(\pm 0.039)\sin(\text{elevation}), \qquad (6)$$

with an r.m.s. residual of 0.043 mm.

The coefficient of temperature dependence is comparable to that seen for the change in the best focus position seen in the AEG radiometric measurements of the whole system, which indicates that the change in focal length of the dish is the dominant effect (rather than changes in the apex structure).

For the AEC antenna, Figure 2.3.3 shows the focal length vs. elevation curves for the runs from Night 2. For the unweighted BFP case the best-fit curve is

$$f_{unwtd} = 4799.898(\pm 0.051) + 0.245(\pm 0.072)\sin(\text{elevation}), \qquad (7)$$

with an r.m.s. residual of 0.070 mm; and for the weighted BFP case we calculate

$$f_{wtd} = 4799.735(\pm 0.049) + 0.302(\pm 0.069)\sin(\text{elevation}), \qquad (8)$$

and an r.m.s. of 0.067 mm.

Figure 2.3.4 shows, for the AEC antenna, scatterplots of BFP focal length vs. air temperature for all the runs at 90° elevation (three from Night 2, and eight from Night 3). There is no strong correlation with temperature. For the unweighted case, we calculate a correlation coefficient of $\rho = 0.172 \pm 0.306$ for f vs.T_{air}. For the illumination-taper weighted BFP calculation, we find $\rho = -0.034 \pm 0.295$ for f vs.T_{air}. We have not done correlations against time-lagged air temperature, nor against BUS temperature measurements.

It appears that there is no need to repeat, for the AEC prototype antenna, the same regressions vs. temperature as were done for the Vertex prototype.

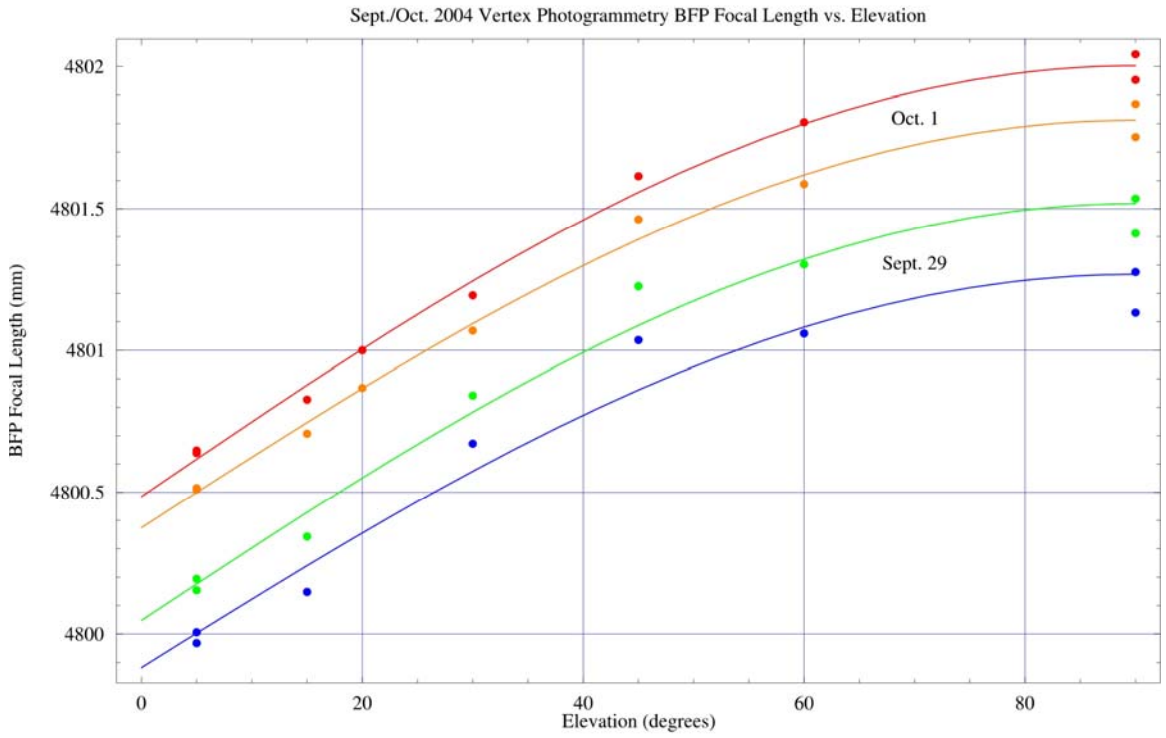

Figure 2.3.5. This figure shows the BFP focal length vs. elevation curves for the Sept./Oct. 2004 Vertex photogrammetry runs, together with the best-fitting sin(elevation) regression curves. The data from Sept. 29 (Runs 1 and 2 combined) are shown in Green and Blue; those from Oct. 1 (Runs 3 and 4) in Red and Orange. The Red and Green curves represent the unweighted BFP focal lengths; Orange and Blue the illumination-taper weighted fits.

2.3.3 Sept./Oct. 2004 Vertex photogrammetry data.

According to the chronology provided by Victor Gasho, "prior to the measurements taken on Sept. 29, all sunshades were removed from the Vertex prototype antenna, in order to inspect and re-torque all of the 480 BUS connection bolts. A total of three bolts were found to be completely loose, two between sectors 13 and 14.... It was determined that the structure was not behaving properly. [Apparently this means that an excess focal length excursion was observed over the 5°–90° elevation range.] New targets were then installed." Then, upon inspection of the BUS to Invar cone interface, it was determined that the turnbuckle bolts were tightened to 30% (or one-half?) of the proper specification, and that twelve hub bolts were loose. The bolts and turnbuckles were then re-torqued to proper specification before the photogrammetry runs of the evening of Oct. 1. The photogrammetry targeting pattern was the same as for the Nov. 2002 runs: five targets per panel, one adjacent to each one of the panel adjustment points, for a total of 1320 targets.

Table A3 gives a summary of the BFP focal length fits to the data of Sept. 29 and Oct. 1. For these we have approximate times of most of the measurements on Oct. 1, but none for Sept. 29. No valid air temperature measurements from the ATF weather station exist for these dates. There apparently are no BUS temperature data for these dates, either. There are, however, VLA weather station temperature data. The so-called "Run 1" and "Run 3" measurements, at 5° and 90° elevation were taken just after sunset on Sept. 29 and Oct. 1. "Run 2" and "Run 4" refer to the sequence of observations (at 5°, 90°, then 15°,…, 60°) later on in each of the two evenings.

Figure 2.3.5 shows the BFP focal length vs. elevation curves for the Sept./Oct. 2004 Vertex photogrammetry runs. For Sept. 29, Runs 1 and 2 combined, the best-fit regression curve to the unweighted BFP focal lengths is

$$f_{\text{unwtd}} = 4800.048(\pm 0.055) + 1.470(\pm 0.082)\sin(\text{elevation}), \qquad (9)$$

with an r.m.s. of 0.073 mm. For the weighted case the best fit is

$$f_{\text{wtd}} = 4799.882(\pm 0.070) + 1.385(\pm 0.105)\sin(\text{elevation}), \qquad (10)$$

with an r.m.s. of 0.093 mm. The total focal length variations between elevations 5° and 90°, for these two cases, are 1.342 mm and 1.264 mm, respectively.

For Oct.1, Runs 3 and 4 combined, the best-fit regression curve to the unweighted BFP focal lengths is

$$f_{\text{unwtd}} = 4800.485(\pm 0.027) + 1.518(\pm 0.043)\sin(\text{elevation}), \qquad (11)$$

with an r.m.s. of 0.039 mm. For the weighted case the best fit is

$$f_{wtd} = 4800.374(\pm 0.029) + 1.438(\pm 0.045)\sin(\text{elevation}), \qquad (12)$$

with an r.m.s. of 0.041 mm. Here the total focal length variations between elevations 5° and 90° are 1.386 mm and 1.313 mm, respectively.

Figure 2.3.6. This is a plot of the measured air temperature at the VLA weather station beginning in the evening hours of Sept. 29 and Oct.1, 2004. (No ATF weather station temperatures were recorded on these dates, nor were there Vertex antenna BUS temperature measurements taken on those two nights.) Note that 18:00 local time (MDT) Sept. 29 and Oct. 1 corresponds to 0^h Universal Time Sept. 30 and Oct. 2, respectively, and to 0^h UT on the modified Julian calendar dates (MJADs) of 53278 and 53280. (Data in the VLA monitor system database are time-tagged by MJAD; recall that JD=MJAD+2400000.5.) The black dots show the temperatures at the midpoints of the periods of each of the Oct. 1 measurements. We do not know the times at which the Sept. 29 runs were taken.

Plots of the measured air temperatures at the VLA weather station are shown in Figure 2.3.6, for the evenings of Sept. 29 and Oct. 1. Now, compare with Figure 2.3.5: The evening temperature on Sept. 29 is relatively more constant than that of Oct.1, and the

Oct.1 evening temperatures are consistently higher. The Oct.1 BFP focal lengths are greater than those of Sept. 29, but the temperature difference is not enough (assuming a 30-34 μm coefficient of thermal variation, as seen in the Jan. 2005 photogrammetry data and in the radiometric data mentioned previously) to explain the offset between the curves of Oct.1 with respect to those of Sept. 29. So it would seem that the offset must be due to the additional bolt re-torquing that was done between these photogrammetry sessions.

Another thing to note in Figure 2.3.5, and in the fits Eqs. (9)–(10) and (11)–(12), is that the best-fit sin(elevation) regression curves for Oct.1 are closer together than those for Sept. 29, suggesting that the bolt tightening efforts did make a change in the shape of the dish (see section 2.4.5 below). Thus, these data suggest a better-behaved surface after the further bolt tightening that was done in between the two photogrammetry sessions.

We have one final, more puzzling result: if, for the Oct. 1 data, we regress on both sin(elevation) and temperature, we see nothing similar to the fits to the Jan. 2005 data. Fitting to the unweighted BFP focal lengths we find

$$f_{\mathrm{unwtd}} = 4800.358(\pm 0.098) + 1.525(\pm 0.041)\sin(\mathrm{elevation}) + 0.011(\pm 0.008)\, T_{\mathrm{air,VLA}}, \qquad (13)$$

with an r.m.s. residual of 0.035 mm. For the weighted BFP case

$$f_{\mathrm{wtd}} = 4800.259(\pm 0.107) + 1.444(\pm 0.044)\sin(\mathrm{elevation}) + 0.010(\pm 0.009)\, T_{\mathrm{air,VLA}}, \qquad (14)$$

with an r.m.s. of 0.042 mm. (One might wonder why the r.m.s. residual is slightly larger for Eq. (14) than for Eq. (12), when an additional parameter has been added to the model. The explanation is that, in calculating the r.m.s.'s quoted here we always have divided the sum of squared residuals by $n–p$, rather than n, where n is the number of data points, and p is the number of parameters. The square root of this quantity is the unbiased estimate of the population r.m.s. about the regression line - the sample r.m.s. is biased low). The best-fit coefficient of thermal variation is about one-third the value seen in the Jan. 2005 data, and the Oct.1 data are not significantly better modeled when the thermal variation term is included. (The calculated "*P*-value" for the fitted coefficient is ~0.3. This means, according to the standard normal distribution theory, that the probability that this parameter is irrelevant in modeling the data is high. In contrast, for the Jan. 2005 data the calculated *P*-value was of order 10^{-8}, as for the sin(elevation) term, meaning that both terms were very significant.) It is not a matter of having an insufficient number of data points to determine the temperature dependence, for if we fit to just the Night 1 Jan. 2005 data (only 8 points) we get essentially the same fit as in Eqs. 3 and 4 (and a tiny *P*-value).

We should remark, again, that the HVAC thermal controls for the receiver cabin walls were off during the Sept./Oct. runs.

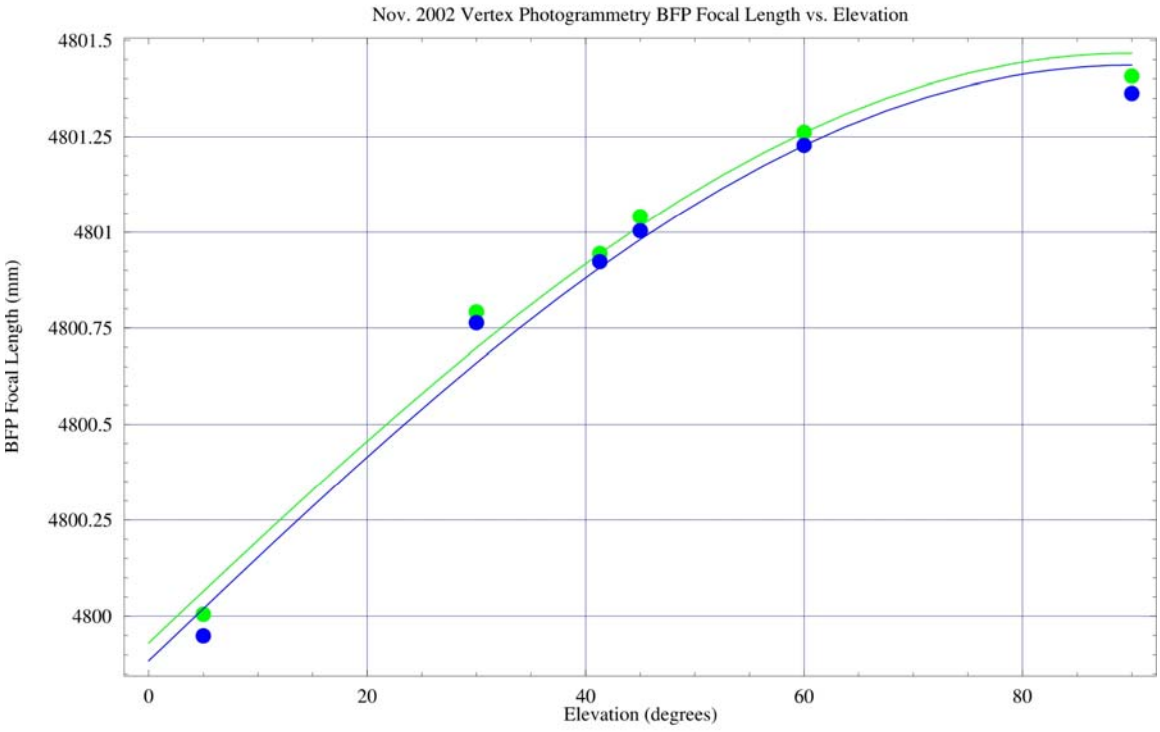

Figure 2.3.7. This figure shows the BFP focal length vs. elevation curves for the Nov. 2002 Vertex photogrammetry runs, together with the best-fitting sin(elevation) regression curves. The results for the illumination-taper weighted fits are shown in Blue; the unweighted fits, in Green. Note the near coincidence of the two curves, and compare with Figs. 2.3.1, 2.3.3, and 2.3.5. The larger separation of the curves seen in the previous figures evidently is primarily attributable to the spherical aberration that was built in when holographic measurements without the proper near-field correction were used for panel setting.

2.3.4 4. Nov. 2002 Vertex photogrammetry data

Here, a 1.4 mm variation in focal length (between 5° and 90° elevations) was observed and reported by VA, who claimed that the large variation must be due to poor-quality photogrammetry data. They argued that, intrinsically, focal length is poorly determined by photogrammetric measurements. They cited, in support of this argument, the fact that the fit at 45° elevation had a significantly higher r.m.s. than the measurement at the nearby 41.3° rigging angle elevation. They argued that their measurement at 5° elevation had to be in error. This was the one measurement that showed a significant deviation from homologous behavior.

We suspect that their argument is incorrect. A few hours' difference in the time of measurements, together with large temperature changes, might explain the anomalies. We have never seen any time log information for this photogrammetry run, nor do we have BUS temperature measurements or air temperature. We do not know the order in which the runs occurred —nor the time of day— so we can make no knowledgeable assumption as to whether the environmental temperature was rising or falling during the sequence of observations. In our own experience we find, in general, that focal length estimates from photogrammetry are robust and quite insensitive to measurement error.

According to Victor Gasho's chronology, the HVAC thermal control system for the receiver cabin walls was operating during this run.

Summary results from our own fits to the Nov. 2002 data are shown in Table A4 and Figure 2.3.7. For the unweighted BFP case the best-fit curve is

$$f_{\text{unwtd}} = 4799.930(\pm 0.063) + 1.536(\pm 0.090)\sin(\text{elevation}), \qquad (15)$$

with an r.m.s. residual of 0.064 mm; and for the weighted BFP focal lengths we have

$$f_{\text{wtd}} = 4799.884(\pm 0.072) + 1.552(\pm 0.103)\sin(\text{elevation}), \qquad (16)$$

with an r.m.s. of 0.074 mm. (The total focal length excursion between elevations 5° and 90° is 1-sin 5° ≈ 0.913 times the coefficient of the sin(elevation) term —or 1.40 mm and 1.42 mm, respectively, for the two fits— so this is all in accord with VA's 1.4 mm.

The focal length constants for the two fits differ by only 0.046 mm, an amount which is smaller than the standard errors: see Figure 2.3.7. For the Jan. 2005 Vertex data the difference is much larger (0.258 mm, *cf.* Fig. 2.3.1); and likewise for the Jan. AEC data (0.163 mm, *cf.* Fig. 2.3.3). Zernike polynomial fits to the Nov. 2002 Vertex photogrammetry data show no dominant spherical aberration term. We believe that this explains the closer proximity of the focal length vs. elevation curves which is seen in Figure 2.3.7, as compared with Figures 2.3.1, 2.3.3, and 2.3.5. The November 2002 photogrammetry preceded any panel adjustments which were based on holography.

2.3.5 Conclusions

The Jan. 2005 data for the Vertex prototype antenna show a strong correlation with temperature. When the photogrammetrically derived focal lengths are fit to a model with a sin(elevation) dependence and a linear temperature dependence, the observed total variation in focal length is consistent, to within 10%, with the finite-element model prediction.

We remain puzzled, however, that the same temperature dependence is not seen in the Oct. 1, 2004, photogrammetry data. Here, in fact, there is no strong correlation with temperature. (Note, however, that only VLA weather station data were available; we have no ATF weather station or BUS sensor measurements.) The Sept./Oct. 2004 data do suggest that the bolt tightening that was performed between Sept. 29 and Oct. 1 made an improvement to the non-homologous behavior of the surface of the Vertex prototype. The bolt tightening did not however remove the excess gravitational coefficient in the focal length seen in these data, which remain discrepant with those taken in January 2005.

The Nov. 2002 Vertex photogrammetry data also show an excess total variation in focal length, in comparison with the FEM prediction. The Nov. 2002 weighted vs. unweighted BFP sin(elevation) curves nearly coincide (unlike the case for the Sept./Oct. 2004 and the Jan. 2005 data). This is probably due to the absence of any significant spherical aberration from holographic panel setting adjustments, with a near-field error.

The Jan. 2005 holography data on the AEC antenna show no surprises. The total variation in focal length is only about 0.25 mm, with a well-behaved sin(elevation) dependence. No strong temperature dependence was discovered. The weak temperature dependence that is seen (if one ignores two outliers) is consistent with that measured radiometrically (around 10μm per °C).

2.3.6 Appendix – Tables

Table A1. Vertex antenna BFP focal length summary data from the Jan. 2005 photogrammetry runs.

Run	Night	UT (hrs.)	elev.	$T_{\rm air}$ (C)	$\overline{T_{\rm BUS}}$ (C)	$f_{\rm unwtd}$ (mm)	$f_{\rm wtd}$ (mm)
VPG1-90	1	2.5	90°	2.58	5.44	4801.601 ± 0.014	4801.418 ± 0.014
VPG1-5	1	6.1	5°	−3.93	0.56	4800.408 ± 0.015	4800.147 ± 0.015
VPG2-90	1	6.6	90°	−4.34	0.15	4801.335 ± 0.014	4801.153 ± 0.013
VPG1-60	1	7.3	60°	−3.99	−0.14	4801.250 ± 0.014	4801.060 ± 0.013
VPG1-45	1	7.9	45°	−4.22	−0.30	4801.021 ± 0.014	4800.808 ± 0.013
VPG1-30	1	8.9	30°	−5.43	−0.88	4800.782 ± 0.014	4800.567 ± 0.013
VPG1-15	1	9.2	15°	−6.60	−1.18	4800.629 ± 0.014	4800.387 ± 0.014
VPG2-5	1	9.5	5°	−6.58	−1.47	4800.351 ± 0.015	4800.112 ± 0.014
VS1	3	0.2	90°	14.50	17.18	4801.891 ± 0.014	4801.709 ± 0.015
VS2	3	0.3	90°	14.04	17.02	4801.834 ± 0.014	4801.664 ± 0.014
VS3	3	2.1	90°	3.01	9.96	4801.599 ± 0.014	4801.441 ± 0.014
VS4	3	2.2	90°	3.01	9.53	4801.579 ± 0.013	4801.419 ± 0.013
VS5	3	5.1	90°	0.04	4.42	4801.419 ± 0.014	4801.265 ± 0.015
VS6	3	5.2	90°	0.04	4.35	4801.481 ± 0.015	4801.328 ± 0.015
VS7	3	5.6	90°	−0.94	4.04	4801.432 ± 0.014	4801.264 ± 0.014
VS8	3	5.7	90°	−1.27	3.93	4801.424 ± 0.014	4801.245 ± 0.014

Table A2. AEC antenna BFP focal length summary data from the Jan. 2005 photogrammetry runs.

Run	Night	UT (hrs.)	elev.	$T_{\rm air}$ (C)	$f_{\rm unwtd}$ (mm)	$f_{\rm wtd}$ (mm)
APG1-90	2	3.2	90°	1.72	4800.003 ± 0.013	4799.892 ± 0.014
APG1-5	2	3.9	5°	2.85	4799.890 ± 0.011	4799.730 ± 0.012
APG2-90	2	4.45	90°	0.51	4800.193 ± 0.014	4800.089 ± 0.015
APG1-60	2	5.1	60°	−4.05	4800.093 ± 0.013	4799.969 ± 0.014
APG1-45	2	6.55	45°	−2.97	4800.138 ± 0.012	4800.012 ± 0.013
APG1-30	2	7.55	30°	−4.88	4800.142 ± 0.015	4799.978 ± 0.015
APG1-15	2	8.15	15°	−6.38	4799.938 ± 0.012	4799.808 ± 0.013
APG2-5	2	8.75	5°	−4.77	4799.881 ± 0.012	4799.729 ± 0.013
APG3-90	2	8.85	90°	−4.56	4800.151 ± 0.013	4800.067 ± 0.013
AS1	3	1.15	90°	8.54	4800.072 ± 0.013	4799.937 ± 0.015
AS2	3	1.21	90°	7.87	4800.101 ± 0.013	4799.970 ± 0.015
AS3	3	2.35	90°	3.36	4799.996 ± 0.013	4799.896 ± 0.014
AS4	3	3.0	90°	3.61	4799.992 ± 0.012	4799.876 ± 0.013
AS5	3	6.32	90°	−3.82	4799.993 ± 0.012	4799.895 ± 0.013
AS6	3	6.42	90°	−3.82	4799.974 ± 0.012	4799.878 ± 0.013
AS7	3	6.6	90°	−3.2	4799.980 ± 0.012	4799.880 ± 0.013
AS8	3	6.8	90°	−3.25	4800.019 ± 0.012	4799.938 ± 0.013

Table A3. Vertex BFP focal length summary data from the Sept./Oct., 2004, photogrammetry runs.

Run	Date	UT (hrs.)	elev.	$T_{\rm air,VLA}$ (C)	$f_{\rm unwtd}$ (mm)	$f_{\rm wtd}$ (mm)
V-Run1-5	Sept. 29	—	5°	—	4800.154 ± 0.017	4799.968 ± 0.016
V-Run1-90	Sept. 29	—	90°	—	4801.536 ± 0.018	4801.275 ± 0.018
V-Run2-5	Sept. 29	—	5°	—	4800.194 ± 0.015	4800.006 ± 0.015
V-Run2-90	Sept. 29	—	90°	—	4801.412 ± 0.018	4801.132 ± 0.018
V-Run2-15	Sept. 29	—	15°	—	4800.343 ± 0.016	4800.148 ± 0.015
V-Run2-30	Sept. 29	—	30°	—	4800.841 ± 0.016	4800.672 ± 0.015
V-Run2-45	Sept. 29	—	45°	—	4801.225 ± 0.016	4801.036 ± 0.016
V-Run2-60	Sept. 29	—	60°	—	4801.302 ± 0.017	4801.059 ± 0.017
V-Run3-5	Oct. 1	0.88	5°	15.1	4800.639 ± 0.016	4800.510 ± 0.016
V-Run3-90	Oct. 1	1.21	90°	13.8	4802.043 ± 0.018	4801.869 ± 0.018
V-Run4-5	Oct. 1	1.92	5°	12.0	4800.648 ± 0.016	4800.515 ± 0.016
V-Run4-90	Oct. 1	2.50	90°	11.7	4801.953 ± 0.018	4801.753 ± 0.018
V-Run4-15	Oct. 1	3.28	15°	10.7	4800.827 ± 0.015	4800.707 ± 0.015
V-Run4-20	Oct. 1	3.68	20°	9.9	4801.000 ± 0.017	4800.868 ± 0.016
V-Run4-30	Oct. 1	3.97	30°	9.5	4801.193 ± 0.016	4801.069 ± 0.015
V-Run4-45	Oct. 1	4.67	45°	11.2	4801.615 ± 0.016	4801.462 ± 0.016
V-Run4-60	Oct. 1	∼5.0(?)	60°	9.9	4801.805 ± 0.019	4801.587 ± 0.019

Table A4. Vertex antenna BFP focal length data from the Nov. 2002 photogrammetry runs.

Run	UT (hrs.)	elev.	$T_{\rm air}$ (C)	$\overline{T_{\rm BUS}}$ (C)	$f_{\rm unwtd}$ (mm)	$f_{\rm wtd}$ (mm)
V5	—	5°	—	—	4800.005 ± 0.021	4799.949 ± 0.022
V30	—	30°	—	—	4800.792 ± 0.023	4800.764 ± 0.024
V41.3	—	41.3°	—	—	4800.944 ± 0.020	4800.923 ± 0.021
V45	—	45°	—	—	4801.041 ± 0.023	4801.004 ± 0.024
V60	—	60°	—	—	4801.262 ± 0.021	4801.228 ± 0.022
V90	—	90°	—	—	4801.407 ± 0.021	4801.363 ± 0.022

2.4 Photogrammetry (Hills/Schwab)

2.4.1 Introduction

Photogrammetry is a well-established technique for making accurate measurements of the shapes of large objects. The basis of the method is to make high-resolution images of the object from many different directions and then use geometry to reconstruct its three-dimensional form from these images. Determining the surface errors of antennas is one of the standard applications of photogrammetry. The fact that the measurement can be made at any orientation of the dish makes it especially valuable to us for studying gravitational deflections. Our requirements are, however, so demanding that we are pushing the accuracy of the technique to its limit.

The common practice, which was used here, is to attach retro-reflecting targets to the object and to use a ring flash around the lens of the camera to illuminate them. The cameras used have high-quality optics and extremely uniform CCD detectors, which makes it possible to locate the centroids of the images of the targets to about $1/50^{th}$ of a pixel. The CCD's have 2k square pixels, so the basic accuracy of each 2-D image is of order 1 part in 10^5. The accuracy of the reconstruction depends on the geometry and would generally be lower than this if only a minimum number of images were taken (say 3). By combining a large number of images (typically 40 to 100 in each of the measurement sets we are working with), one can however beat down the noise. The redundant information available with many images means that good internal estimates can be made of the uncertainty in the position of each target. In the data discussed here these estimated errors were usually in the range 15 to 25 microns for each coordinate, implying an impressive accuracy of better than 2 parts in 10^6. Various steps to reduce systematic errors, such as taking some shots with the camera rotated by 90 degrees about its optical axis, were also taken. As will be seen below, the analysis is generally consistent with the data being free of serious systematic errors and having random noise at about the level indicated by the internal estimates.

Systematic errors, due to things like the gradients in the air temperature inside the dish and the fact that slightly different sets of camera locations were used for measurements at different elevations, must start to come in at some level. It is not known what this level is, but it seems likely that non-random errors must be present at a level of at least a few microns over scales of several meters.

Note that the absolute size of the object and its location are not fixed directly from the images. In most of the data discussed here Invar bars, ~3 meters long, were attached to the antenna and used to establish the scale. It turns out that the errors in this scale determination are not entirely negligible, but this is only significant in the focal length measurements.

2.4.2 The Data

The VertexRSI antenna was measured on three separate occasions: in Nov 2002, in Sept/Oct 2004 and in Jan 2005. The AEC antenna was only measured in Jan 2005 because a different method (laser metrology) had been used to carry out the initial panel alignment. The measurements in 2002 and 2005 were carried out by Geodetic Services Inc., Melbourne, Florida, USA, and those in 2004 by GDV Ingenieurgesellschaft, Bad Schwartau, Germany, using very similar equipment and software.

In 2002 and 2004 the targets were placed near the adjustment points – typically 5 per panel, giving a total of 1320. In 2005 a more uniform distribution of targets was used, as shown in the pictures below, with 1080 targets – typically 4 per panel on the VertexRSI antenna and 9 per panel on the AEC antenna.

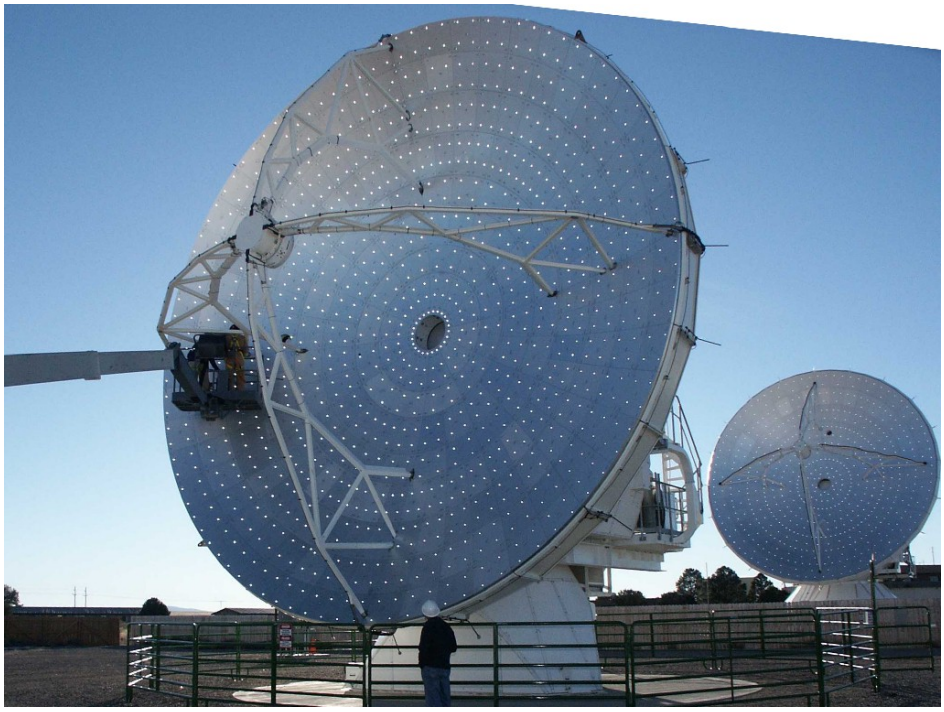

The retro-reflecting targets on the Vertex dish in Jan 2005. The targets are in 17 rings with from 24 to 96 targets per ring.

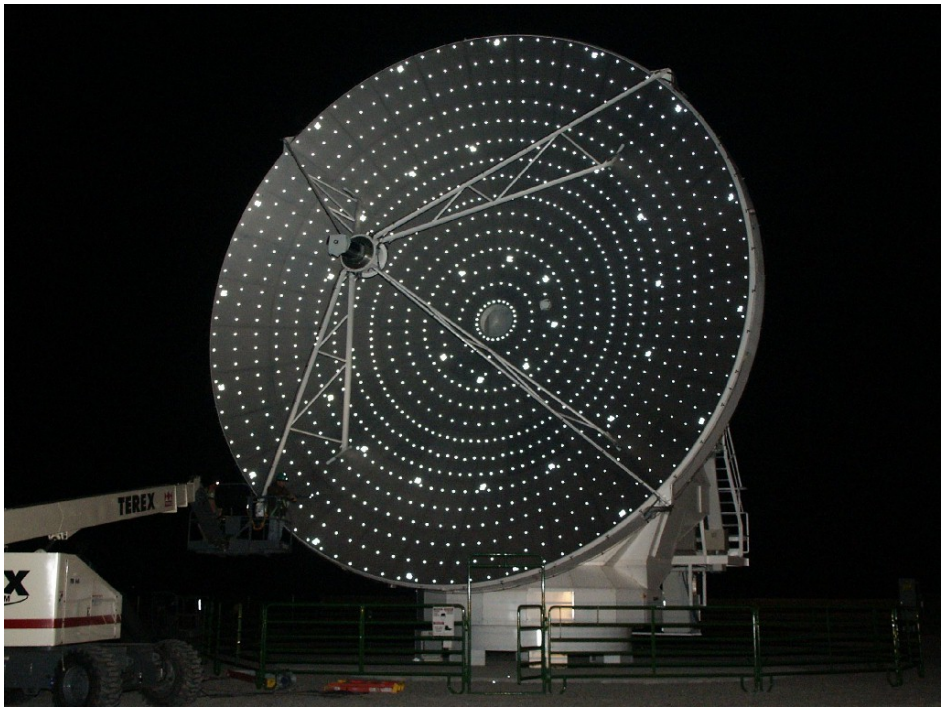

The pattern on the AEC antenna was very similar but with 15 rings of targets instead of 17. The "coded" targets used to find the approximate camera positions are in place here.

The measurements were made at night, to give better contrast and to reduce thermal effects. In most cases the measurements started shortly after sunset. In retrospect it might have been better (but even more arduous for the staff involved) to have started the measurements after midnight when the temperatures were even more stable.

In 2002 a series of photogrammetric measurements of the VertexRSI antenna were made at a fixed elevation and used to adjust the dish. We have not reanalyzed those initial data sets, but we have re-examined the final set of measurements from that run, which include observations at 5, 30, 45, 60 and 90 degrees elevation. The more recent sets of measurements consist of two observations at each of 5 and 90 degrees elevation followed by observations at intermediate angles, e.g. 60, 45, 30, and 15 degrees. In 2004 there were two complete runs, one taken on 29th Sept, immediately after the three inter-sector bolts had been tightened, and one on 1st Oct, after all the other bolt tightening activities had been completed. Both these sets were taken without the rear covers on the BUS and with the thermal control not in its normal state. (Victor Gasho's note says it was turned off, whereas a recent message from Dr K. Pausch at VA says, "The HVAC system was partly in operation", but emphasizes that, "The telescope was thermally not fully stabilized, in particular during the measurements shortly after sunset.")

In January 2005 a full set of measurements of the VertexRSI antenna was taken on the night of 17/18th and a similar set on the AEC antenna on the 18/19th. It was clear from the initial analyses of these data that significant thermal deformations were taking place and that these might be obscuring the true gravitational deflections. Further data sets on both antennas were therefore taken on the 19/20th on both antennas to study their thermal stability. For this the antennas were left pointed to the zenith and measured repeatedly over a period of several hours while the temperature was monitored.

2.4.3 Data Processing

The results described here were all produced using Excel spreadsheets. These take as input the lists of x, y and z coordinates of the targets produced by the photogrammetry software ("V-STARS"). The estimated errors are also read in but these are not used in the analysis except for deciding whether any points should be removed because they show unusually large errors.

The first step is to find the best-fitting paraboloid. We allow six parameters to vary: the x, y and z shifts of the vertex; rotations of the dish around the x and y axes; and the focal length. The quantity minimized is the weighted rms path-length error. The changes in the focal lengths are discussed in a separate section of this report. The analysis here concentrates on the residuals from these fits in the direction normal to the surface. It is worth noting that it may also be possible to derive useful insights from the deformations in the plane of the surface, which are also available from these photogrammetric measurements.

To a good approximation the changes in the best fit parameters can be taken out by a combination of pointing offsets and shifts in the position of the subreflector, but the residual errors, the non-homologous deformations, cannot be compensated in this way and it is these that are our main concern.

To visualize the form of the deformations we have plotted them in false color in a uniform manner, i.e. the color scale has been set to run from –100 to +100 microns and the coordinate frames have been rotated to be consistent with the ALMA convention (Y downwards and X to the left when looking into the dish). To make such a plot it is necessary to interpolate or smooth the data from the individual targets in some way. As a compromise between maintaining resolution and reducing the noise, all the plots shown here have been smoothed with a Gaussian of 0.6 metres full-width half-maximum. Since the typical spacing between data points is about 0.3 metres this has the effect of reducing random, noise which is uncorrelated between neighbouring points, by about a factor of 2. The quantity plotted is the normal surface error, but in calculating the weighted rms error (which is given in microns in the heading to each plot) only the boresight component of this error has been counted and this has been weighted with the amplitude illumination pattern for a 12dB edge taper, as allowed by the ALMA antenna specifications.

2.4.4 The VertexRSI measurements from November 2002

There are five data sets which were, we believe, all taken on the evening of 8th November 2002, at elevations of 5, 30, 45 60 and 90 degrees. We have no information about the times when the data were taken, the weather conditions or the thermal state of the antenna, although it is possible that such records exist. It is however possible to look for temperature changes in the data itself because the thermal expansion of the panels relative to the BUS can be seen as differential motions. These motions are quite small in these data, which suggests that the temperatures were reasonably stable.

The data was processed as described above, but in this case the target positions had already been adjusted to put them in the frame of the best-fitting paraboloid, so the only parameter that was found to vary significantly was the focal length. It is worth noting that internal evidence suggests that the 5 degree elevation set had been scaled in a way which produced a slightly smaller overall size for the dish than for the other sets, and that when the scales of all the data sets are adjusted so that the radii of the outer ring of targets match, the apparent change in focal length with elevation is somewhat reduced and the fit to a sin(elevation) function is improved.

The dish was only poorly adjusted at this time, so there is no useful information here on the actual shape of the surface. The changes in shape with elevation should however have been measured accurately – the irregularity of the surface has no effect on the ability of the photogrammetry technique to measure changes in shape. These have been assessed in two ways. The "Diff 90 – 5" plot on the left below shows simply the differences between the normal residuals in the 90 and 5 degree maps. The right hand

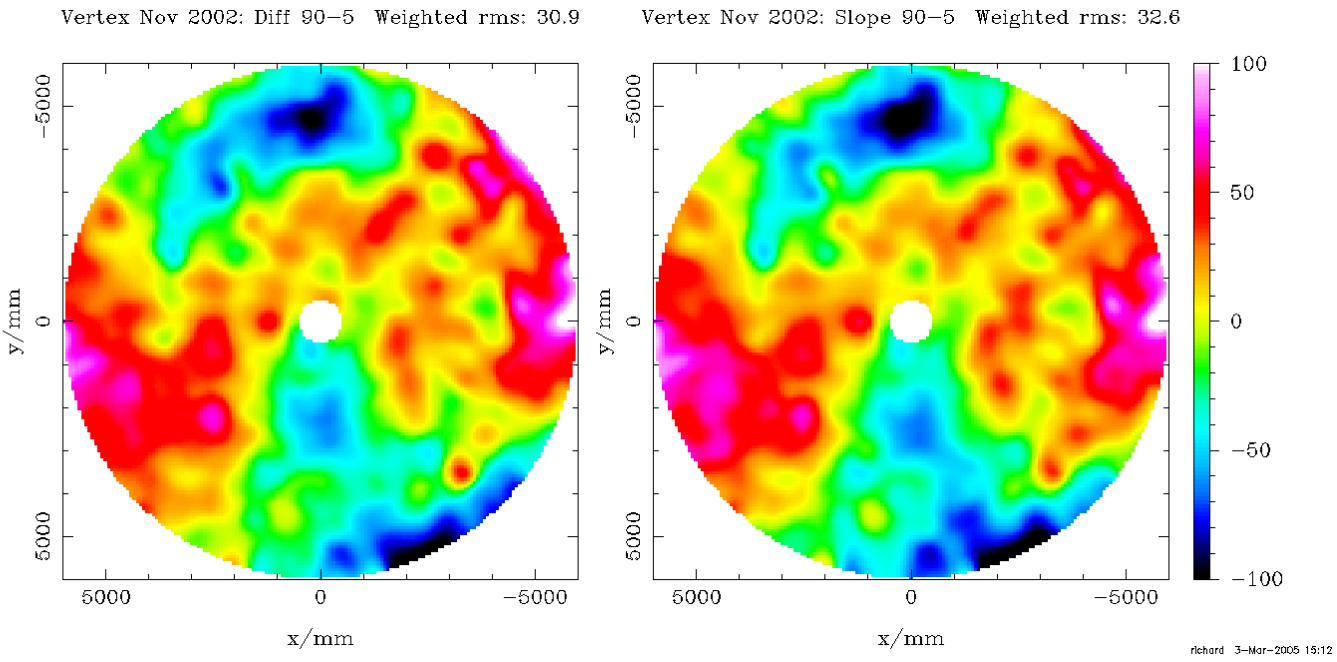

plot, “Slope 90 – 5”, includes data from all the sets at intermediate angles. Here a fit has been made to residual for each of the targets as a function of elevation and the slope of this fit, normalized to the interval 90 to 5 degrees is displayed. A minor point here is that one does not know whether the dish shape is varying as a function of sine or cosine of elevation or a combination of the two. All three were tried but this was found to make little difference. In the plot here the fitted function was sin(Elevation-45 degrees).

Clearly these two ways of treating the data give very similar results, but it should be appreciated that the plots are not at all independent because the 90 and 5 degree data sets are also used in the fitting of the “slopes”, and indeed they get the strongest weighting.

The apparent deviations from homology are quite large (~30 microns rms even taking into account the weighting) although some of this must be due to noise in the measurements. The large coherent structures cannot however been interpreted as noise and in particular a substantial amount of astigmatism is evident. The amplitude of the measured astigmatism at the edge of the dish is ~ +/–100 microns. The fact that significant non-homologous deformations appeared to be present in these data was one of the causes for concern when we first analyzed them in November 2004. The more recent investigations have not found any reason to discount these measurements. Indeed, as discussed below, the recent work has generally confirmed that photogrammetry does provide remarkably accurate results.

In addition to the photogrammetry data, we also have the predicted gravitational deformations of the antenna as calculated by finite element modeling. The FEA output available to us is identified as “model: alma10, state 12.04.02”. The figures below show the predicted deformations and the residual found by subtracting the FEA prediction from apparent deformation (the “difference” above) seen in the photogrammetry results.

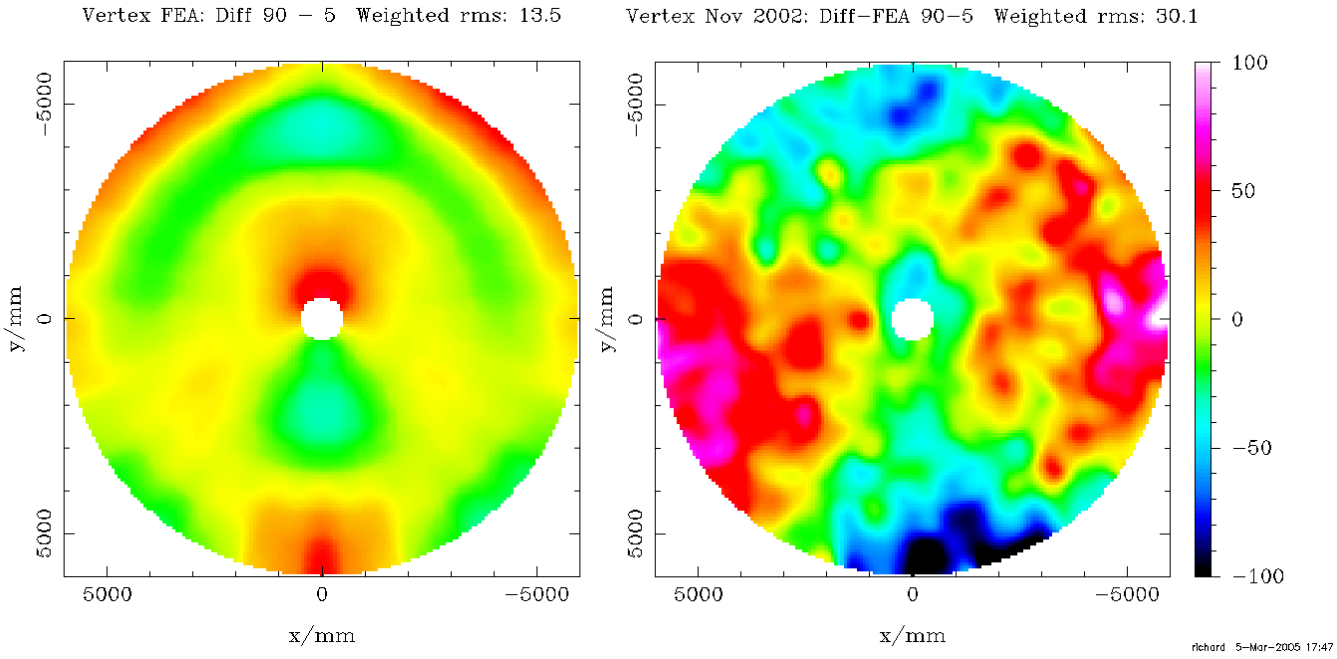

It can be seen that only a few of the apparent deformations in the photogrammetry data correspond to features in the FEA predictions. In particular the astigmatic deformation is still present.

2.4.5 The VertexRSI measurements from Sept/Oct 2004

During 2003 the antenna surface was adjusted using holography to an accuracy which was believed to be better than 20 microns rms. This was done at an elevation of about 8 degrees. It was therefore expected that the photogrammetry data taken in September 2004 would show a relatively good surface accuracy, especially at low elevation. The first point to be looked at in this data is therefore the actual shape of the surface. Shown below are maps taken at 90 and 5 degrees elevation on 29th Sept.

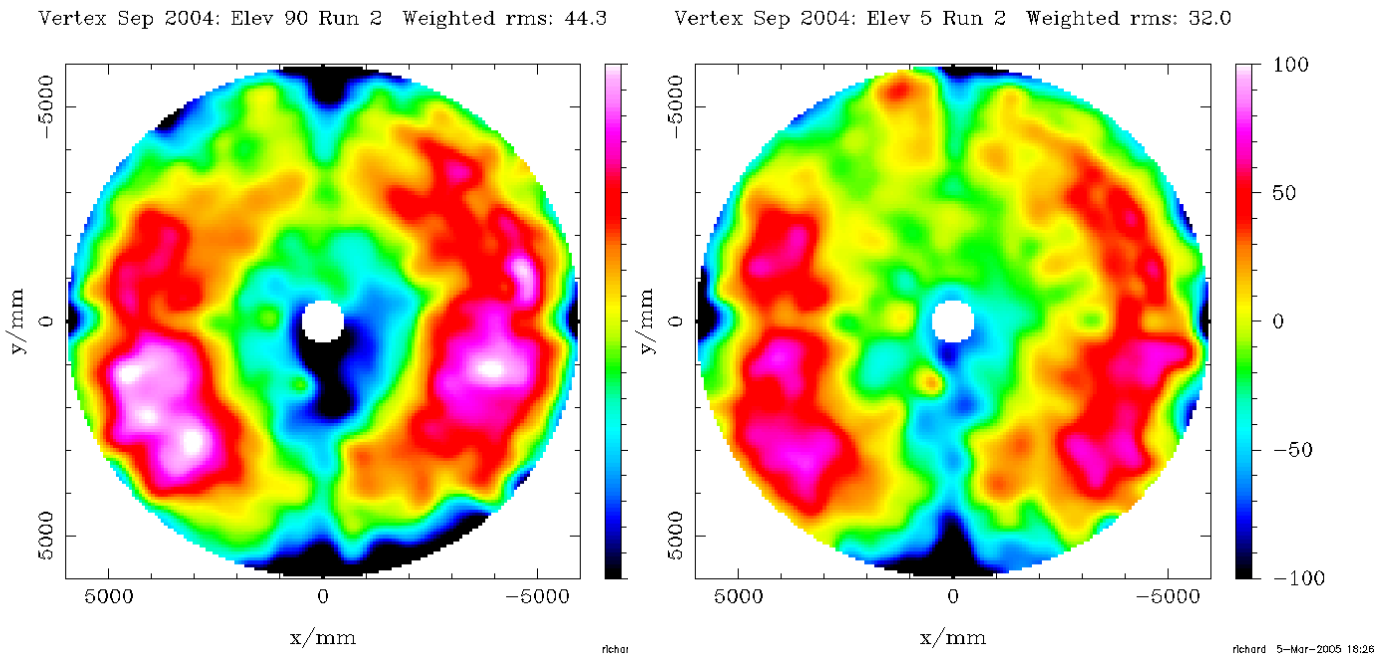

(The two other maps taken earlier in the same evening were thought to be of less good quality because the temperature conditions were less stable, but they are in fact very similar.)

These data clear show that the dish surface was well out of specification at this time. As explained in the holography section of this report there was in fact a systematic error present in the setting of the antenna which produced a circularly symmetric deviation in the surface from that intended.

In the next two plots we show the form of this error and the average of the 5 degree elevation photogrammetry maps with a correction applied.

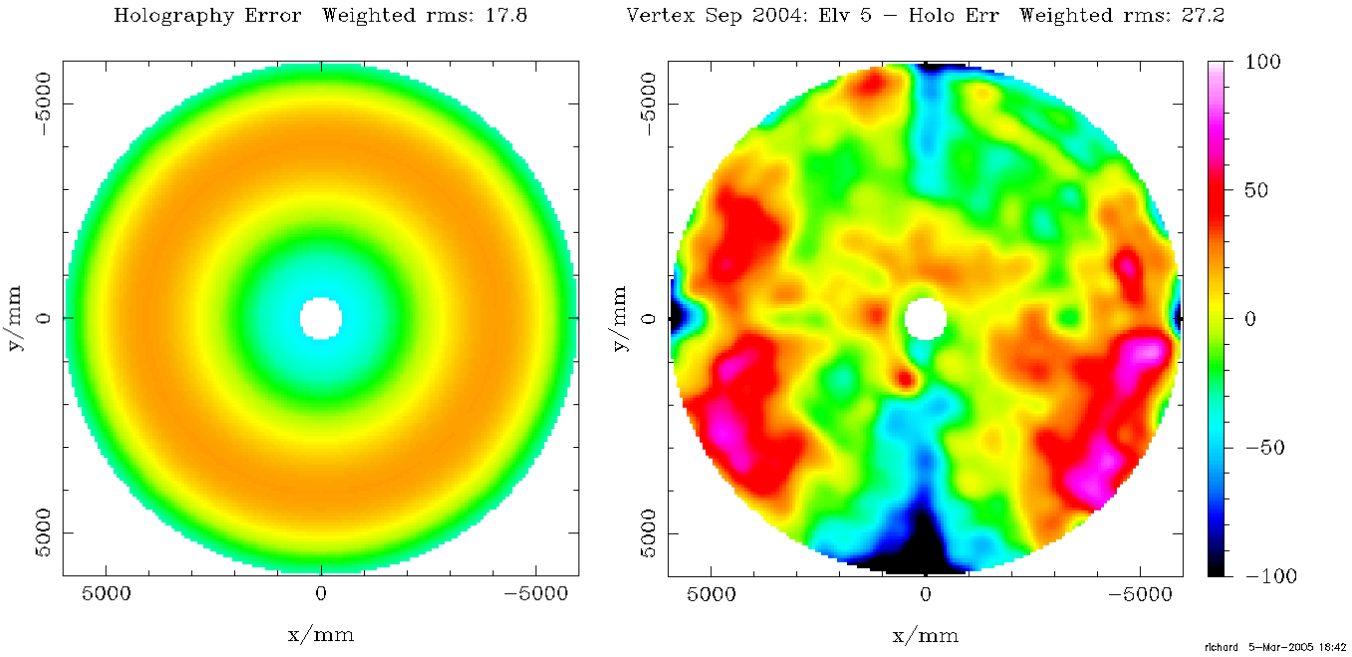

It is clear that some of the error in the shape of the dish that was present at that time was due to the problem with the holography, but not all of it by any means. The presence of this distortion was confirmed by holography measurements made in January 2005 and the possible causes are discussed elsewhere in this report.

The next question to look is whether the tightening of the bolts that was carried out between Sept 29th and Oct 1st caused any changes in the surface. Here are maps of the apparent change in shape between these two dates.

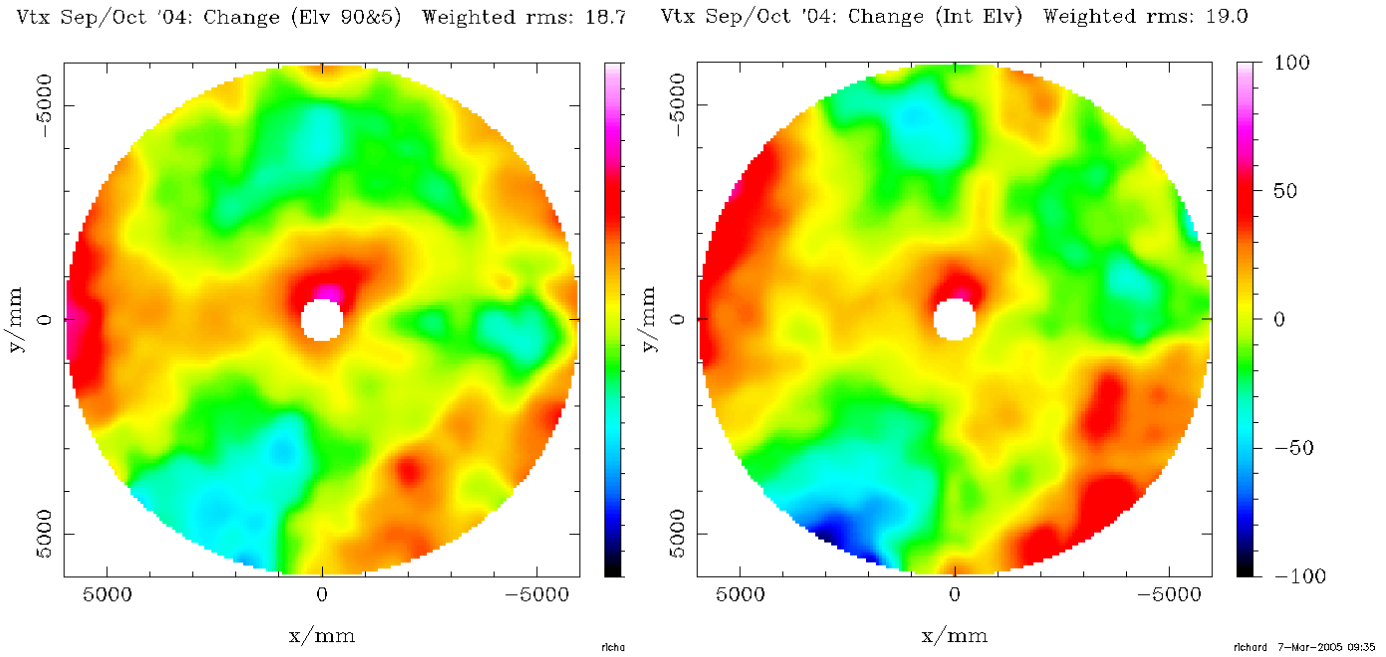

To do this we have taken the differences between the data sets taken on the two days and averaged the differences together to increase the signal to noise ratio. On the left are all the data at 5 and 90 degrees and on the right all the data at intermediate elevations. This is an arbitrary division of the data just to give two separate estimates of the change in shape of the dish between these dates.

Given that these are independent data sets, the fact that we see a consistent pattern means that we are detecting a real change in shape here, although the changes detected are near the limit of what can be seen with this technique. Note that there was also a significant change in the focal length of the dish between these dates. These changes in the shape of the surface are probably a result of the tightening of various sets of bolt in the BUS which was carried out by the manufacturer between these dates.

Turning now to the non-homologous changes in shape with elevation, here are the differences between 90 and 5 degrees elevation, averaging two data sets in each case.

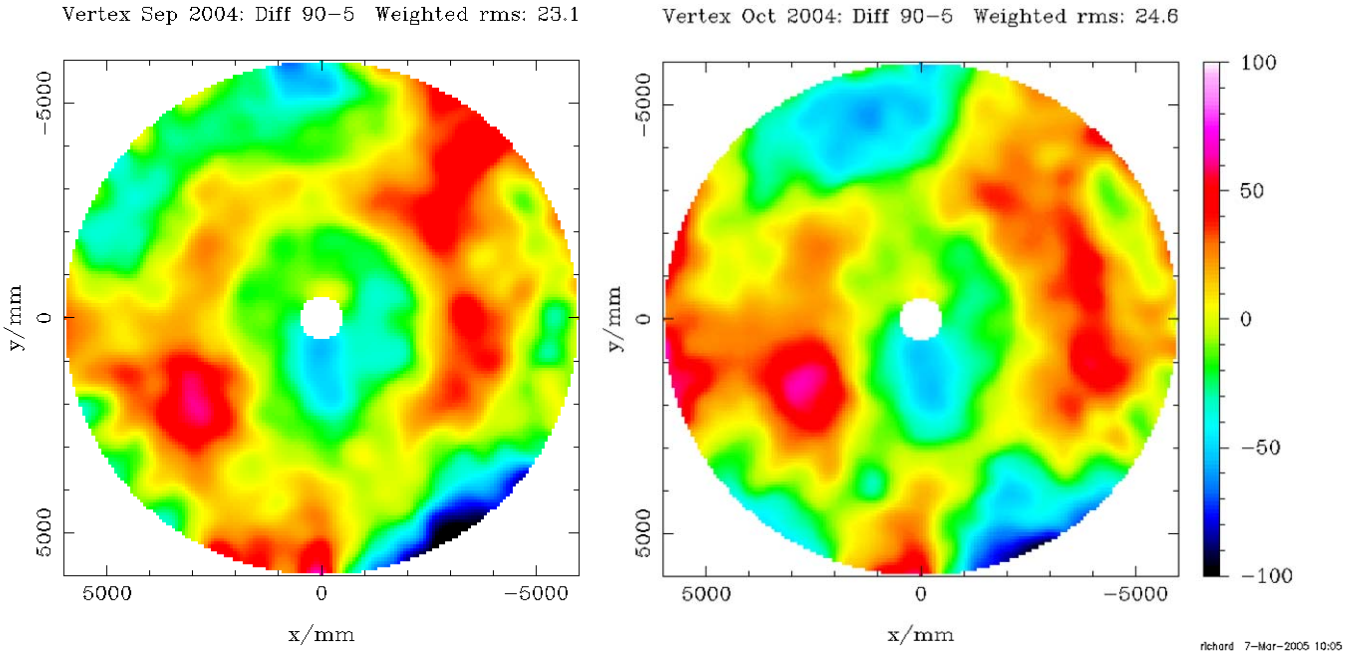

In this case (remembering that the errors in these plots due to noise are expected to be at a level of ~14 microns rms) there is no obvious difference in the behaviour between the two dates. Comparing back to the equivalent plots from November 2002, however, it does appear both that the magnitude of the non-homologous deformations is smaller and that most of the astigmatic term has gone.

Taking the data at face value, this seems to imply that the adjustments that were made to the BUS before the photogrammetry measurement on Sept 29th 2004 had the effect of correcting whatever was causing the astigmatic deformation as a function of elevation, while those made between the 29th Sep and 1st Oct had little effect on the stiffness of the structure, although they did cause some change in its static shape.

2.4.6 Measurements of January 2005 (1) - Thermal

As already noted, it became apparent in the course of these measurements that thermal effects were important and a whole evening (Jan 19/20th) was devoted to studying them. We start by looking at that data since we can use it to establish the reliability of the measurements. There are eight data sets for each antenna, taken in pairs at the fixed elevation of 90 degrees, over the period from ~0:30 to 07:00 UT (17:30 to midnight local time). The next figure shows the temperature record during this period, along with an indication of the times at which the data sets were taken.

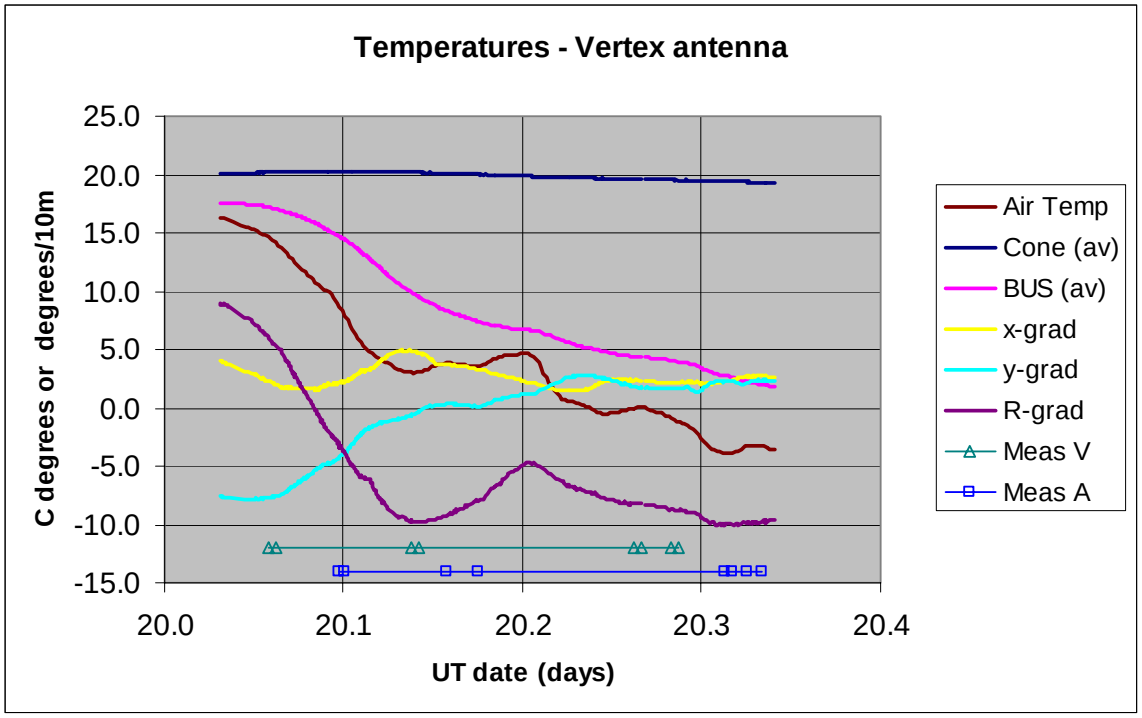

It can be seen that the air temperature was falling fast, especially in the early part of the evening, and that the mean BUS temperature follows it with a lag of 1 to 2 hours. There are 24 sensors in the structure, arranged in 4 rings, typically 0.3m behind the front surface of the dish. Linear temperature gradients have been fitted to the readings from these sensors and are shown here in units of degrees per 10 meters, i.e. there was ~10 C from top to bottom (y-axis is downwards) at the start of these experiments. We have temperature monitoring data from the AEC antenna but not from inside the BUS. It is likely that at least the mean temperature inside the BUS of the AEC antenna would have followed a similar track to that of the Vertex antenna.

Although this was not seen as one of the original goals of these measurements, we can clearly use the photogrammetry data to set limits on the amount of non-homologous

thermal deformations. For example, to look at the period when the temperature was changing most rapidly, we can take the average of the first pair of measurements and subtract the average of the second pair. The maps of these differences look like this:

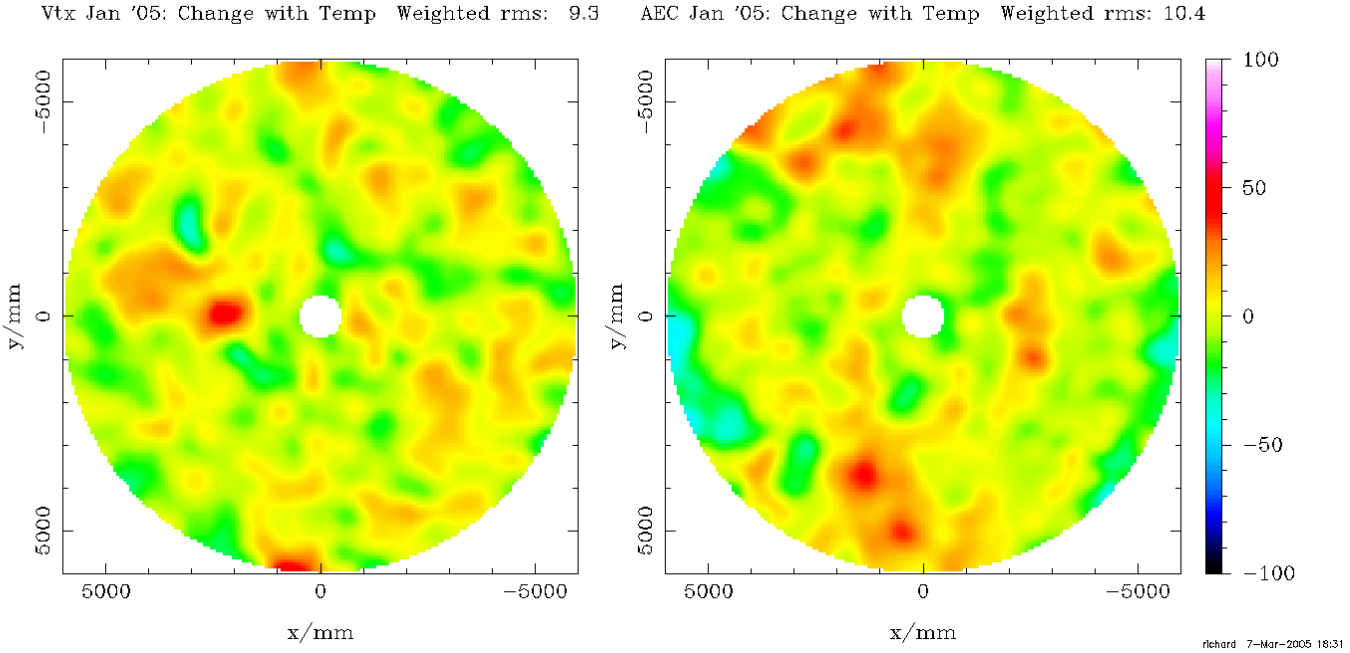

In fact these differences are at most only slightly above the noise in the data. To see this we can reverse the signs of the residuals on the second data sets in each pair and repeat the exercise. The resulting images are then:

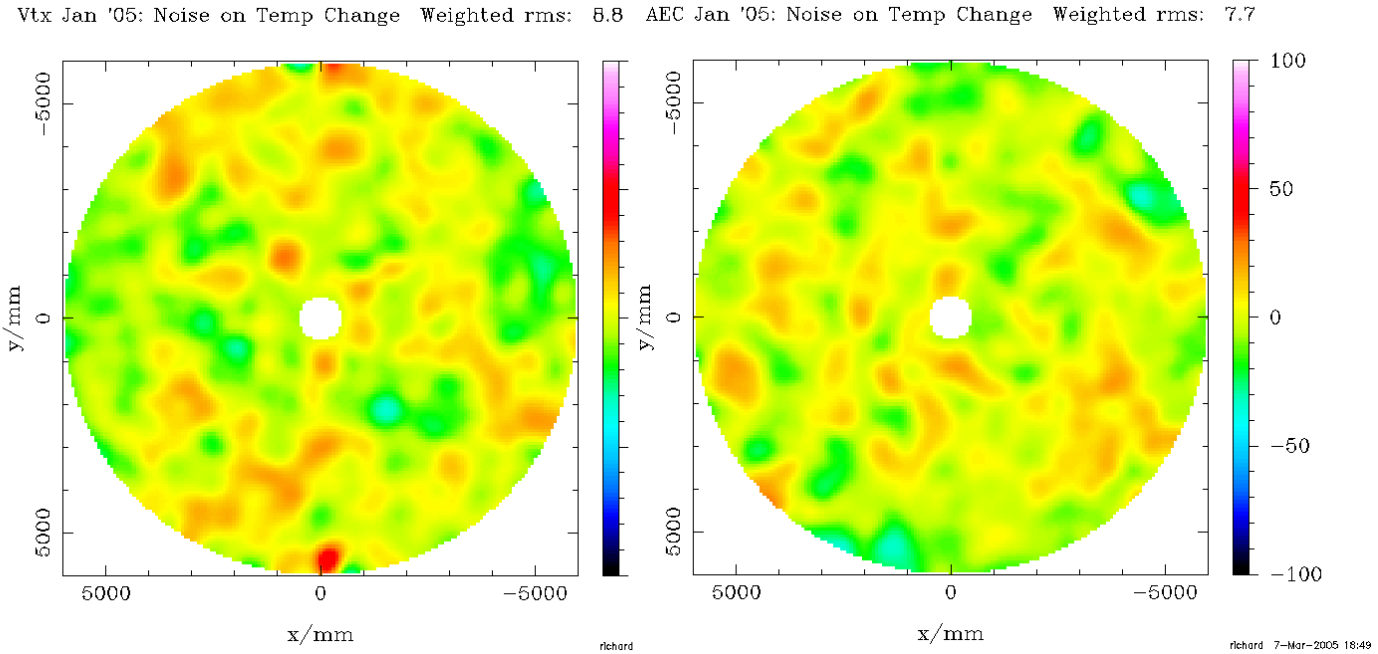

It is seen that the differences in these plots are at a similar level, even though any correlation with temperature changes should have been destroyed. Formally one could do a quadratic subtraction of the rms figures shown above which gives values of 3 and 7 microns for the "real" thermal changes in the Vertex and AEC data sets, but it is clear that this is below the level at which we can expect to rely on the photogrammetry data.

Some further numerical investigations of these data were undertaken which led to the following conclusions:

1. the derived noise levels on the normal displacements of the individual points are ~20 microns, which is consistent with the internal error estimates that are provided by GSI's software;
2. the noise goes down more or less as expected when two or more data sets are averaged together;
3. the noise also goes down when the individual points in a map are averaged together by area. (This has already been done to a small extent in the plots shown above.) The reduction in the rms is in fact rather smaller than would be expected for pure noise – presumably we are starting to see some systematic effects here;
4. upper limits on the non-homologous thermal deformations in both antennas can be set at about 10 microns in the weighted rms half-path error.

This limit is above the values in the surface error budgets for either ambient temperature effects or temperature gradients. Note also that we have not by any means covered the full range of operating conditions for which the antennas are specified – these measurements were all made at night. A more sensitive measurement of thermal deformations can be obtained from analysis of the holography data as a function of temperature and this is reported in section 2.8. The levels of deformation found there are consistent with the estimates above.

The main conclusions from this exercise are that the photogrammetry data from separate measurement sets is repeatable at the level indicated by the internal error estimates and that the non-homologous thermal errors are not large enough to confuse the measurement of the gravitational effects seriously.

The behaviour of the antennas as a function of elevation had been investigated on the two previous evenings, i.e. 17th and 18th Jan 2005. The plot below shows the run of temperature during this period. Note that all the structural temperatures refer to the Vertex antenna. The elevations of the antennas when they were measured are indicated in the lines "Meas V" and "Meas A" with 90 degrees just below the -10 C line and 5 degrees just above -15.

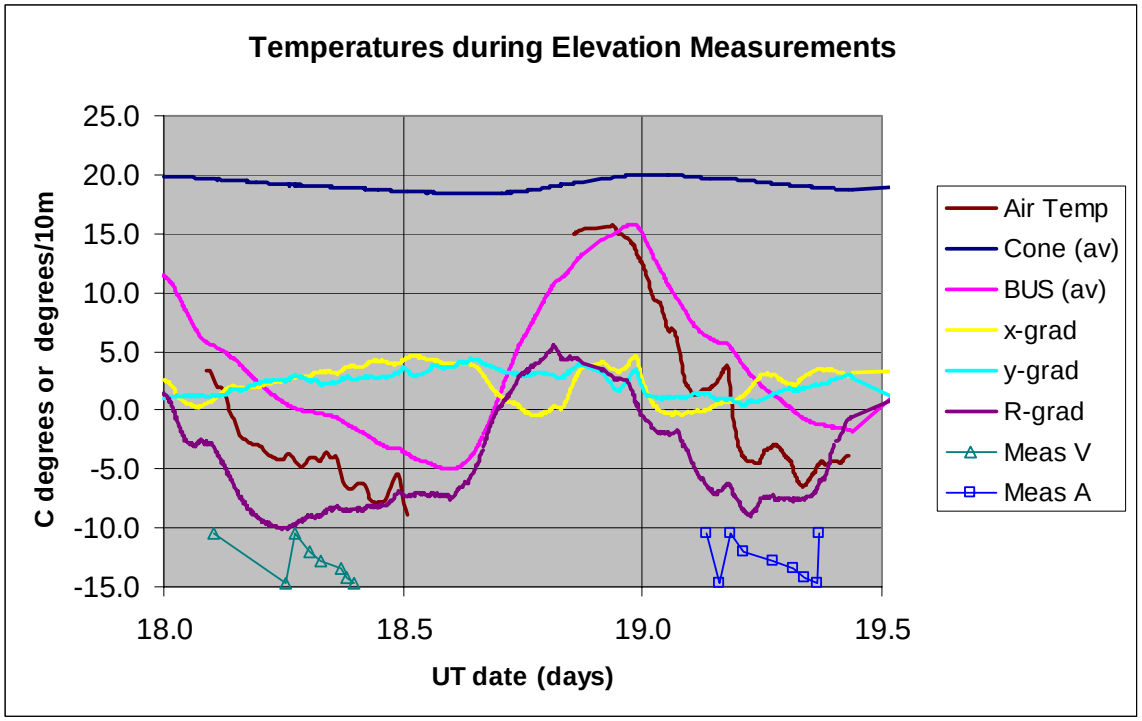

It can be seen that the run of temperatures was roughly the same on these nights as on the night when the stability tests were made. We can therefore be reasonably confident that thermal changes will not contribute more than about 10 microns to the weighted rms of any non-homologous deformations seen in that data.

2.4.7 Measurements of Jan. 2005 (2) - Gravitational Changes in Surface Shape

We now look at the data from the two nights where the changes with elevation were measured, by taking at least two sets of images at 5 and 90 degrees and one at each of the intermediate angles 60, 45, 30 and 15 degrees. As explained previously we can process this data in various ways. The simplest approach is to take the difference of the means of the two maps at 90 degrees and the two maps at 5 degrees. Doing this for the Jan 2005 data produces the following maps.

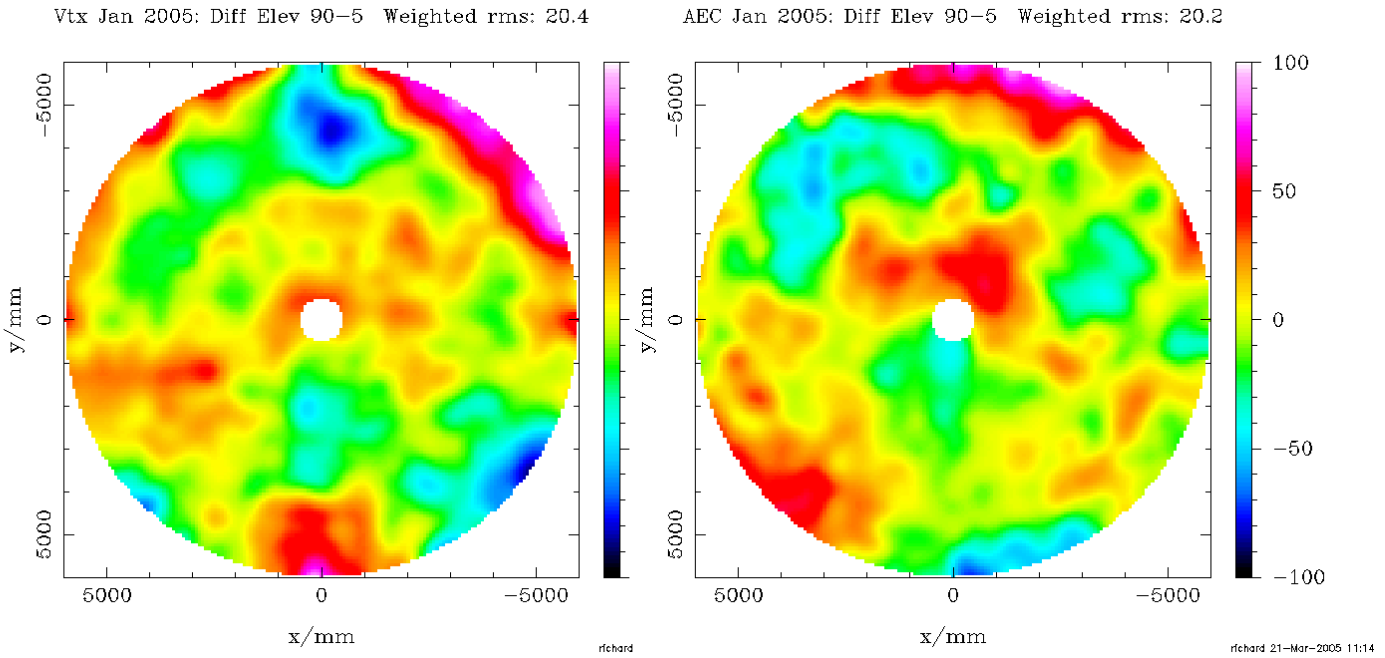

In both cases it is clear that we are measuring real effects. In particular we do see features which are predicted by the FEA models. Here are the two models:

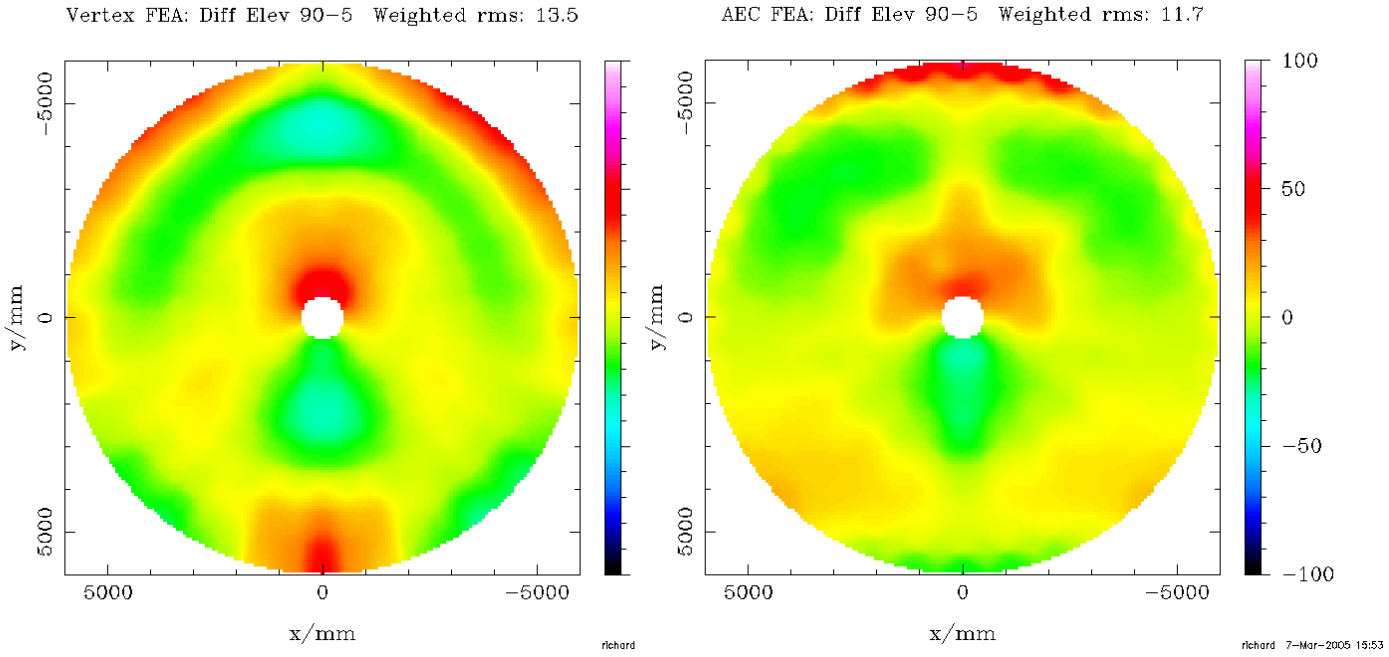

The Vertex one was already shown in the discussion of the Nov 2002 data and is just repeated here for convenience. The AEC data is from a recent run by Franz Koch using the model provided by the AEC.

Clearly there is a strong correlation between the observed pattern of deformations and that predicted by the FEA. In fact the correlation coefficient on the normal residuals is 0.79 for the Vertex case and 0.74 for the AEC. Alternative ways of analyzing the photogrammetry data, such as using all the data from intermediate elevations and fitting for the terms that varied with elevation in various ways, were also tried. These gave very similar results but if anything slightly lower correlations with the prediction, so they were not pursued.

It was found that simply subtracting the predicted deformations from the measurements left residuals that still showed traces of the predicted pattern. To minimize the residuals and remove this correlation required that the FEA predictions be scaled up by a factor of about 1.2 to 1.4 for both antennas. (The exact factor required depends on whether one minimizes the weighted or unweighted residuals[1].) The plots below show the residuals obtained using a scaling factor of 1.35 in both cases.

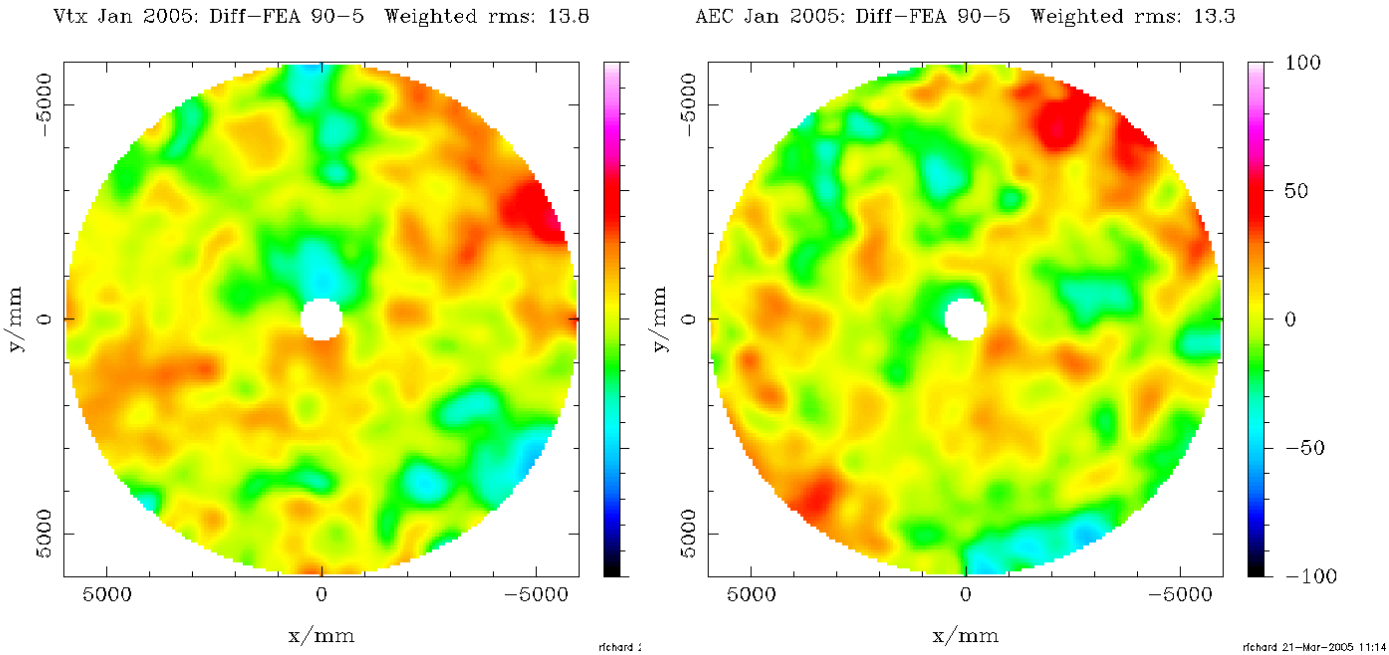

It is remarkable that the two plots are so similar in both the magnitude of the residuals and, to some extent, their form as well.

[1]This is telling us that the behaviour of the inner and outer parts of the dish is different. In fact on the Vertex antenna it appears that, if anything, the deformations in the inner part of the dish are less than predicted, but that in the outer part they are up to 50% larger. The behaviour of the AEC data suggests a more uniform behaviour with an excess of measured deformation over prediction of about 35%.

One possibility is that everything that we are seeing on these residuals maps is due to errors in the photogrammetry. This would however require systematic effects effects to be present in order to produce the relatively large-scale structures seen. As before the random noise in the photogrammetry data can be estimated by reversing the signs of half the maps being included in the analysis. This produces the following plots.

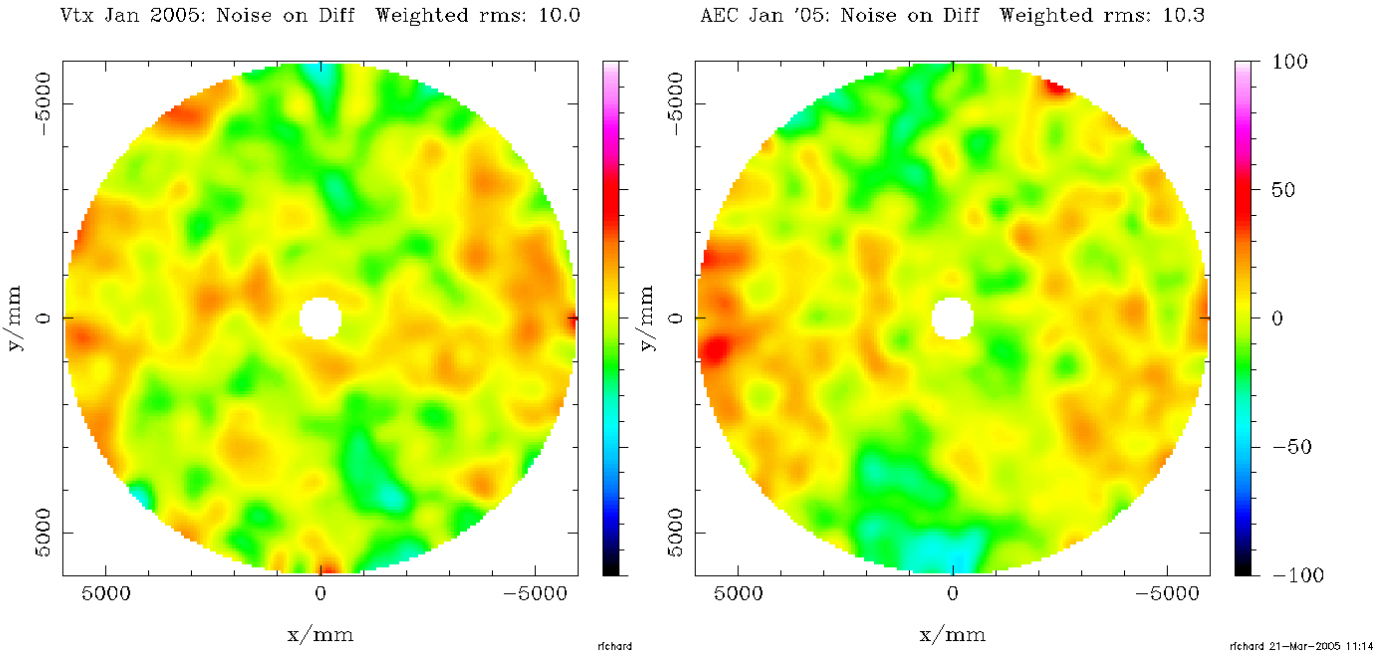

Comparing the measured residuals, which have deviations exceeding +/– 50 microns and which appear to form coherent structures, with the smaller deviations and less ordered structures seen in these noise estimates, it does appear that we are probably seeing real changes with elevation that are not predicted by the FEA models. Clearly we are, however, again reaching the limits of what can be done with this measurement technique.

To provide a “best” estimate of the total non-homologous gravitational deformations, we can take the measured rms deviations of 20.4 and 20.2 microns (for the Vertex and AEC antennas) and perform a quadratic subtraction of the “noise” values of 10.0 and 10.3 microns, giving values of 17.8 and 17.4 microns respectively.

These values are for the weighted half-path errors, as allowed in the specifications. They are however for the whole elevation range from 5 to 90 degrees. Since the bulk of the deformations do appear to have a predictable form (i.e. that given by the FEA but with an additional scaling factor applied), it should be possible to set the surface with a built-in bias such that it will be optimized at an intermediate elevation (the rigging angle). If this is done then the residual gravitational deformations over the range of operational elevations will be about a factor 2 lower than the 90 to 5 degree estimates above, i.e. 8.9 and 8.7 microns respectively.

2.4.8 Conclusions from the Photogrammetry Measurements

1. The most important point is that the data taken in January 2005 give no evidence for really excessive gravitational deformations in either of the prototype antennas. Upper limits in the region of 20 microns on the weighted rms half-path errors for the elevation change from 90 to 5 degrees can be set from these data.
2. Non-homologous deflections are clearly present with roughly the form predicted by the finite element analysis. It appears that magnitude of these deformations is larger than predicted by factors of 1.2 to 1.4.
3. Some residual deformations which do not have the predicted form – e.g. lacking the expected symmetry with respect to the vertical axis – do also appear to be present at a level of about 9 microns rms. This detection is however stretching the photogrammetry technique to its absolute limits.
4. The much larger non-homologous deviations that were seen on the Vertex antenna in data taken in November 2002, which included a gravitational astigmatism, appear to be real, but we have less detailed information on exactly what was done at that time, so measurement problems cannot be ruled out.
5. These large gravitational deformations are not seen in any of the later data, so if they were real, the gravitational behaviour of the dish changed. In this case, the most likely explanation for this apparent change in the gravitational behaviour of the Vertex antenna between 2002 and the present is the work done on the antenna on September 29th 2004.
6. The data taken in 2004 at the time this work was being done are not fully consistent with those taken in January 2005. The discrepancies may be due to thermal effects, but there is no direct evidence to support this.
7. An upper limit of around 10 microns can again be set, for both prototype antennas, on any non-homologous thermal deformations under these conditions. Although there were substantial changes in the shape of the Vertex antenna with temperature, these appear to be largely homologous under the conditions present for these tests.

2.4.9 Acknowledgements

We should like to record the extremely dedicated and professional efforts of Russell Morrison and Dave Lucas from GSI, and of Nick Emerson, Pascal Martinez and Remi Rabut who all worked extremely long hours, much of it on top of cherry-pickers in very cold conditions to obtain these data. John Richer's help with software was also much appreciated.

2.5 Out-of-focus Radiometric Beam Cuts (Emerson, Lucas, Mangum)

Abstract:

The antenna beamwidths are measured radiometrically, using astronomical sources and over a range of elevations. By comparing the beamwidths measured in orthogonal directions, whilst offsetting the axial focus by known small amounts, the astigmatic term of the dish surface can be measured. These measurements are performed over a range of elevation angles and give an estimate of how astigmatism of the antenna surface varies as a function of elevation.

2.5.1 Introduction

The technique of deriving astigmatic antenna distortions by using the measured azimuth and elevation beamwidths, as a function of focus offset, has been known for many years; see reference (1). The most obvious indication of astigmatism in an antenna surface, besides a reduction in overall boresight gain, is a broadening of the beam in one direction relative to the orthogonal direction. The optimum antenna focal position, as defined by the minimum beamwidth of the antenna, then depends on which beam diameter is being minimized. The optimum focal position as defined by maximum antenna boresight gain is usually near the mid-point between the 2 focal positions defined by minimum beamwidth. By studying precisely how the relative beamwidths vary as a function of focus offsets, the amplitude of the astigmatic term can be determined very easily and with good precision.

This note describes measurements made on the ALMA prototype antennas to determine the amplitude of astigmatism and how it varies with elevation angle. To determine astigmatism in the general case, beam cuts in just Azimuth and Elevation are insufficient, and additional beam measurements in a coordinate frame rotated by 45 degrees to Az-El are required. A mathematical model of an antenna surface with astigmatism was created in Mathcad. The beamwidths for a given amount of astigmatism and for a given defocus were computed numerically. The most convenient parameter derived from the model is the ratio of orthogonal beamwidths as a function of focus offset; measurements of this parameter were fit to the model, to derive the astigmatic term.

2.5.2 The Antenna Model

A model was created in the program Mathcad, based on the ALMA antenna parameters: dish diameter 12 meters, focal length 4.8 meters, at a frequency of 265 GHz. The

antenna response in a given direction, for a given defocus and for a given degree of astigmatism, was calculated by numerical integration. For a given focus offset, the beam angular response was calculated simply by adding a linear phase gradient to the antenna aperture, and solving numerically for the peak response and the half-power response, as a function of the phase gradient. The astigmatic term was generated by raising the surface of the dish, in the "Z" direction and normal to the dish aperture, by an amount:

$$\mathbf{A.(r/R)^2.\cos(2.\{\theta-\theta_0\})}$$

where **A** is the peak amplitude of the astigmatism at the edge of the dish, **r** is the radius from the center of the dish in the plane of the aperture, **R** is the radius of the dish (here 6 meters), θ is the position angle in the same plane, and θ_0 defines the position angle of the main axis of astigmatism. A central blockage of diameter 0.75 meters was assumed. For the model fitting, an illumination edge taper of -15 dB was used, matching the radiometry measurements, although in converting peak astigmatism into a weighted rms component an edge taper of -12 dB was assumed. A quadratic form of taper was used, but other forms were tried and the analysis is very insensitive to details of this illumination function.

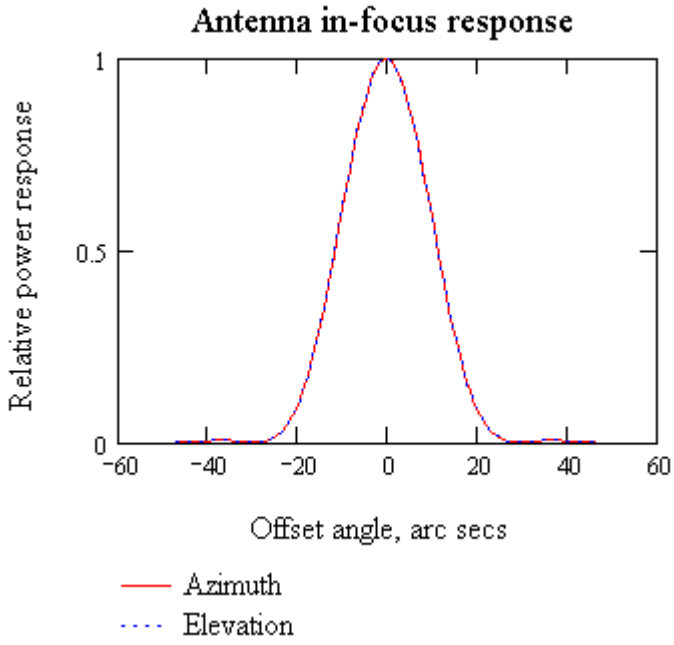

Figure 2.5.1. The model beam shape calculated in focus and with no astigmatism. The FWHP is 22.9".

Mathcad was used to solve the field integral numerically, but as a consistency check computations were compared with analytic functions available elsewhere. Figure 2.5.1 shows the computed beam in-focus response in the absence of astigmatism; the computed fwhp is 22.92". Figure 2.5.2 shows the computed in-focus gain variation on boresight as a function of axial focus offset, with no astigmatism; the gain falls to half power with a focus offset of 0.85 wavelengths, or 0.96 mm.

Figure 2.5.3 shows an example of orthogonal beamwidths predicted from the Mathcad model for 20 microns peak astigmatism, aligned in the azimuth-elevation frame – i.e. $\theta = 0$. In this case, the maximum and minimum beamwidths occur precisely along azimuth and elevation offset angles.

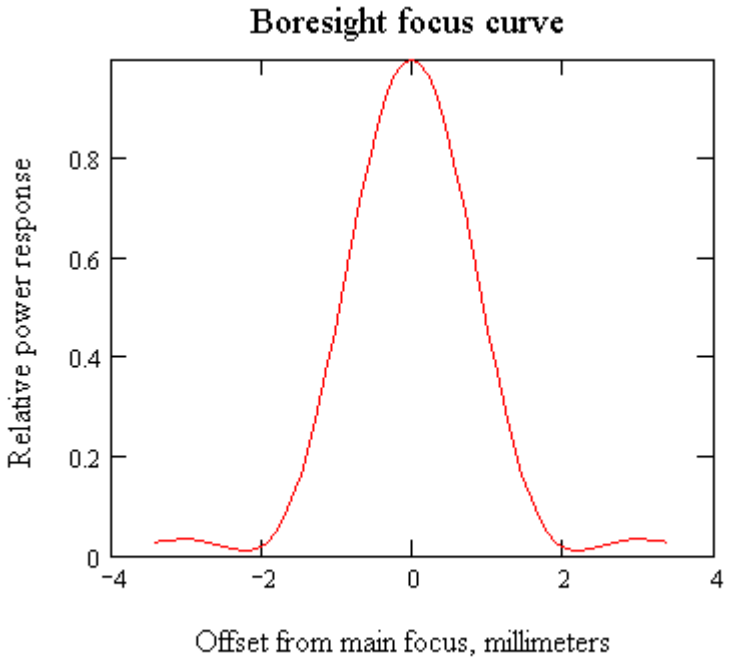

Figure 2.5.2. The computed change of gain on boresight, with no astigmatism. The gain falls to half power with an offset of 0.85 wavelengths, or 0.96 mm.

From Figure 2.5.3, the ratio of (e.g.) Azimuth/Elevation beamwidths, as a function of focus offset, may be derived. Examples of the ratios for peak astigmatism values of 10, 20 and 30 microns of this are shown in Figure 2.5.4. At a given value of astigmatism, the plot of orthogonal beamwidth ratio against focus offset is linear for small focus displacements, but begins to deviate significantly from linearity at about +/- 1 wavelength

of defocus. The slope of the curve is proportional to the magnitude of the astigmatism; for peak astigmatism up to about 50 microns, the linear relationship holds within a few tenths of one micron. This slope is a convenient parameter to use for fits with observational data.

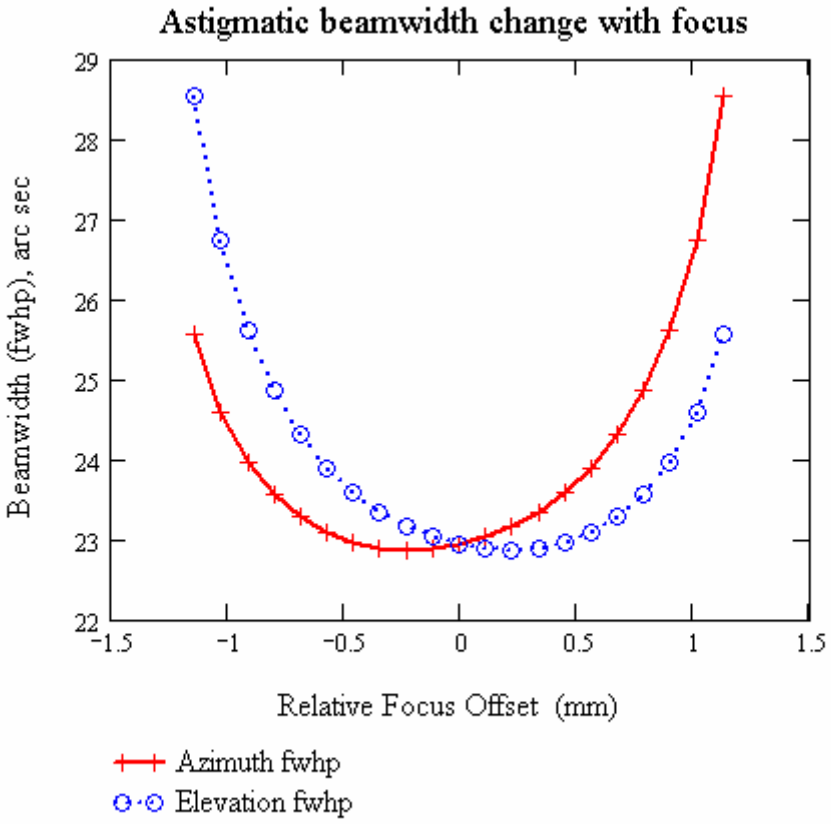

Figure 2.5.3. The computed beamwidths (fwhp) in Azimuth and in Elevation, for a peak astigmatism aligned with the elevation axis of 20 microns (5.4 microns weighted rms).

Figure 2.5.5 shows the best fit model beamwidth ratios, together with points derived from measurements on Venus, at an elevation of 33 degrees; the measurements have been corrected for the source diameter of 10.3". The correction for planetary diameter used a model of a disk, representing the planet, convolved with a gaussian beam. For this observation, the derived best fit astigmatism is 15.9 microns peak, giving a radiometric weighted rms of 4.3 microns. The conversion from peak astigmatism to radiometric weighted rms gives a constant ratio of

(Peak edge astigmatism/Weighted rms) = 3.67.

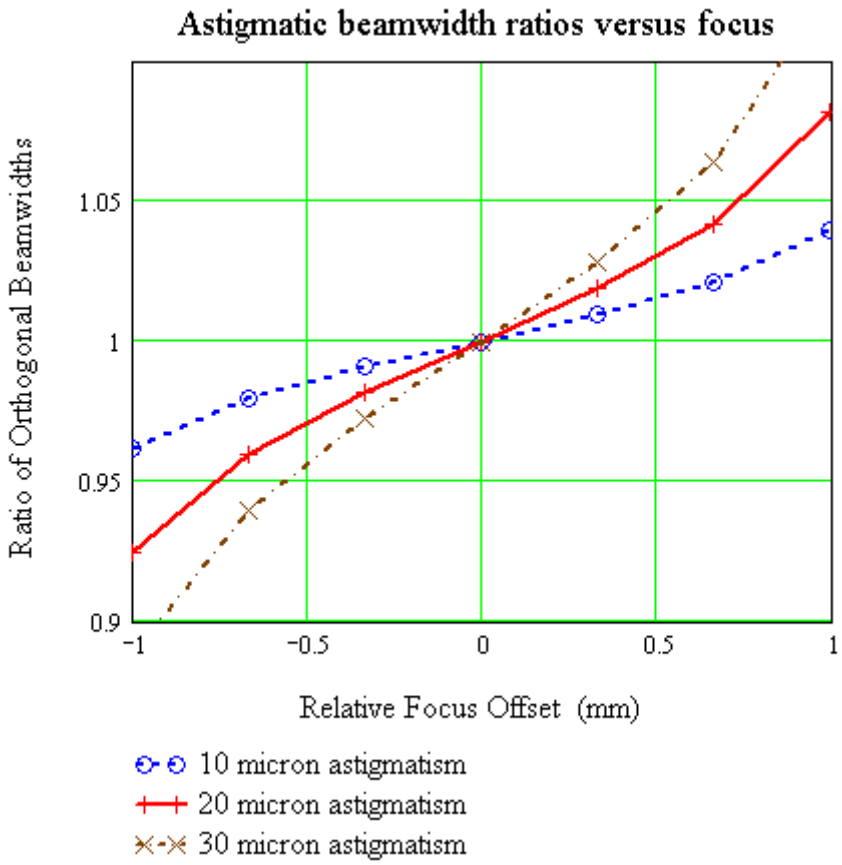

Figure 2.5.4 The ratio of Azimuth beamwidth over Elevation beamwidth for different offsets of the axial focus. Curves are shown for peak astigmatism values of 10, 20 and 30 microns. The slope of the curve of beam ratio to focus offset is linearly proportional to the magnitude of astigmatism.

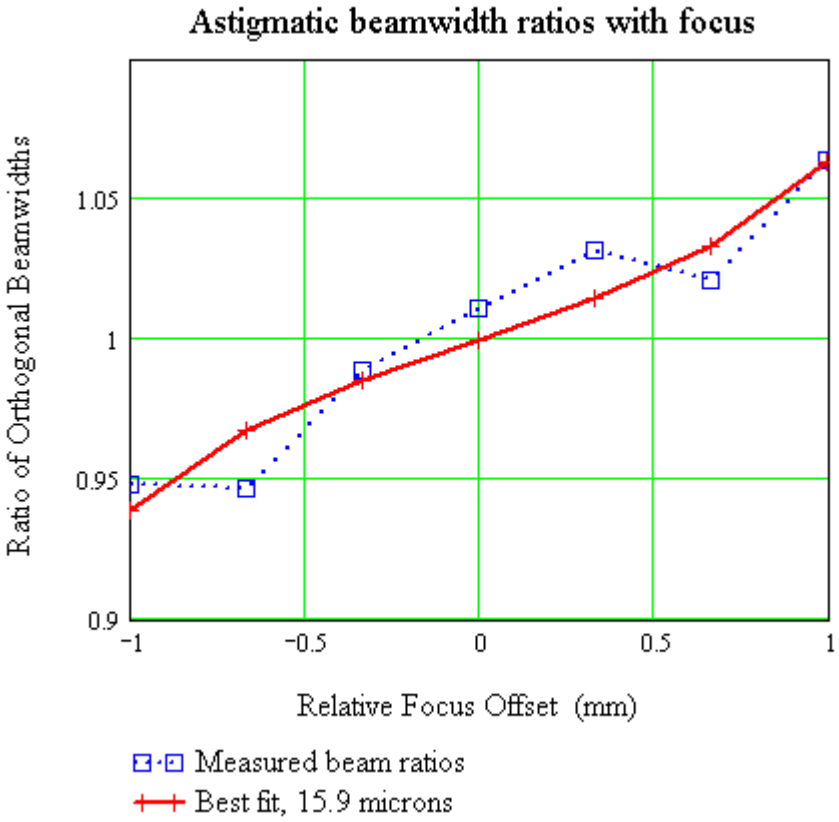

Figure 2.5.5. Measured beam ratios, Azimuth bw/Elevation bw, on Venus on January 25th, when the planet was at elevation 33 degrees. Before computing ratios, the beamwidths have been deconvolved for the circular planetary disk diameter of 10.2", using a model Gaussian beam convolved with a 10.2" disk. The solid line shows the best fit model of astigmatism, which has a peak amplitude of 15.9 microns, corresponding to 4.3 microns weighted rms.

2.5.3 The Observations

The data were taken by rapid on-the-fly scanning of the telescope beam across the source – for the Vertex measurements, either Saturn or Venus was used. The scans were made in orthogonal directions either in the Azimuth-Elevation frame, or in a frame rotated by 45 degrees. Scans were made with axial focus offsets of -1, -0.67,

-0.33, 0, .33, .67 or 1.0 mm; observations were at 265 GHz, a wavelength of 1.13 mm.
For the observation on Venus shown in Figure 2.5.5, the scan was made while nutating the subreflector. For subsequent observations, the data were taken in total power mode with no switching of any kind.

2.5.4 Analysis

- Data
The beamwidths of each pair of orthogonal scans were determined by fitting a Gaussian, superposed on a sloping linear baseline. The Gaussian amplitudes and beamwidths were then used in the subsequent analysis – the model fitting itself uses only the measured beamwidths, but the amplitude information is useful as a check that the zero focus offset measurement corresponds to the peak amplitude, so that there were no additional focus offsets.

- Beamwidth corrections
The available strong astronomical sources were all planets. It is important to correct the observed beamwidth to true antenna beamwidth; Venus had a diameter of 10.2", while Saturn was 18.8" x 20.5"; the in-focus beamwidth of the antenna at this frequency is nominally 23". The deconvolution from observed beam size to real beam size, allowing for the planetary diameter, was based on a model disk convolved with a guassian beam. For a given planetary disk diameter, predicted observational beamwidths were tabulated for various values of real antenna beamwidth. A polynomial fit to these tabulations was then used to derive true antenna beamwidth from the beamwidth as measured from the planetary observations.

After correcting for the size of the planetary disc, the ratios of beamwidths from each pair of orthogonal beam cuts, against focus offset, were tabulated for the subsequent model fitting.

- Model fitting
In a series of tests, model orthogonal beamwidth ratios were computed, as a function of axial focus offsets, for a number of values of peak astigmatism ranging from 0 to 50 microns. It was found that the slope of the curve of beamwidth ratios against focus offset was extremely linear as a function of peak astigmatism. From these calculations, a template of the curve of beamwidth ratio against focus offset with a fixed but somewhat arbitrary value of 10 microns of peak astigmatism was computed. This template was then compared to the corresponding observational data, and the value of astigmatism was found by minimizing the squares of the differences between the data and the scaled 10-micron template. The best scaling factor then determined the best fit value of peak astigmatism. This may be converted to weighted rms astigmatism by dividing by 3.67.

- Correction to weighted rms

The model computations incorporated the known -15 dB edge taper of the ALMA prototype antenna evaluation receiver feeds. To convert values of peak astigmatism used in the model to an equivalent rms surface error, an edge taper of -12 dB was used. It was found that the rms defined this way is a factor of 3.67 below the peak astigmatism. This weighted rms value is the relevant quantity to use in a calculation of aperture efficiency using the Ruze equation.[2]

2.5.5 Results

Measurements on the ALMA Vertex Prototype Antenna

The tables below summarize the measurements on the Vertex antenna. Measurements in the Azimuth-Elevation frame are shown separately from the 45-degree frame. The **sign of the Azimuth-Elevation astigmatism** is such that the left and right edges of the dish are bent towards the prime focus. The **sign of the 45-degree astigmatism** is such that, looking at the back of the dish and looking in the same direction as the radio beam, the lower right and upper left edges are bent away from the prime focus. The first Az-El measurement at elevation 33 degs is on Venus, all the other points were measured on Saturn. Note that there is a wide range of parallactic angle in the course of the measurements, so any systematic errors caused by the elongation of Saturn or its rings should show up. There is no obvious strong correlation of measured astigmatism either with parallactic angle or with rate of change of parallactic angle.

Note that the weighted rms microns given in column 6 are calculated with respect to the ray paths, so may be compared directly with other aperture efficiency factors that might be used with the Ruze equation. The values in column 6 are the weighted rms multiplied by the sign of the astigmatism. The Delta-Parallactic Angle values in column 7 are calculated from the total difference in parallactic angle between the finish and the start of a given set of measurements of 7 different focus offsets.

[2] Strictly speaking this is not allowed, because Ruze assumes an ensemble of error areas of random size with randomly distributed profile errors, with the condition that the scale size (correlation length) of the error areas is much larger than the wavelength and much smaller than the reflector diameter. A more rigorous treatment treats different scale sizes separately before deriving a total efficiency factor. However, Greve, Kramer and Wild (Ref. (4)) show that the error in treating all scale sizes together, deriving a single rms value to apply to the Ruze formula, involves an error in efficiency calculation of only 1-2%. Thanks to Jaap Baars for pointing this out.

Summary Az-El results

Date (2005)	Scan Number	Elevation (degs)	UT	Astigmatism, Peak Microns	Weighted rms microns	Parallactic Angle	Delta-Parallactic Angle
Jan 25	0	**33**		**15.9**	**4.32**		
Jan 29	629	**73.76**	5:26	**28.5**	**7.75**	36.875	1.27
	665	**74.355**	6:55	**24.8**	**6.75**	-35.005	2.31
	694	**61.35**	8:09	**26.3**	**7.15**	-57.875	0.53
Feb 03	820	**58.325**	3:38	**8.93**	**2.43**	59.63	0.4
	853	**69.04**	4:34	**17.0**	**4.62**	49.355	1.21
	898	**74.27**	6:34	**12.3**	**3.34**	-35.75	2.28
	931	**63.85**	8:24	**24.6**	**6.69**	-56.075	0.67
	984	**21.27**	11:03	**1.5**	**0.41**	-60.465	-0.19

Summary 45-degree scan results

Date (2005)	Scan Number	Elevation (degs)	UT	Astigmatism, Peak Microns	Weighted rms microns	Parallactic Angle	Delta-Parallactic Angle
Jan 29	644	**76.57**	5:51	**-13.3**	**-3.64**	19.82	2.12
	666	**74.33**	6:55	**-19.1**	**-5.21**	-35.11	2.3
	695	**61.31**	8:09	**-2.0**	**-0.54**	-57.94	0.6
Feb 03	821	**58.36**	3:39	**-17.0**	**-4.64**	59.61	0.4
	834	**59.565**	3:45	**-6.7**	**-1.83**	58.975	0.29
	854	**69.07**	4:35	**-16.7**	**-4.56**	49.295	1.21
	867	**69.98**	4:41	**-6.9**	**-1.88**	47.63	0.88
	899	**74.245**	6:35	**-15.5**	**-4.24**	-35.86	2.26
	912	**73.585**	6:41	**-13.8**	**-3.77**	-38.47	1.34
	932	**63.815**	7:36	**-13.4**	**-3.66**	-56.105	0.67
	945	**62.88**	7:41	**-9.7**	**-2.64**	-56.89	0.4
	985	**21.23**	11:03	**-5.4**	**-1.47**	-60.465	-0.19
	998	**20.36**	11:09	**-2.9**	**-0.81**	-60.25	-0.12

The figures below plot the derived astigmatism, in terms of weighted rms of the surface, as a function of elevation; peak astigmatism is 3.67 times the weighed rms value. The Az-El astigmatism increases from nothing at low elevation (corresponding to where the dish was measured and set holographically) up to around 7.5 microns at the highest elevation. The relatively large scatter (from ~2.4 up to >7 microns in values of weighted rms) in values above 60 degrees is somewhat greater than is expected from measurement errors.

The 45-degree astigmatism ranges from around 2.5 microns rms (9 microns peak) at low elevation up to around 3.5 microns rms (13 microns peak) at higher elevation, but this

increase is marginally statistically significant. If the measurements above 50 degrees elevation are assumed to be of a constant value of astigmatism, then the rms scatter gives an estimate of the random error of the technique, which is 1.4 microns in the weighted rms values (5.2 microns in peak values)

Taking just the Az-El measurements above 50 degs elevation, the rms scatter in the weighted rms measurements is 2.1 microns (7.6 microns in peak values).

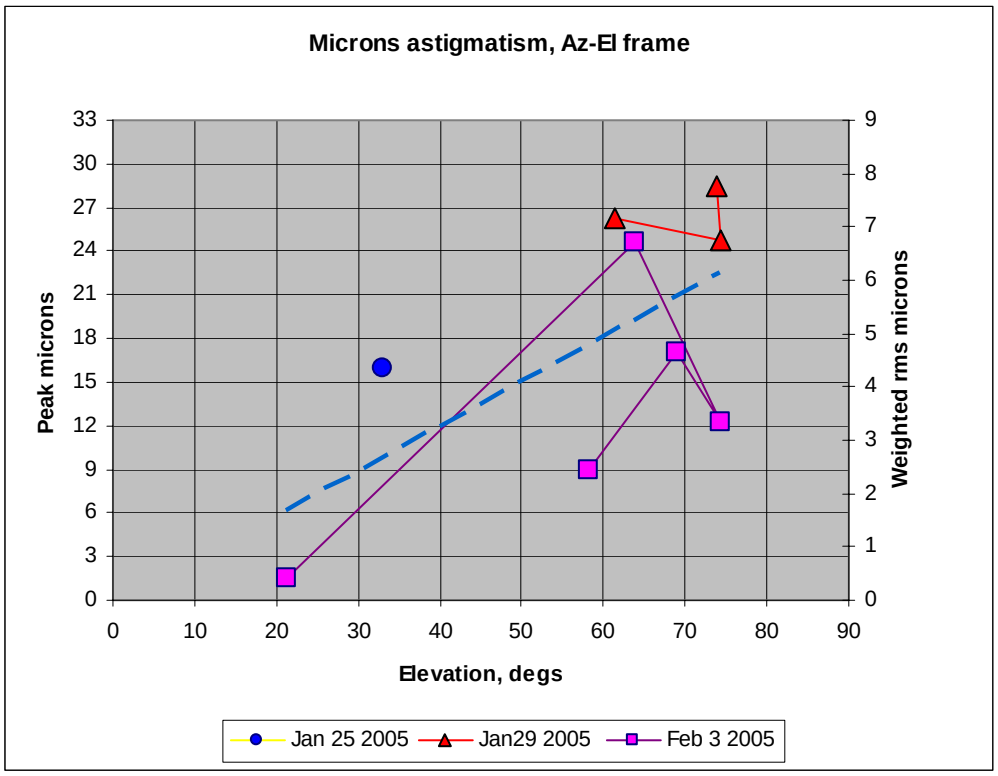

Figure 2.5.6. A plot of the derived weighted rms astigmatism as a function of elevation, for the beam cuts measured in the Azimuth-Elevation frame. The left vertical axis indicates the peak value of astigmatism A, and the right axis the corresponding weighted rms values, calculated for the ray paths and as might be applied in the Ruze equation. A continuous line joins the points to indicate the chronological order in which data were taken on a given date. Observations were spread over 3 different sessions on different days. The dashed line is just a straight line fit to all data points, and does not necessarily have any physical significance.

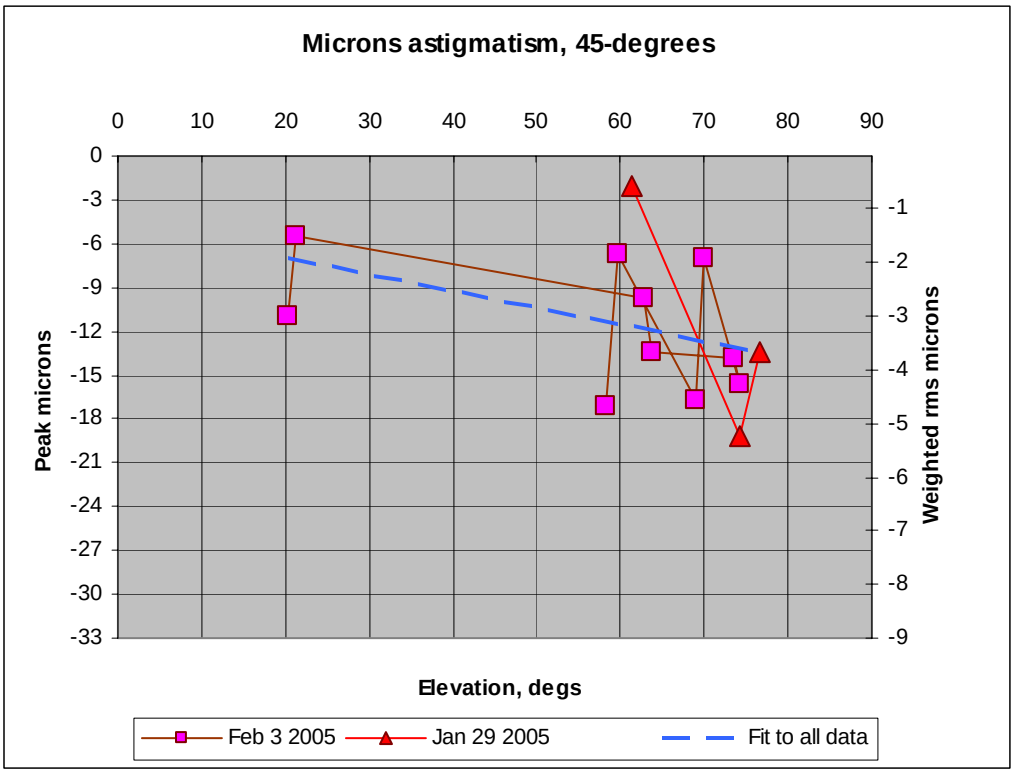

Figure 2.5.7. A plot of derived astigmatism against antenna elevation pointing for the beam cuts at 45 degrees. As above, a continuous line joining the points indicates the chronological order in which data were taken on a given date; the observations occurred on 2 different days, as indicated. The dashed line is a straight line fit to all points, but does not necessarily have any physical significance.

Measurements on the ALMA Alcatel (EIE) Prototype Antenna

Due to weather issues and hardware problems in the latter parts of the JATG test program, at the time of writing this report, data from radiometric beams cuts on the AEC prototype were not yet available.

2.5.6 Error Analysis

This technique is fairly insensitive to many types of potential error. In particular, since the absolute beamwidth is not used in the analysis, but just the variation of beamwidth as focus is varied, other causes of apparent beam distortion such as coma, or elongation of

the astronomical source used for the measurements, have only minor influence on the derived results. For example, a fixed offset of beam size in one coordinate (e.g. Azimuth) would, to a first approximation, merely provide a constant bias on the curve of ratios of Az/El beamwidths, with little effect on the slope of that curve. Similarly, a fixed beam enlargement in both orthogonal directions would cause only a minor change in the slope of beamwidth ratio versus focus displacement.

- Elongation of the astronomical source

Disk of Saturn: Most of the observations reported here used Saturn as the source. At the time, the equatorial diameter of the planet's disk was 20.5", with the polar diameter 18.8". In the analysis, Saturn was treated as a circular disk with diameter the mean of these two values.

The deconvolution from observed beam size to real beam size, allowing for the planetary diameter, was based on a model disk convolved with a guassian beam. For a given planetary disk diameter, predicted observational beamwidths were tabulated for various values of real antenna beamwidth. A polynomial fit to these tabulations was then used to derive true antenna beamwidth from the beamwidth measured from the planetary observations

As an example, if the observed beam width on Saturn were 30", using the circular disk approximation the deconvolved antenna beamwidth would be 27.46". If the true planetary diameters were used, the deconvolved antenna beamwidths would be 27.69" by 27.22". In the worst case, this would introduce a near-constant offset of the mean ratio of antenna beamwidths of only 1.7%. Tests confirmed that the error introduced in the derived astigmatism is somewhat less than this – a true 10 micron of astigmatism might be measured as only 9.9 microns. The possible error is only a scaling factor on the measured astigmatism. However, for constant parallactic angle, this is a constant offset with very little effect on the slope of the plot of beam ratios against focus offset. Elongation of the planet does not introduce spurious measured astigmatism if none is present. In the observations reported here, change of parallactic angle is negligible (see below). Errors introduced by the circular planetary disk approximation will be less than ~0.1 micron in derived astigmatism amplitude.

Rings of Saturn: At the time of the observations, the outer edge of Saturn's rings had an extent of 46.5" by 18.4". The emission from the rings may introduce an error in the measured beamwidths, although the emission from the rings is low compared to the total emission from the planet's disk. However, as explained above, if any broadening of the measured beam is constant for the duration of a focus change cycle, minimal error is introduced into the derived astigmatism.

The greatest change of parallactic angle during one set of focus change measurements was 2.3 degrees. The worst case would be if the major axis of the rings were aligned with one of the orthogonal beam directions. To calculate an order-of-magnitude impact, assume the rings to be edge on – again, a worst case. After 2.3 degrees change of parallactic angle, the rotation of the edge-on rings would give an apparent extent in the orthogonal direction, for a beam 30" in extent along the major axis, of 30" * sin(2.3) = 1.2". Convolved with an antenna beam of ~25" normal to the major axis, this would introduce a change of apparent beamwidth in one coordinate of approximately 0.03", or an error in the beamwidth ratios by a factor of 1.0014. This would introduce spurious astigmatism at a level of less than 0.2 microns peak, or 0.07 microns rms. So, errors introduced by change of parallactic angle causing a rotation of the major axis of Saturn's rings during a set of focus scans are quite negligible.

- Coma aberrations.

To some approximation, beamwidth variations from coma distortion, such as might be produced by a large translational error of the subreflector in the X- or Y- direction, are equivalent to elongation of the astronomical source. From the same arguments, one would expect errors in derived astigmatism from this cause to be a scaling factor, roughly proportional to the fractional increase of the width of the main beam, and not to result in appearance of spurious astigmatism if none is present on the antenna. This surmise is confirmed by some preliminary simulations using Mathcad, although this issue has not been pursued in any detail. Errors from this cause are estimated to be at most a very few per cent in calibration of the magnitude of derived astigmatism. Note that photogrammetry measurements do not in any case indicate significant coma in the antenna surface.

- Circularly symmetric distortions – aberration from the surface donut

At the time of the observations on the Vertex antenna, the "donut" surface error was set into the surface. Robert Lucas estimated the weighted rms of the donut deformation to be 18 microns. At 265 GHz this corresponds to a Ruze efficiency factor of 0.96. If all of this aberration resulted in widening the main beam, then that would be a 2% beam broadening. This results in error in computed astigmatism of ~2%, or about ~0.4 microns peak, ~0.1 microns rms, on this particular measurement. This error is insignificant.

- Random receiver noise

The signal-to-noise in these observations was typically several hundred to one. In any measurement of beamwidth, that might introduce an error of one part in several

hundred – a 25" beam might be measured as 25.1". This will contribute less than 1 micron to the errors in measured peak astigmatism values.

- Pointing errors

The dominant contribution to random errors in the measurement may be the telescope tracking errors. If this were to cause a 0.1" pointing error in the time it takes to scan across the beam, then potentially a 25" beam could be measured as 25.1". A 0.1" error in measured beamwidth from this cause could introduce nearly 1 micron error in measured peak astigmatism.

- Model approximations – prime focus vs. moving secondary mirror

The model calculations have all been for a prime focus system, with focus movements meaning motion of the prime focus. The ALMA antennas are Cassegrain systems, where the focus movement is a motion of the secondary reflector. This introduces (see e.g. ALMA Memo 456) a small error, of about 0.38% of the real astigmatism. For 20 micron peak astigmatism, that corresponds to an error of ~0.08 microns peak, which is quite negligible in the current context.

Approximations in the model fitting procedure may introduce a further error of order 0.2 microns in the peak astigmatism.

- Form of astigmatism

The model of astigmatism used here has assumed a surface deviation varying as $\mathbf{A.(r/R)^n.cos(2.\{\theta-\theta_0\})}$, with **n=2.** Higher orders of astigmatism may be present, such as a component with **n=4.** However, the precise order of astigmatism has surprisingly little impact on the derived magnitude of astigmatism using this technique. The outer edges of the dish play the dominant role in determining the beam FWHP. With astigmatism defined by the above equation, the peak amplitude of the astigmatic deformation **A,** which occurs at the edge of the dish at **r=R**, is the same for all values of **n.** It was found empirically that, for a given set of measured orthogonal beamwidth ratios and for -15 dB edge taper, the derived peak astigmatism **A** would be ~25% lower by assuming **n=4** rather than for **n=2.** However, the conversion from a given peak value **A** to a weighted rms value would give a value ~30% lower for **n=2** than for **n=4.** The net effect is that weighted rms values of surface error derived from beamwidth ratios only change by ~5% between **n=2** and **n=4.** Real astigmatism is likely to be a combination of various orders of deformation, but the weighted rms quantities are almost independent of the precise order of the astigmatic terms.

This can be understood qualitatively in the following way: the dominant beam deformation from astigmatism is a broadening of the main beam in one direction.

The loss of aperture efficiency from this cause is approximately proportional to the increase of beam volume, so proportional to the broadening. A given loss of efficiency then implies about the same additional mean square surface error, no matter whether the error is distributed across the dish as $\mathbf{r^2}$ or as $\mathbf{r^4}$**. [See also the comment in footnote 1 and Reference (4).]**

- Feed Pattern

The feed illuminating the antenna, via the subreflector, during these measurements will have both amplitude and phase imperfections. Unfortunately only amplitude data is available; see:

Denis Urbain and Christian Holmstedt: "*Beam measurements on Evaluation Receiver*", for #1 and #2. EDM number AFTD-41.08.00.00-001-A-VER and AFTD-41.08.00.00-002-A-VER .

Evaluation receiver #1 was in use for the measurements on the Vertex antenna; these reports show a possible ratio of feed pattern widths of 1.5%. Such an effect will not introduce any spurious astigmatism into the measurements described here (see below), but may introduce an amplitude scaling error of any astigmatism that is found, by of order 1.5%.

Surface errors in the subreflector will also be indistinguishable from primary surface errors, but should be at a sufficiently low level not to be a cause for concern here.

- Summary of errors

Random errors: from the fits of the model to measurements of beamwidth ratios as a function of focus offset, the formal error is about 0.8 microns in weighted rms values, or 3 microns in the peak edge value of astigmatism. From the spread of measurements on the 45-degree cuts, if there is assumed to be no real variation of astigmatism with elevation for those measurements above 50 degrees, the rms scatter of those points is an upper limit measure of the statistical error. This is **1.5 microns weighted rms,** or **5.5 microns peak astigmatism.**

Systematic errors: On a given measurement set, the mean (either geometric or arithmetic mean) of all 7 measurements should be 1.0. It is sometimes found to be up to ~10% greater, or smaller than, 1.0. Some of this variation may originate in the structure of Saturn and variations of parallactic angle from measurement to measurement. As discussed above, this **could introduce a ~10% error** in the derived magnitudes of astigmatism, although because only the slope of this curve is used to derive astigmatism, no spurious astigmatism will be introduced if there is none present on the dish. We could find no obvious correlation between magnitude of derived astigmatism and the deviations of the mean ratio from 1.0.

Spurious astigmatism: Because of the differential nature of the analysis – i.e. dealing only in ratios of orthogonal beamwidths, not the absolute values, and fitting for variation in the ratios as a function of focus offset - the only possibility we can think of for false astigmatism potentially appearing in the results, is a combination of elongated structure in the source and a rapid change of parallactic angle during the measurements. As discussed above, any such effect is estimated to be **less than 0.1 microns rms**.

Measurements of the amplitude response of the feed are available in reference (3). These reports show a possible difference in orthogonal feed pattern widths of 1.5%. Such an effect will not introduce any spurious astigmatism into the measurements described here (see below), but may introduce an amplitude scaling error of any astigmatism that is found, by of order 1.5%.

In our measurements any **astigmatism in the phase response of the feed,** equivalent to the phase center of the feed in the horizontal plane being displaced from that in the vertical plane, is indistinguishable from astigmatism of the prime surface. Unfortunately, no phase measurements of the feed are available, but fortunately any such astigmatism would appear as a constant value independent of elevation. Surface errors in the **subreflector** should be insignificant.

Form of astigmatism: The model of astigmatism used here is of a term varying in the plane of the aperture as $\mathbf{A.(r/R)^n.cos(2.\{\theta-\theta_0\})}$ **,** with **n=2**. Higher order terms may be present, such as a component with **n=4**. However, when expressed in terms of weighted rms surface error, the measurements here will give **approximately the same result** no matter what order **n** of astigmatism is actually present on the dish surface.

Unknown errors: The treatment of possible errors from the structure of Saturn may be oversimplified, and does not for example consider antenna sidelobes falling on the rings. It is difficult to quantify this, except to note that sidelobes of the antenna are known to below -20 dB at this wavelength. In any case, no systematic change in derived astigmatism as a function of parallactic angle was found. Similarly, no strong correlation between rate of change of parallactic angle and derived astigmatism magnitude was found, so this is probably not a significant cause of error.

2.5.7 Conclusions

The technique of measuring variations of antenna beamwidth as a function of axial focus offsets has been used to measure the astigmatism of the prototype ALMA antenna(s) as a function of elevation angle. The differential nature of the technique makes it

substantially insensitive to other dish degradations or to elongation of the astronomical source.

On the Vertex antenna, astigmatism in the 45-degree coordinate system is found with a value of ~2.5 microns weighted rms (peak ~9 microns) at low elevation, and a value of ~3.5 microns weighted rms (peak ~13 microns) at high elevation. The rms scatter of all 45-degree measurements above 50 degrees is a 1.4 microns in the weighted rms values. All these values are derived assuming a $(r/R)^2$ form of astigmatic components of the dish surface, but the derived weighted rms astigmatism is insensitive to the order of astigmatism.

For astigmatism aligned with the Azimuth-Elevation frame, the Vertex antenna shows zero astigmatism at low elevation, rising to perhaps 7.5 micron weighted rms (~27 microns peak) at high elevations. If confidence can be established in the magnitude and form of this astigmatism varying with elevation, then in principle the dish could be set at an appropriate rigging angle and so potentially halve the peak amplitude.

References:

(1) *Astigmatism in reflector antennas*, Cogdell, J. & Davis, J., IEEE Trans. Ant. Prop., AP {21, 565 - 567}, 1973

(2) ALMA Memo #456, available at
http://www.alma.nrao.edu/memos/html-memos/abstracts/abs456.html ,
Characteristics of a Reflector Antenna: Parameters, graphs and formulae for Cassegrain systems with Mathematica expressions for numerical computation, by Jaap Baars.

(3) EDM ATFD-41.08.00.00-001-A-VER Beam measurements on Evaluation Rx #1. Christian Holmstedt & Denis Urbain 2003-09-11 18:04
EDM ATFD-41.08.00.00-001-A-VER Beam measurements on Evaluation Rx #2. Christian Holmstedt & Denis Urbain 2003-09-11 18:06

(4) *The beam pattern of the IRAM 30-m telescope*, Greve A., Kramer C. & Wild W., Astron. Astrophys. Suppl. Ser **133**, 271-284 (1998).

2.6 Out of Focus Beam Maps (Hills/Nikolic)

2.6.1 Introduction

"Out-of-focus" (OOF) holography is a relatively new technique for measuring surfaces of radio antennas using astronomical sources and receivers[3]. It is based on solving the non-linear inverse problem of recovering the phase distribution of the aperture given a set of beam-maps at a number of defocus settings. By optimizing the choice of defocus and the parameterization of the aperture, it is possible to make useful measurements of large scale errors in surfaces of antennas in this way, provided that the signal to noise ratio on the in-focus beam is of order 100:1 or better.

2.6.2 Observations

Some out of focus beam maps were taken using the VertexRSI antenna early in 2004. These were taken with the chopper operating which helps greatly in removing atmospheric fluctuations and receiver noise, but slightly complicates the processing of the data. The best set of maps, using Venus as the source at an elevation of about 59 degrees, were taken in March 2004 and are shown in these plots.

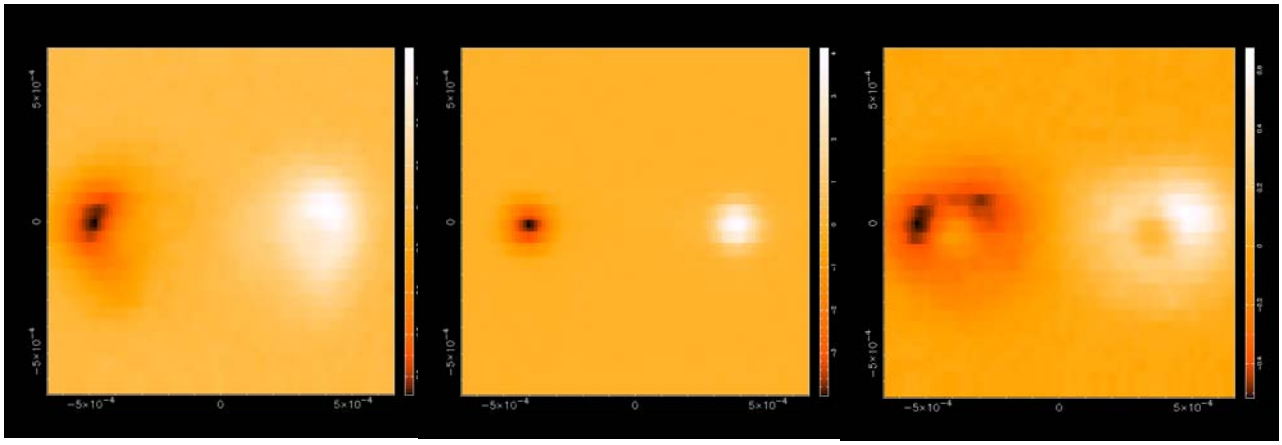

These show the beam shape with +2mm defocus (left), nominal focus (centre), and –2mm defocus (right). The maps were made by scanning in the Azimuth direction while chopping in the same direction. In each map there is a positive and negative image corresponding to the two positions of the secondary mirror during the chop. The amount of defocus chosen is such that, for an ideal antenna, the defocused maps should be circular rings. It is evident that the observed shapes are quite distorted, but some of this is due to the fact that the secondary mirror position had not been fully optimized when these observations were made, so some coma was present.

3 Nikolic, Richer and Hills, proceedings of URSI, Maastricht, 2002

The recent data obtained for the VertexRSI antenna were taken in January 2005, using Saturn as a source. In this case the pointing and focus in all three axes were optimized before making each set of OOF maps, using scripts prepared by Robert Lucas.

Unfortunately the chopper was not operational, so data were taken in a total power mode by making rapid scans across the source with fast sampling (16 milliseconds sample interval). The scans took only 1 second to cover the 200 arc-second extent of the map and the telescope then turned around, stepped to the next row and scanned back in the opposite direction. The turnaround took approximately 3 seconds, during which time data were not taken.

The maps were made in pairs, the first scanned in azimuth and the second in elevation. A full OOF data set consists of three such pairs, one with the axial focus at –2mm from nominal, one pair in focus, and one at +2mm from nominal. The time taken to complete a full such set was about 25 minutes. An example data set is shown in the diagram below, with the three focus positions going from left to right, while the azimuth scanning is in the upper row and the elevation scanning in the lower.

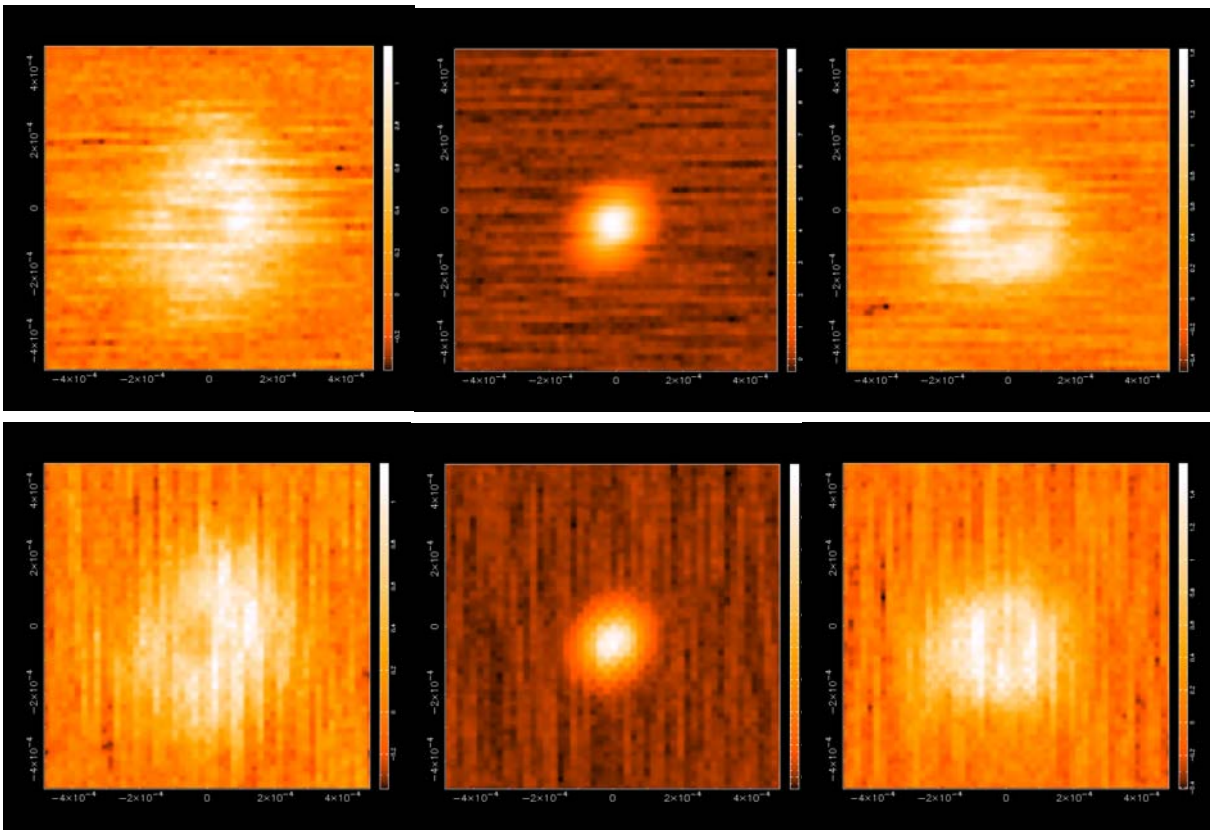

The majority of usable data sets were taken at elevations in the range 55 to 70 degrees. In addition there is one good-quality set which was taken at a lower elevation of ~28 degrees.

2.6.3 Pre-processing of the Data

The first step is to remove the effect of a "lag" in the data sampling, which shows up as a displacement in alternating scans. The magnitude of the applied correction was 9 arc-seconds with the sign of the correction alternating between scans.

Atmospheric subtraction was carried out on a scan-by-scan basis by removing a linear baseline found by fitting a straight line through the end sections of each scan. This has already been done in the plots above and it is evident that, in the case of the total power maps, the linear baseline subtraction is not able to remove all the spurious signals present, as the scan direction can be clearly seen. It is not clear whether the noise present is mostly due to the receiver, the atmosphere or something else. It appears to be non-Gaussian, but we have not yet investigated its statistical properties. Since the maps are highly over-sampled in both directions the fine structure in the noise should not have a big systematic effect on the results.

2.6.4 Derivation of the Antenna Surface Errors

The model used for fitting to the data describes the antenna as a perfect dish to which smoothly varying surface errors, described by Zernike polynomials, are added. The illumination function due to the feed is described by a Gaussian and we assumed this to be correctly centered and circular. Some of the analyses were carried out with the edge taper of the feed as a free parameter; and the derived best fitting value for the taper was close to –15dB in all cases. Although this value is greater than that intended in the design of the evaluation receiver, it is close to that measured in the laboratory, so it was adopted and held fixed for the final processing. The known phase changes due to the deliberate axial focus offsets are added as appropriate. The intensity beam patterns are then calculated and convolved with a model for the emission of the planet. In the case of Venus this was just a uniform disk of the appropriate diameter. For Saturn we employed a detailed model kindly provided by Melvyn Wright, which is based on recent OVRO and BIMA observations. The ellipticity seen in the in-focus maps above is primarily due to the emission from Saturn's rings. Obviously the model takes into account the changing orientation of the planet with respect to the Az-El coordinate frame the antenna.

These models were compared to the observed data by interpolating the model beam-maps to the position of each data point. This has the advantage that no interpolation or convolution of the observed data needs to be made. The free parameters of the surface model, together with the source intensity, were adjusted to find the least-squares fit to the data.

Because the data are noisy, this process will tend to over-estimate the errors in the dish surface because it tries to account for features in the data which are in fact noise. It is possible to reduce this effect by assigning a higher "prior" probability to models with smaller rms surface errors. This makes it possible to use a larger number of Zernike polynomials in the fit without the results becoming too sensitive to noise. Assigning a good prior is, however, made complicated by the correlated nature of the noise in the maps. In practice the strength of the prior was set by trial and error to find the set of parameters which gave the smallest rms surface error while still fitting the data well. All of the parameters describing the surface were in common for a given set of six maps, but it was found to be necessary to allow for pointing shifts between the individual maps. Jeff Mangum has explained that the data were taken without using a proper model of the radio pointing of the antenna and this may explain these drifts in the pointing.

2.6.5 Sources of Uncertainty and Limitations

The limited signal-to-noise ratio and the modest size of the maps mean that the OOF technique is sensitive only to relatively large-scale surface errors. For this reason, the maximum order of Zernike polynomials which is used to represent the surface is limited to a value in the range n=5 to n=7 (20 to 35 terms). The consequence of this is that any surface errors on scales smaller than 2 to 3 meters would not be detected.

The strong taper of the feed means that constraints on the outer part dish are significantly weaker than for the central parts and that, as a result, errors on the derived surface for the outer parts are correspondingly larger. These parts of the dish are however weighted down in the calculation of the weighted rms surface error.

Another consequence of the strong taper is that it introduces mixing between related Zernike polynomials, for example between the defocus and spherical aberration and between third-order coma terms and fifth-order polynomials of azimuthal order +/–1. This means that power due to lateral focus errors (normally dominated by the third-order terms) will couple to these polynomials as well.

2.6.6 Results 1: The VertexRSI data from March 2004.

These have been processed using polynomials of up to 7th order and a prior on the surface errors (see the description of "run 2" below). The resulting fit to the data is good and the map of the surface looks like this.

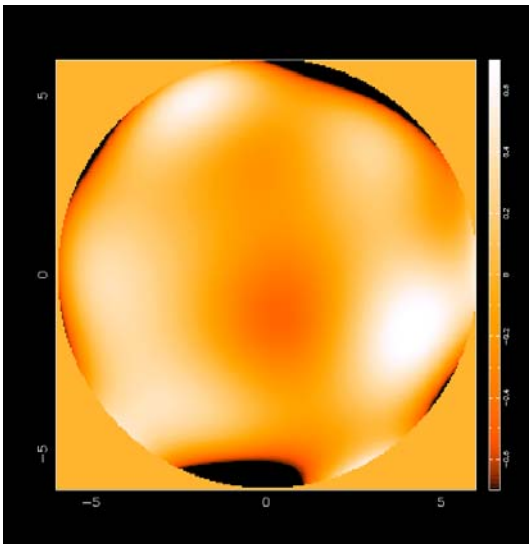

The color scale runs from approximately –60 to +60 microns and it is in the sense that the white sections are points on the surface which are too high. The terms in the fit which are likely to have been due to the displacement of the secondary mirror have been removed from this map of the surface. The weighted rms error of this fitted surface is 28 microns. The relatively large surface errors that were derived from these data were of course a cause for concern when this analysis was first made in November 2004, since it had been thought that the antenna surface was good at the time when this data was taken. Subsequent measurements, using photogrammetry and conventional holography, confirmed the presence of substantial surface errors, as described elsewhere in this report.

2.6.7 Results 2: The VertexRSI data from January 2005.

Visual inspection shows that, despite the relatively poor signal to noise ratio, the beam shapes in the out-of-focus maps are relatively close to the round ring expected for a perfect dish. The models that are produced by the fitting process appear to be a reasonably good fit to the data with most of the features repeatable between the azimuth and elevation scans reproduced. Although the position of the secondary mirror was

optimized before each OOF run, the aperture phase functions derived from these observations are still dominated by Zernike polynomials which correspond to errors in the position of the secondary mirror. We do not consider these terms when calculating the accuracy of the surface, but for the reasons described above, they are not entirely decoupled from other Zernike polynomials.

Results from two reduction runs are presented in the table below: the first represents what is probably the worst case (although it must be remembered that errors on small scales and those coupled to the position of the secondary are excluded); the second is the our present best estimate of the level of large-scale errors that are present. The main differences between the two runs are: the number of Zernike terms being fitted; which terms are eliminated from calculation of the rms surface error; and whether or not a prior on the surface rms value is introduced, specifically:

- Run 1: The fits go up to fifth order polynomial Zernike polynomial, so a total of 17 coefficients describe the surface. No prior is applied. In calculating the rms value only the tilt, defocus and coma terms are removed.

- Run 2: The fit includes all Zernike polynomials up to 7^{th} order. A prior is used. Higher-order coma terms (n=5, l=+/- 1) are eliminated from the calculation of rms.

The rms values quoted are defined as required by the antenna specifications – i.e. half-path errors and weighted with the amplitude illumination for an edge taper of 12dB.

Starting Scan #	Elevation (degrees)	Date	Run 1 RSS (micron)	Run 2 RSS (micron)
601	57	29th Jan	20	14
608	63	29th Jan	19	17
683	70	29th Jan	18	17
813	55	3rd Feb	19	12
846	63	3rd Feb	19	17
924	69	3rd Feb	18	16
975	28	3rd Feb	19	14

In the next figure, the surface maps derived from two sets of maps taken at similar elevation are compared. It can be seen that they are very similar. The weighted rms of their difference is approximately 8 micron, which suggests that the repeatability of these measurements is of order 5 microns rms.

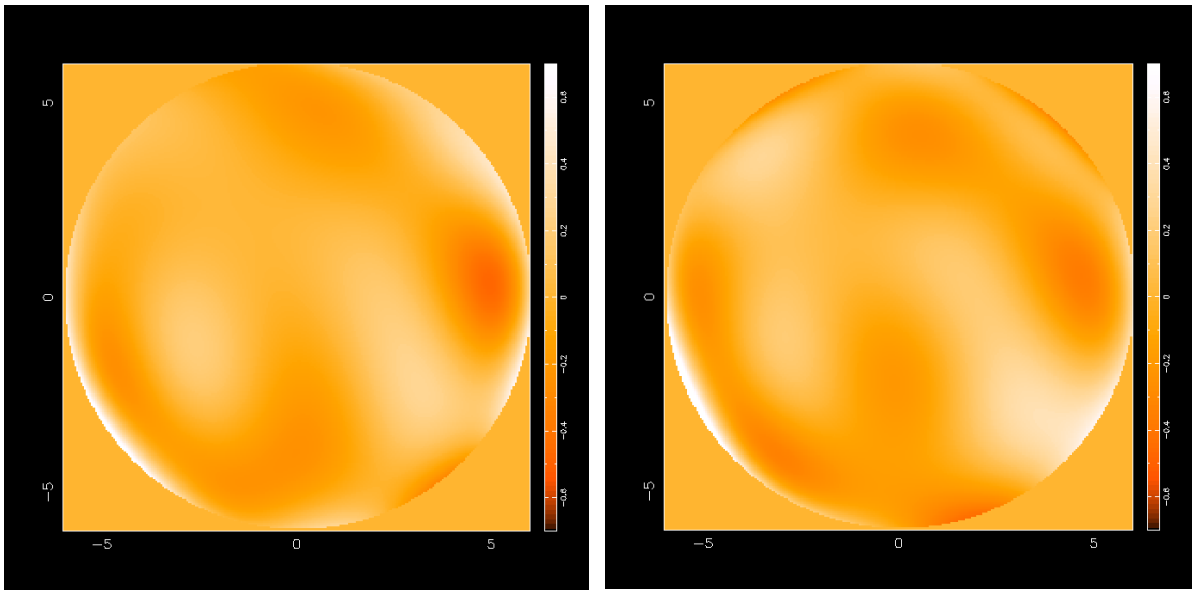

Derived surface maps from Run 2 for scans 601 and 813. The color scale runs from about +60 to –60 microns. The next plot shows the surface map derived from the low elevation data set (975).

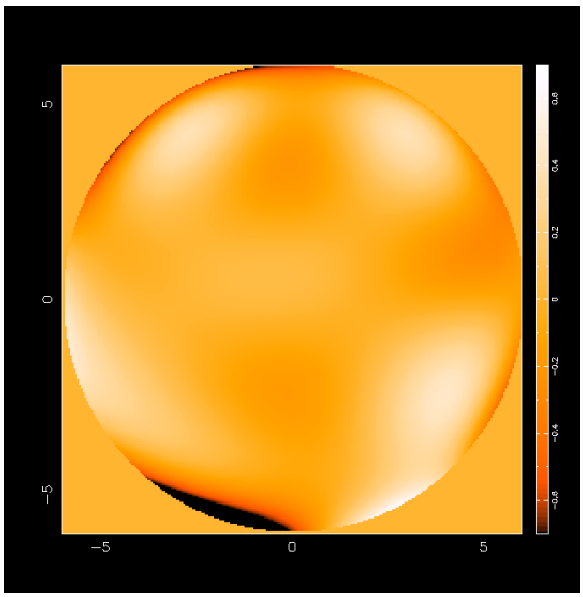

The form of the surface appears to be rather different, although the data is not good enough for us to be able to state that it is different with any confidence. Note that, as explained above, the surface at the edge of the aperture is not well determined because of the strong taper.

2.6.8 Discussion / Conclusions

The signal-to-noise ratio in the maps obtained in January 2005 with the VertexRSI antenna is lower than had been hoped, but it is good enough to put an upper limit of around 20 microns on the weighted rms surface errors on scales larger than about 3 metres. It appears that the surface is substantially better than in March 2004.

It is difficult to assess the significance of the pattern seen in the surface errors because the noise present in the maps is clearly highly structured rather than random and there are many possible sources of systematic error present. At present no clear correspondence has been established between the features seen in these maps and those measured by other techniques. Rather than trying to set an exact figure on the errors, for example, one which could be used in the surface error budget, these results are probably best treated as supporting evidence for the conclusion that there are no gross surface errors in the VertexRSI antenna at present.

2.7 Optical Pointing tests (Mangum/Wallace/Wirenstrand)

This report describes results from optical pointing telescope (OPT) measurements of the AEC antenna all-sky pointing performance made in 2005/01/07-02/09 by the Antenna IPT and the JATG.

2.7.1 Standard AEC Pointing Model

The initial pointing model used was that derived from earlier OPT analyses (See Wallace2004 for details). The default model is:

1	IA	-74.200	
2	IE	-695.300	
3	HASA2	-1.700	fixed
4	HACA2	+2.940	fixed
5	HECE	-16.850	fixed
6	HESA2	-0.990	fixed
7	HECA2	+1.530	fixed
8	NPAE	+28.620	fixed
9	HVSA2	-2.250	fixed
10	HVCA2	-2.080	fixed
11	CA	-829.500	
12	AN	+7.700	
13	AW	-0.800	

The analysis of these new data followed standard pointing measurement analysis procedures. The previously-derived model terms listed above were used to make an initial pointing model solution to the new OPT measurements. The need for changes to the selection of terms used in the pointing model was then considered based on the existence of systematics in the model solution residuals.

Through the course of the analysis of these new OPT measurements, we have found some differences between the pointing model derived by the AEG and the best-fit pointing model derived from these new measurements. Specifically:

- Two terms -- HVSA2 and HVCA2 -- are no longer significant and need not exist in the pointing model solution. The HVSA2 and HVCA2 terms represent changes in the Az/El non-perpendicularity as the mount rotates. The insignificance of these terms suggests that the Az axis has become less wobbly. Removing these terms from the model fit would improve the knowledge of the remaining terms but would make the RMS figure slightly worse.
- The small amount of curvature seen in some of the residual plots of dZ versus Z can be accounted for by adding a suitable term to the model. Such a term could be interpreted as a small adjustment to the refraction, a change to the elevation encoder run-out or a non-Hooke's-Law vertical flexure component. However, the

available improvement is in general not large. Nonetheless, we have included the HESE term in all subsequent model analyses.

2.7.2 Pointing Analysis Results

Figure 2.7.1 shows the cumulative AEC optical pointing model results. For each total RMS value shown we also show the contributions to this total RMS due to cross-elevation and elevation pointing residual.

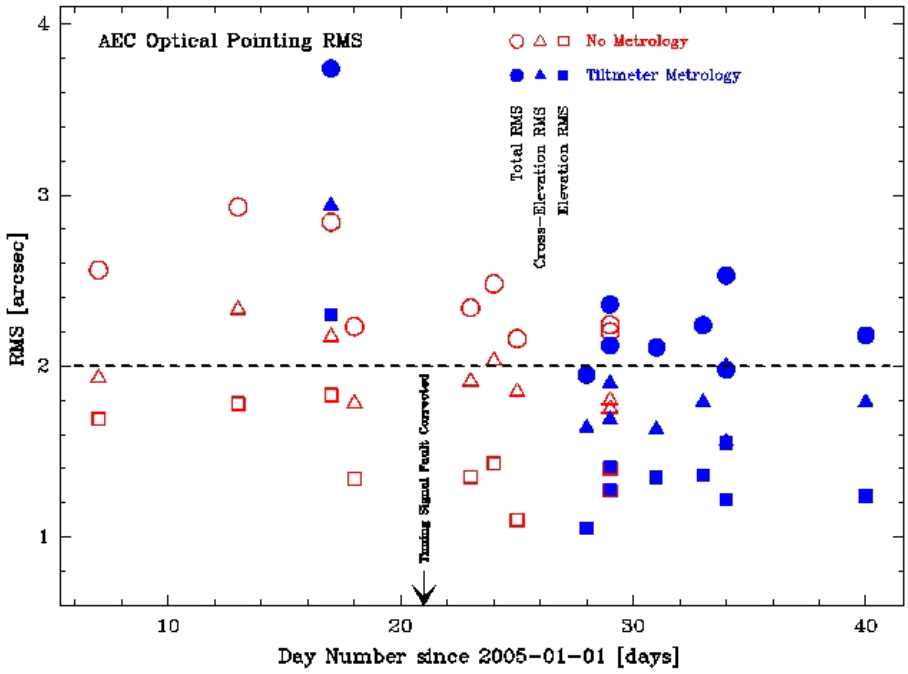

Figure 2.7.1: AEC optical pointing results.

2.7.3 Summary

- Strictly speaking, the model fits should fix the known “core" terms to their previously-determined values. A much less strict interpretation is used here, where all 12+ terms are allowed to float in all model fits, and hence the resulting RMS figure is optimistic. Applying a core model analysis to these data leads to a degradation of the best-fit RMS of at most 0.1 arcsec.
- The uniform 5 arcsec radial cutoff used to mask errant measurements was in many cases too extreme, likely eliminating acceptable measurements and producing a much more optimistic resultant residual RMS.

- The RMS figure is also optimistic simply because it is *a posteriori*, applying to the observations used in the fit and not to the population from which they were drawn. The PSD figure (population standard deviation) attempts to correct for this by allowing for the combination of number of observations and number of terms being fitted. The correction is imperfect because the different pointing terms do not affect the pointing residuals randomly but tend to apply more to one axis than the other in each case. Despite this, the reported PSD is likely to be a more reliable indicator of the true pointing than the RMS, which is bound to be optimistic. Experiments where individual runs were split into two (observations 1, 3, 5… being one set and observations 2, 4, 6… being the other) verified this: fitting the model from one set and applying it to the other set gave a pair of *a priori* RMS values that bracketed the original PSD and were each worse than the original RMS figure. When the results are being assessed, the RMS should really be disregarded and the PSD used as the figure of merit.
- The consistently large change to the IA and AW terms, relative to the previously-derived pointing models reported in the AEG pointing report, are quite unusual. The shift in these terms is a pretty clear indication of a timing error in the monitor and control system of approximately 13 seconds. This timing error does not affect the resultant pointing RMS values derived. On 2005/01/20 this timing error was corrected.
- A timing signal cable problem was fixed on 2005/01/23. This cable problem is likely to have disturbed the pointing measurements done shortly before repair, and thus the results from the first weeks of January may be suspect.
- The pointing model fit appears to be changing over very short (few days) timescales. This could be attributed to the continually changing antenna positioning configuration or possibly to flexure in the contractor-supplied OPT mount.
- Activating the yoke arm metrology correction initially required the inclusion of five more pointing terms. This expanded model fit was worse than model residuals derived from data acquired without metrology correction. After adjustment of the orientation of the tip/tilt sensor and improvement of the correction algorithm, these symptoms were no longer observed.
- A sequential multiple star measurement, where each star measurement was repeated three times, was used to derive seeing. These measurements suggest a seeing contribution of approximately 1.5 arcsec, in line with the results from tracking tests. Extending the interpretation to account for the seeing contribution suggests that the true antenna pointing residual is 1.7~arcsec, assuming the approach to the analysis presented in this document.

2.7.4 Bibliography

Wallace, P.T., Mangum, J.G., & Lucas, R. “Evaluation of the ALMA Prototype Antennas: Pointing" (2004/12/01)

2.8 Further Analysis of AEG Holography Surface Temperature Stability (Lucas, Baars, Mangum)

2.8.1 Summary

A reanalysis of the AEG holography time series data for both the VertexRSI and AEC antennas has been made by making differences of holography maps with different ambient temperatures. The magnitude of the RMS deformations measured (~0.6-0.7 μm/K for the VertexRSI antenna and ~0.8 μm/K for the AEC antenna) corresponds to a temperature-dependent contribution to the surface error budgets of both antennas which is comparable to their respective budgetary contributions.

2.8.2 Analysis

The differencing analysis has been done for the three time series: VertexRSI May 2003, VertexRSI June 2003, and AEC February 2004. The analysis entailed the following:

- For each series the average of all maps in the series was subtracted from all the maps in the series. This removes the spherical aberration and suppresses dependences on any long term effect.
- In each series the maps were divided into several temperature ranges; in each temperature range the average map was computed.
- Finally the differences between the coldest and warmest range averages were computed for each series.

All RMS are the usual 12dB-tapered half-pathlength error.

The maps are plotted in the three summary figures (Figures 2.8.1 through 2.8.3), one for each series. Figure 2.8.4 shows the temperature spans for VertexRSI and AEC assuming a uniform 10 C temperature gradient.

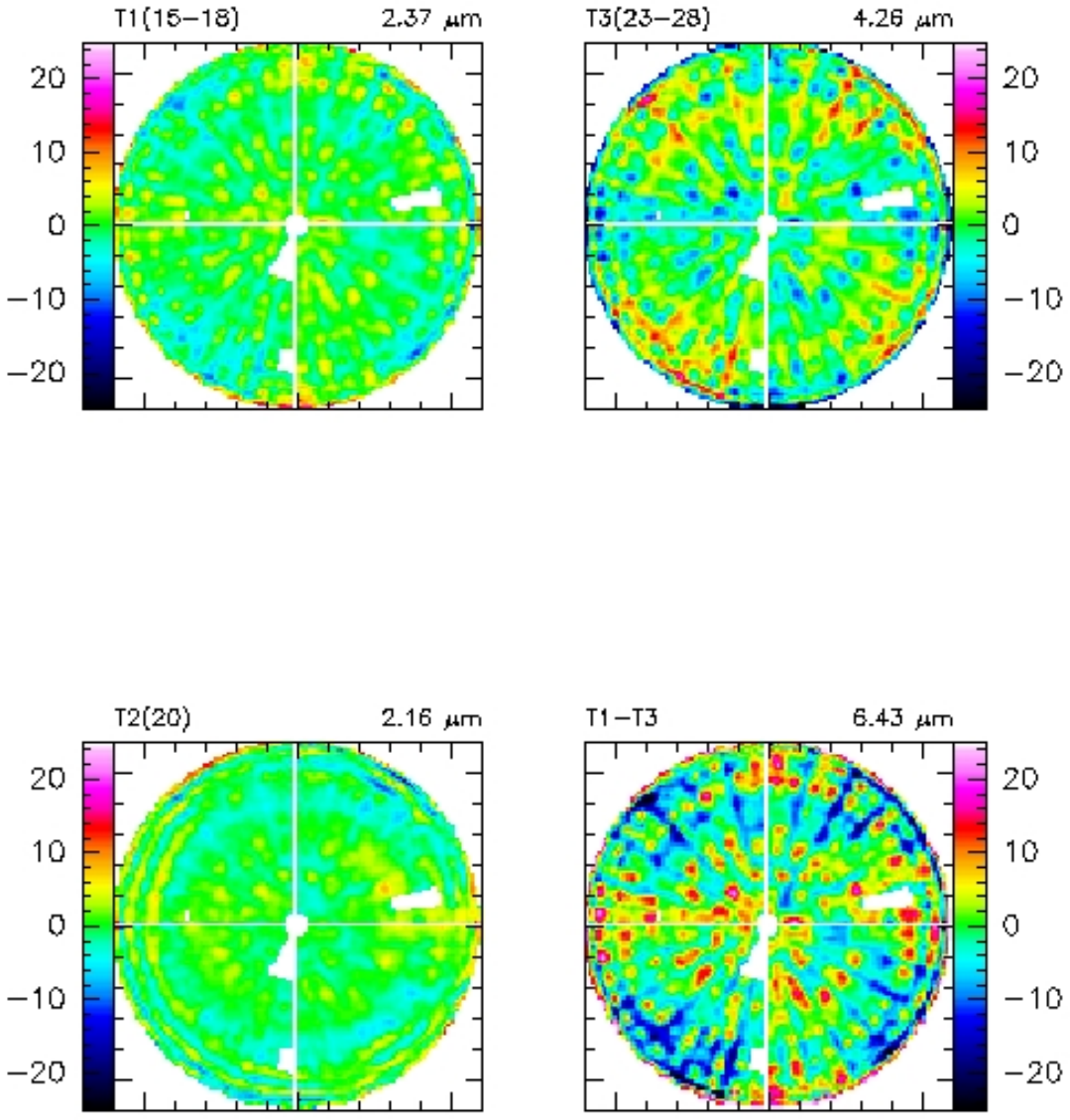

Figure 2.8.1: VertexRSI May 2003 time series. The panels labeled T1 through T3 represent the average difference for the temperature range indicated. The panel labeled T1-T3 shows the temperature span from the coldest to warmest measurement in the series. Note that the high temperature end of this series lies above the upper limit (20 C) for the ambient temperature primary operating conditions.

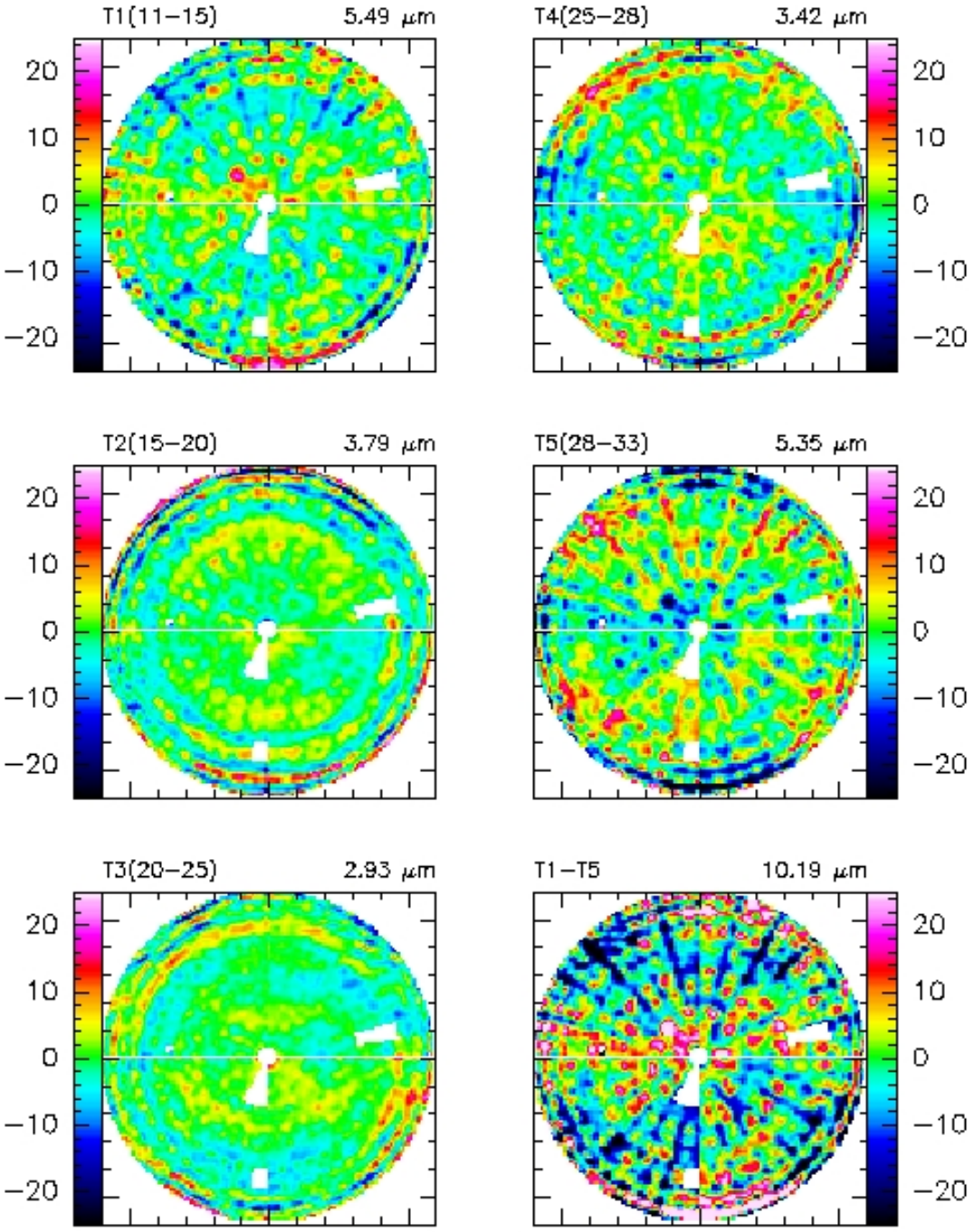

Figure 2.8.2: VertexRSI June 2003 time series. The panels labeled T1 through T5 represent the average difference for the temperature range indicated. The panel labeled T1-T5 shows the temperature span from the coldest to warmest measurement in the series. Note that the T3, T4, and T5 panels lie above the upper limit (20 C) for the ambient temperature primary operating conditions.

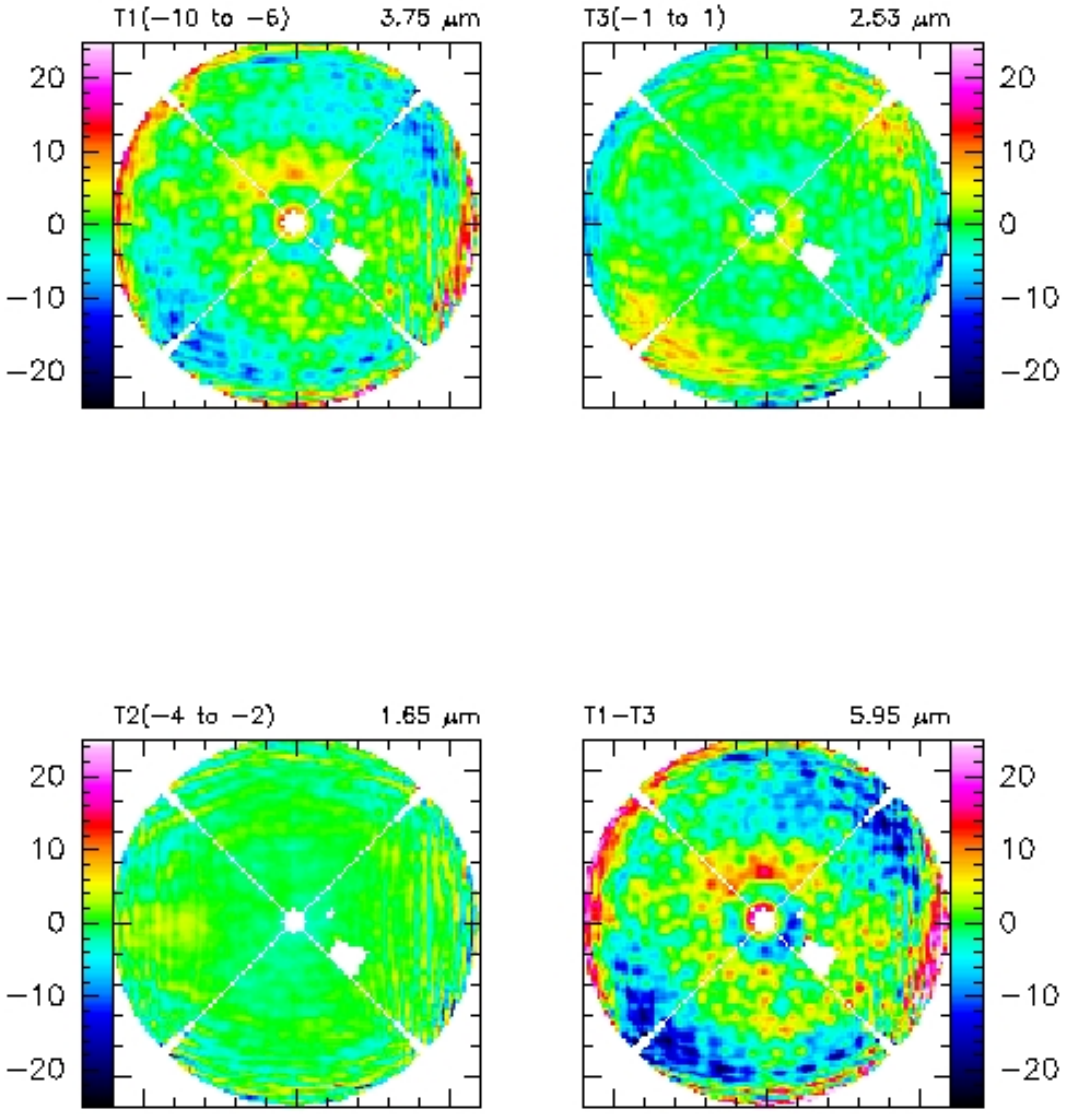

Figure2.8.3: AEC February 2004 time series. The panels labeled T1 through T3 represent the average difference for the temperature range indicated. The panel labeled T1-T3 shows the temperature span from the coldest to warmest measurement in the series.

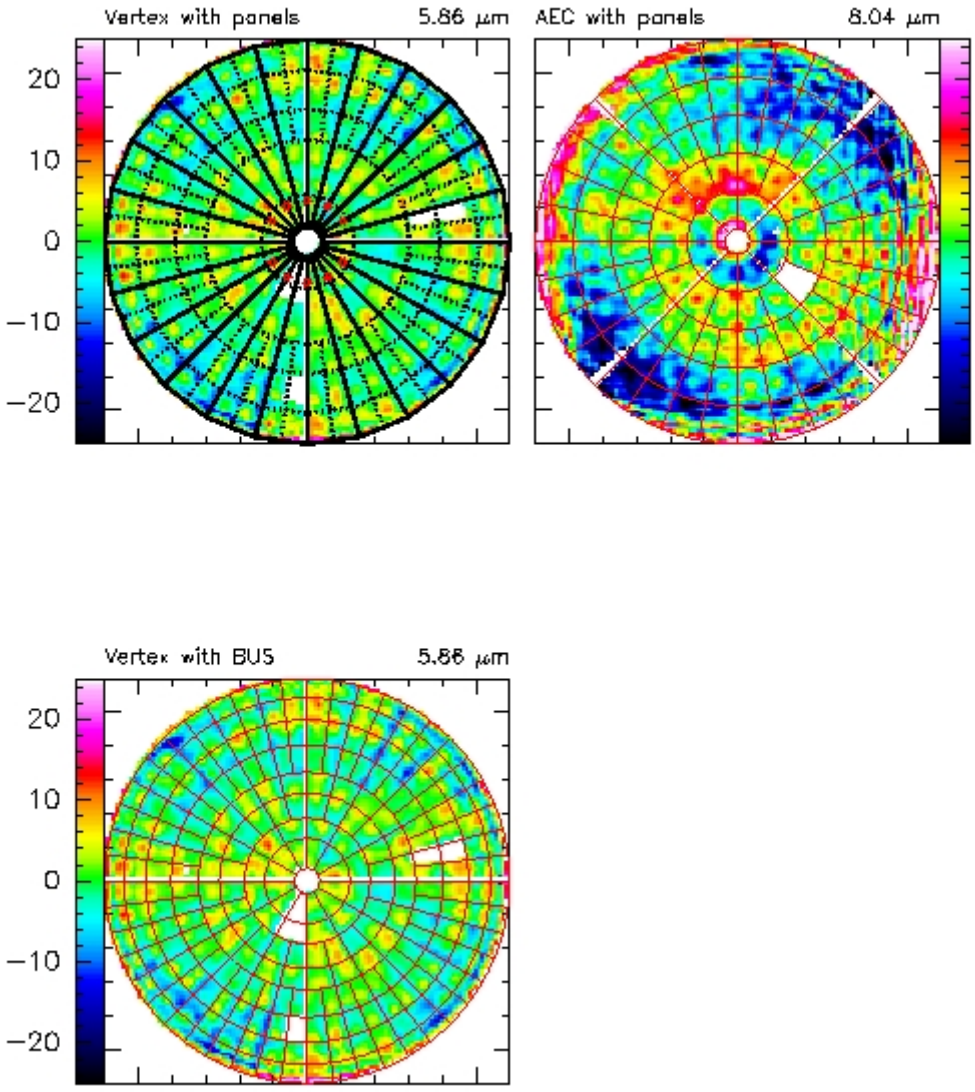

Figure 2.8.4: VertexRSI and AEC temperature span plots with panels (bottom) and VertexRSI BUS (top) boundaries overlain. To put these measurements on the same scale the data have been uniformly scaled to a temperature difference of 10 C.

Note:

- The sampled temperature range is in a large part out of the principal operating conditions (-20 to 20C) for the VertexRSI prototype. It is totally inside the allowable range for the AEC antenna.
- The results for the two periods on the VertexRSI are very consistent with each other.

- The magnitude of the RMS deformations (~0.6-0.7 mum/K for Vertex and ~0.8 mum/K for AEC) appears high; it is not clear to which degree it should be split into panels and BUS and between absolute and gradient terms in the surface error budget. Assuming all effects linear with temperature, and antennas set at 0C, we would expect RMS temperature contributions of ~13 μm for VertexRSI and ~16 μm for AEC at either end of range (+20C or -20C).

2.8.3 VertexRSI Measurements

The thermal deformations for the VertexRSI antenna are a mixture of BUS (the sector edge is sticking out at higher temperature) and panels, not all panels deforming equally.

1. From the BUS overlay drawing it appears that there is a print-through of the connections of the BUS with the Invar cone (the turnbuckles). The small red islands on (or just outside) the second stippled ring are at the diameter of the outer support of the BUS on the cone. We are not certain whether they are at or in between the connections to the cone. In both cases such a print-through can be imagined to happen.
2. The BUS is also supported on the cone towards the center outside the inner stippled circle by about one fifth of the distance between the two stippled circles. Also there we see clear red islands of print-through. These effects are less pronounced in the "lower" section of the dish; actually they seem most pronounced in the left and right quadrants. We don't understand why this would be the case.
3. There are clear, narrow "valleys" along the radials where the sectors of the BUS are joined, especially in the outer half of the radius. They are not equally strong all around, but visible in most cases. The inner part is less clear, presumably because of the already existing effects of the support points.
4. From the map with the panel outline, and ignoring the islands connected to the BUS, as argued above, there is some but not very much evidence for individual panel deformations. It is most likely anyway that individual panel deviations are caused more by forces originating in the stiffer BUS than from the panel itself.
5. The picture of the May series is indeed very similar with the possible exception of the T2 (June) and T1 (May) maps which have about the same temperature range, but seem to show a systematically different shape. It is however at a low level of +-10 μm absolute, hence barely significant, if at all.

2.8.4 AEC Measurements

For the AEC antenna the main deformation is large scale at 45 degrees, with an additional deformation of the inner ring of panels with respect to the rest of the structure. The

vertical stripes on the edges of the AEC maps are an artifact of the measurement not related to temperature.

1. In principle there should be little print-through structure in the difference maps, due to the fact that the BUS design is more homogeneous, being all CFRP, and it should have a continuous transfer of forces to the cabin, which is also the same material.
2. The large-scale deformation at 45 degrees position angle (which looks like astigmatism), along with the additional deformation of the inner ring, are hard to explain. It probably is some effect of the temperature gradients in the cabin and the BUS. It might have something to do with the quadripod connection points.
3. We don't see any individual panel deformation.
4. It is surprising that the deformation per degree is slightly larger for the AEC antenna than it is for the VertexRSI antenna.

2.8.5 Comparison of Measurements to Specifications

The measured variations with ambient temperature changes appear somewhat large. They correspond to a thermal contribution to the surface error of slightly more than 10 μm at the boundaries of the operational range (-20 and +20 C), assuming a setting at 0 C. This is slightly more than we have put in our "standard error budget" and also more than the firms are expecting in their budgets. On the other hand, taking BUS, panel and adjuster contributions all together leads to approximate agreement with these measurements.

The surface budget of the production antennas allows 8 μm contribution due to absolute temperature and 7 μm for gradients for the BUS. The panels are allowed 4 μm for absolute and gradient each. This applies supposedly to the primary operating range of -20 to + 20 C. Let us assume that the dish is set at 0 C and is set to a measured value of 15 μm, which is the value we have been able to set at the ATF. Add the 15 μm maximum of the temperature deformation and the resulting error is 22 μm, more than the goal, but well within the specification. Consider also that at Chajnantor, there will always be wind, which helps smooth the temperature gradients. Especially at the high temperature end, the wind will have a cooling effect and the thermal deformation will be less than the numbers above.

2.9 Further Analysis of Prototype Surface Stability: Acceleration and VertexRSI Receiver Cabin Wall Temperature Stabilization (Mangum, N. Emerson, Meadows, Lucas, Baars)

2.9.1 Summary

To study the influence of:

1. Long-term acceleration motions of the AEC and VertexRSI antennas, and
2. Receiver cabin wall temperature stabilization on the VertexRSI antenna,

a series of additional holography measurements were made January through April 2005.

2.9.2 Acceleration Measurements

One goal of the JATG antenna evaluation was to determine if the surface of the prototype antennas would change under accelerations anticipated in array operations. In this stress test, the VA and AEC antennas were subjected to repeated accelerations over a three week period; holographic measurements of the antenna surfaces were made before and after the testing period and the images compared for changes.

The stress test on consisted of two parts:

a) fast switching the two antennas in a quasi-continuous manner for over 80,000 cycles, and
b) Bringing the antennas to full slew speed in azimuth and elevation and then abruptly applying the brakes using the emergency stop.

The fast switching (FS) test was accomplished by continuously tracking a circumpolar position in the sky while switching in declination to the south by 1.5 degrees. The position chosen was Declination = +70 d and Right Ascension 02h 38m. In this way, over 24 hours, the antennas switched in both elevation and azimuth. The elevation varied between 14 degrees and 44 degrees and the azimuth between approximately 335 degrees and 25 degrees. Since the FS ran continuously, the antennas repeatedly experienced the thermal stress of sunrise and sunset while fast switching. The period for the full FS cycle was 11 seconds.

The FS testing began on March 01 for VA and March 4 for AEC and ended on March 17 for VA and March 22 for AEC. At the end of this period VA had completed 84829 cycles and AEC 85444 cycles.

The high speed brake test was run on March 22 on VA and March 30 on AEC. In each case, the antennas were brought to full speed three times and the e-stop applied at 20 degrees, 50 degrees and 80 degrees elevation.

2.9.2.1 AEC

Holography measurements of the AEC antenna made on (2005/01/28) and after (2005/04/01) a series of "shaking" exercises were made. Figure 2.9.2.1 shows the two maps. There are no apparent adverse affects due to the accelerations detected in the "after" holography image (16.8 microns RMS).

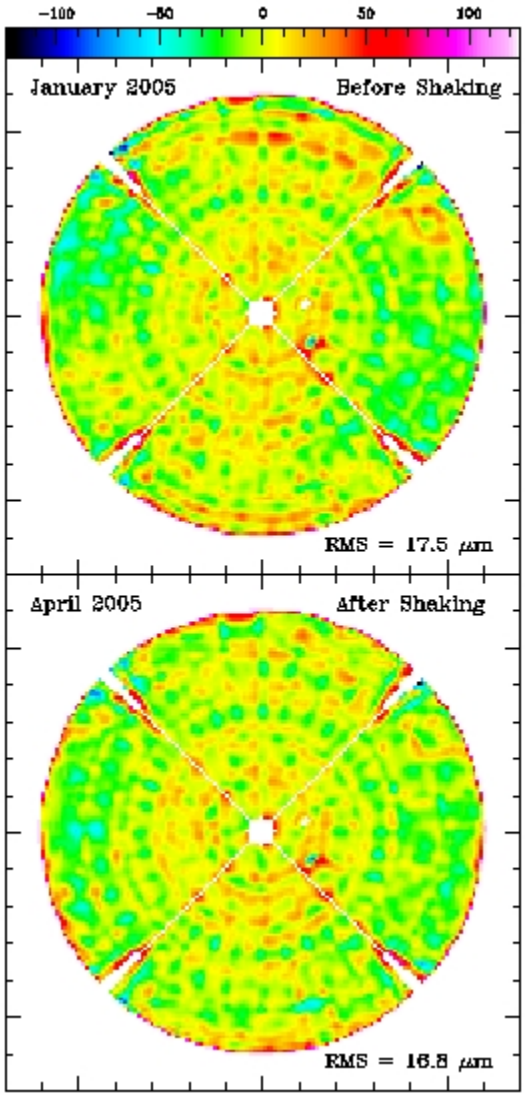

Figure 2.9.2.1: AEC before (top) and after (bottom) shaking test maps.

2.9.2.2 VertexRSI

Holography measurements of the VertexRSI antenna made on before (2005/02/10) and after (2005/03/31) a series of "shaking" exercises were made. Figure 2.9.2.2 shows the two maps. There are no apparent adverse affects due to the accelerations in the "after" holography image (16.1 microns RMS).

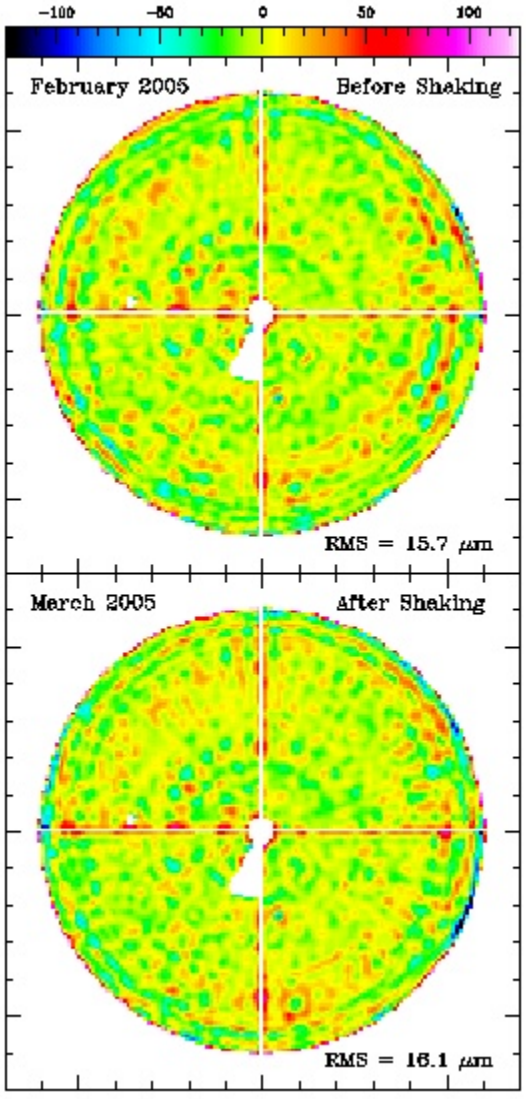

Figure 2.9.2.2: VertexRSI before (top) and after (bottom) shaking test maps.

2.9.3 VertexRSI Receiver Cabin Wall Temperature Stabilization Measurements

The VertexRSI receiver cabin wall temperature is regulated by a glycol cooling/heating system. Glycol is circulated around the walls of the receiver cabin from a Glycol Distribution Unit, eventually out of the receiver cabin into an outside unit under the lower platform, which removes heat from the glycol and circulates it back up to the receiver cabin.

Also in the receiver cabin are 2 air recirculation units that maintain a constant air temperature in the cabin. Heat is removed from the air using glycol from the Glycol Distribution Unit. The air recirculation units have no heating capacity. Twelve fans circulate air throughout the Invar Cone, but have no heating or cooling capacity.

Five different pumps circulate glycol to different zones of the system and to the external unit. Two of these pumps circulate glycol to the left and right wall of the receiver cabin and the lower rim of the Invar Cone, two pumps circulate glycol to the two air recirculation units, and the fifth pump helps to bring cooled glycol back up from the external unit.

For this test the wall temperature control had to be disabled, but the rest of the system had to be kept on to maintain a constant air temperature. To disable the wall temperature control, the breakers for the two pumps circulating glycol around the wall were switched off. It was also necessary to disable the heaters providing heat to those zones, and to add two jumpers to bypass the fault detection that turns off the whole system in case of pump failure.

Measurements of the influence of the VertexRSI receiver cabin wall temperature stabilization were made by making holography maps with temperature stabilization both on and off. To measure the affects, we:

- Calculate the average Rx cooling system off map using four good maps made 2005/03/30-31. Note that the ambient temperature ranged from about +8 to -3 C during the period when these four maps were made.
- Calculate the average Rx cooling system on map using four good maps made 2005/03/31 (a few hours after the data for the cooling on tests were obtained).
- Take the difference of the average on map and the average off map.

The attached plots show the measured receiver cabin wall temperatures during the receiver cabin wall temperating "On" and "Off" measurements on 2005/03/31. A series of additional temperature sensors installed on the receiver cabin interior walls were used to monitor the temperature distribution in the steel structure of the receiver cabin. The receiver cabin temperature sensor measurements during this period are shown in Figures

2.9.3.1(a & b). To accentuate the temperature gradients the antenna was pointed away from the setting Sun (approximate azimuth 0) at intervals during the "On" measurements.

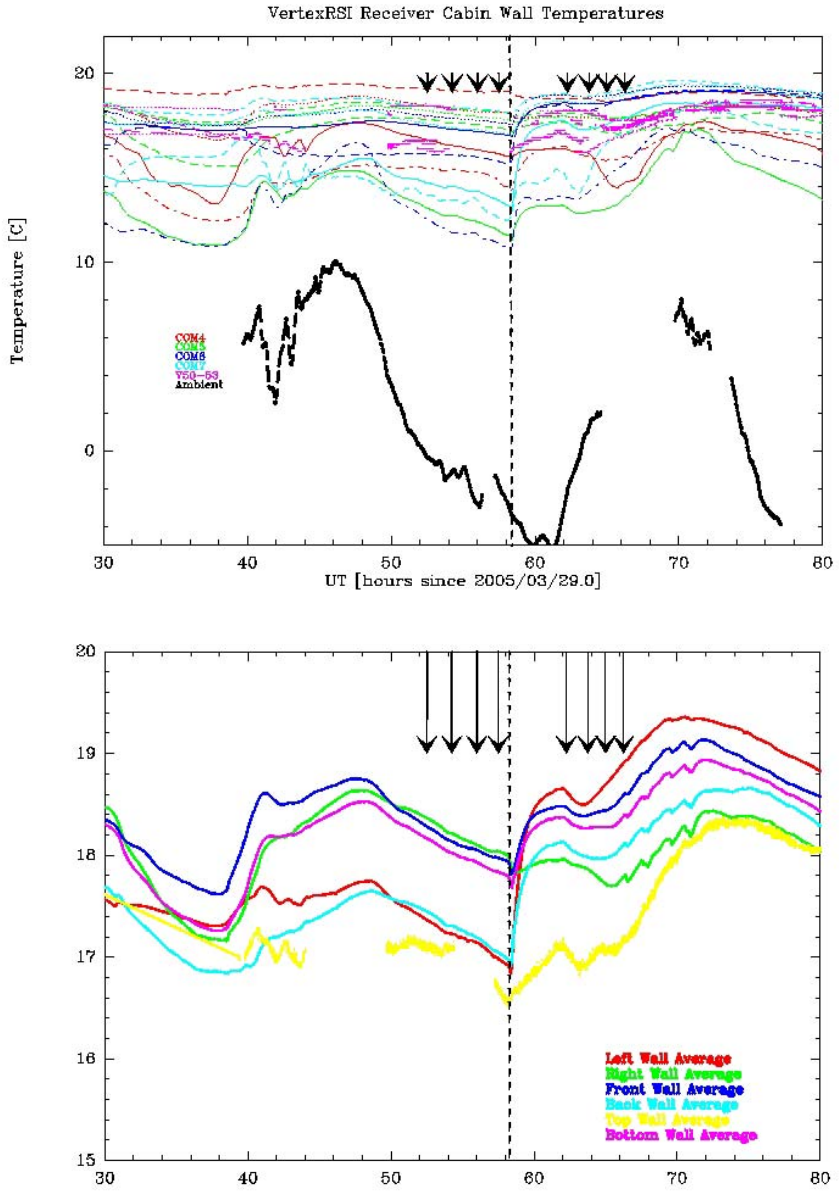

Figure 2.9.3.1 (a-top, b-bottom): Temperature measurements and ambient temperature for Vertex cabin regulation tests. Black arrows indicate the times that holography maps were taken.

One would assume that this directional heating would cause the "front" and "right" sides of the receiver cabin to be warmer than the "back" and "left" sides. Arrows mark the times during which holography maps were acquired. Holography map indicators ***before*** the vertical dashed lines were made with the receiver cabin cooling system

turned ***off***, while those made ***after*** the vertical dashed line were made with the receiver cabin cooling system turned ***on***.

Figure 2.9.3.2 is a plot of the average receiver cabin cooling system on minus off difference. The RMS in this difference image is quite comparable to the noise level in the holography system. This shows that turning off the cabin-wall temperature regulation system does not produce a gross effect on the surface under the conditions present during the tests. It does however appear that, even with the regulation system turned on, the measured temperature differences in the cabin walls are greater than those assumed in the FEA models used in preparing the surface, pointing and delay budgets. Further work, both experimental and analytic, is therefore needed in order to decide whether regulation of the cabin walls is needed and whether the present system does actually provide adequate performance.

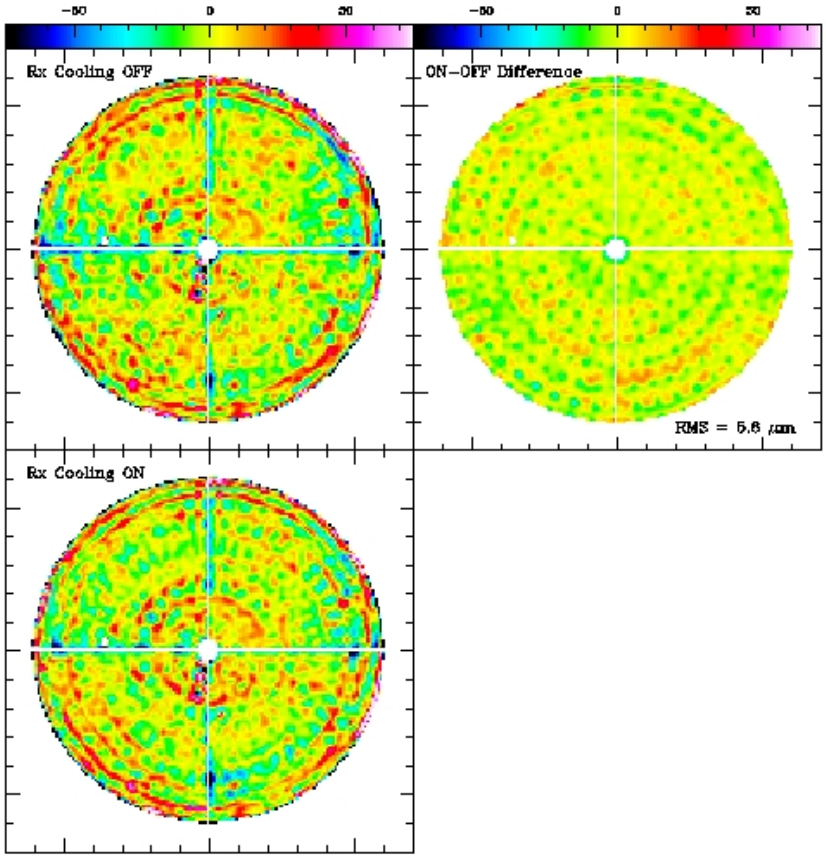

Figure 2.9.3.2: Average VertexRSI holography maps made without (top left) and with (bottom left) the receiver cabin wall temperature control enabled. The upper right image shows the difference of the two images on the left. The residuals in the difference image are dominated by holography systematics, and the RMS is quite comparable to the noise level in the holography measurement system.

3 Discussion

The test programs and analyses carried out by the JATG in late 2004 and early 2005 were designed to address specific concerns raised by technical measurements of the ALMA prototype antennas made by the AEG and other groups (including the prototype vendors). In this section these specific topics are addressed in light of the test results and any other information that has become available.

Surface Stability

Holography measurements of both prototype antennas in December 2004 indicated that both main reflectors had changed shape since their last AEG setting (June 2003 for Vertex, February 2004 for AEC) (Sect. 2.1.2.2 and 2.1.3.1). The exact cause of the changes cannot be determined in either case, but for both prototypes it is felt there are plausible (if untestable) external explanations:

- For the Vertex prototype: a long series of violent shakings of the antenna, resulting from a communications error between the vendor prototype control computers, is suspected (this problem has been resolved in the production design). This problem was resolved in September 2003 (i.e. after the AEG setting of the Vertex surface via holography). The accelerations associated with this shaking are guesstimated to be < 1g, but the shaking occurred on numerous occasions (sometimes multiple times per day), for extended periods. This effect (possibly exacerbated by the loose bolts in the BUS) is the primary candidate for the deformations; the bolt tightening in Sept/Oct 2004 may have contributed, but the AEG March 2004 OOF measurements (i.e. 6 months before the tightening) appear to show the reflector deformations at that time.

- For the AEC prototype: a serious mechanical accident in late 2003 led to damage to the hard stops of the antenna, deformation of the surface and misalignment of the antenna apex structure. The surface of the antenna was reset in early 2004, but correction of the apex misalignment occurred some time later, and stresses may have been introduced into the main reflector at that time.

To gain some confidence that the prototype design surfaces are stable in normal operating conditions, the VA and AEC antennas were subject to repeated accelerations over a three week period; holographic measurements of the antenna surfaces were made before and after the testing period and the images compared for changes. No significant changes were seen in either antenna above the noise expected from the holography measurement.

Surface Accuracy

The accuracy of the antenna surfaces as a function of elevation in the operating conditions expected at Chajnantor has been a primary concern of the project. As explained in the Introduction (Sect. 1) there were indications in mid/late 2004 that at least one of the prototypes (and its derivative production design) may not meet the ALMA specification.

The surface accuracy estimates provided for the Vertex and AEM production designs are shown in Table D1 (taken directly from the bid documentation). The terms of particular interest are the "Gravity (ideal)", "Gravity (non-ideal)", "Wind" and "Temperature Gradients" terms in the BUS section. In the JATG tests outlined below the accuracy of the surface budget terms provided by the vendors were examined.

Quadrant Detector (Vertex)

Quadrant detector measurements of the gravitational deflection of the Vertex BUS (Sect. 2.2) suggest that the BUS is approximately 16% "softer" than the FEM predictions, and indicate a peak amplitude of ~10 microns for astigmatism of the dish. Initial estimates of this difference between the FEM and actual performance of the antenna BUS were 30% or more; careful analysis of the data taken with a new mount (multiple analyses and authors) have converged to a consensus figure of 16%. The minimum correction to the error budget is to apply this factor multiplicatively to the gravity and wind BUS error estimates in Table 1 for Vertex. The measurements were also analyzed to estimate the deviations from the FEM by treating the 8 inner hub plus 8 rim measurements as representative of the whole surface. This gives a conservative value of 9.7 microns (6.2 microns from the Vertex FEM combined in quadrature with 7.5 microns from the deviation of the QD measurements from the FEM) for the net non-homologous gravity deformations.

Holography

Error estimates: From the AEG and now JATG measurements we believe that holography can be used to set the surface of ALMA antennas with an accuracy of 7-10 microns (5 microns reproducibility, the remainder a conservative estimate of the systematic errors underlying the process; see Sect. 2.8); therefore the error budget figures used are correct (Tables D1 and D2).

	Vertex-bid		AEM-bid	
Panels				
Manufacture	8.0		4.5	
Aging	2.0		2.0	
Gravity	2.4		6.9	
Wind	1.1		1.1	
Abs Temperature	0.6		0.9	
Temperature Gradient	2.7		2.6	
Total		9.1		9.0
Backing Structure				
Gravity (ideal)	6.2		6.9	
Gravity (non-ideal)	3.0		2.0	
Wind	8.4		0.7	
Abs Temperature	5.4		5.9	
Temperature Grad	9.3		2.1	
Aging	0.0		3.0	
Total		15.3		10.0
Panel Mounting				
Abs Temperature	0.6		2.0	
Temperature Gradient	0.0		2.0	
Panel location in plane	2.0		3.0	
Panel adjustment parallel to plane	3.0		3.0	
Gravity	0.0		0.0	
Wind	0.0		0.0	
Total		3.7		5.1
Secondary Mirror				
Manufacturing	2.0		5.8	
Gravity	2.0		0.4	
Wind	1.0		0.0	
Abs Temperature	1.0		4.5	
Temperature Gradient	2.0		3.0	
Aging	3.0		2.0	
Alignment	3.0		1.7	
Total		5.7		8.4
Holography				
Holography measurement error	10.0	10.0	10.0	10.0
Other errors	2.0	2.0	2.0	2.0
Total surface performance		**21.6**		**19.5**

Table D1: Production antenna surface error budgets

Photogrammetry

Careful photogrammetry measurements made in January 2005 show no evidence for excessive gravitational deformations in either of the prototype antennas. Upper limits of around 10 microns can be set from these data on components of the error budget due to gravitational deformation of the BUS. An upper limit of 10 microns can also be set on any non-homologous thermal deformations for both antennas under the conditions tested. There were substantial changes in the shape of the Vertex antenna with temperature, but these are of a homologous nature and can be therefore be corrected by refocusing the secondary.

It seems clear that the performance of the Vertex antenna was significantly altered (for the better) by the bolt-tightening effort in September/October 2004. The behavior of the antenna in the photogrammetry observations made in November 2002 and throughout Sept/Oct 2004 is not consistent with that seen in the January 2005 data, which is in substantial (~10%) agreement with the FEM. These discrepancies cannot however all be explained as being due to bolt-tightening. Possible explanations for the discrepant data sets include data processing errors or subtle effects associated with the locations of targets on the surfaces.

The large astigmatism derived from these earlier photogrammetry datasets by the ATWG is not apparent in more recent Vertex measurements, using three different techniques (quadrant detector – Sect. 2.2, photogrammetry – Sect. 2.4 and Beam cuts – Sect. 2.5.5). The current levels of astigmatism seen in both prototypes are not considered to be a significant problem.

The large non-homologous distortions detected previously by ATWG in the Vertex data are not apparent in the recent JATG measurements; at this time, we speculate that the bolt tightening on Vertex corrected the performance of the dish. The January photogrammetry measurements do indicate non-homologous deformations are present in both antennas at a low level; the apparent rms deviation between 5-90 deg in terms of normal surface deviation is ~25 microns for both antennas (unweighted). When geometrical factors and weighting are taken into account, this figure is more like ~20 microns rms. Assuming the project can implement a method of measuring the surface at a more suitable elevation angle (for example, astronomical holography, as planned), it will be possible to reset the antenna surfaces with the correct bias and this contribution would be approximately halved.

The main reflector best-fit paraboloid focal length as a function of elevation has also been derived from the recent and historical photogrammetry data (Sect. 2.3. The recent photogrammetry measurements indicate that the BUS of the Vertex antenna may be softer than the FEM prediction by 10-15%, consistent with the

QD measurements. The surface parameters for focal length are not consistently fit in the previous (Nov 2002 or Sept/Oct 2004) photogrammetry data, further indicating some inconsistencies in those datasets and/or a change in the Vertex antenna performance after bolt tightening (as suggested previously).

The photogrammetry measurements of the focal length changes in the AEC dish are in accordance with the FEM prediction for that design.

It is important to note that for both antenna prototypes, the apparent surface deformations seen are at or near the predicted sensitivity limits of the photogrammetry techniques used. In both cases, the residual surface deformations derived may, in fact, be systematic measurement artifacts. In this case, the magnitude of the deformations seen provides useful upper limits to any real deformations in the surfaces. If these deformations are real, they are slightly larger than those estimated in the vendors' error budget, but are not so large as to push the overall budget above the specifications by themselves.

Radiometric Out of Focus Beam Cuts (Vertex)

The technique of measuring variations of antenna beamwidth as a function of axial focus offsets has been used to measure the astigmatism of the prototype Vertex antenna(s) as a function of elevation angle. The differential nature of the technique makes it substantially insensitive to other dish degradations or to elongation of the astronomical source.

On the Vertex antenna, astigmatism in the 45-degree coordinate system is found with a value of ~2.5 microns weighted rms (peak ~9 microns) at low elevation, and a value of ~3.5 microns weighted rms (peak ~13 microns) at high elevation. The rms scatter of all 45-degree measurements above 50 degrees is a 1.4 microns in the weighted rms values. All these values are derived assuming a $(r/R)^2$ form of astigmatic components of the dish surface, but the derived weighted rms astigmatism is insensitive to the order of astigmatism.

For astigmatism aligned with the Azimuth-Elevation frame, the Vertex antenna shows zero astigmatism at low elevation, rising to perhaps 7.5 micron weighted rms (~27 microns peak) at high elevations. If confidence can be established in the repeatability, magnitude and form of this astigmatism varying with elevation, then in principle the dish could be set at an appropriate rigging angle and so potentially halve the peak amplitude.

No data from radiometric beams cuts on the AEC prototype were available due to problems in the evaluation receiver.

OOF

The Out Of Focus (OOF) measurements made by JATG (Section 2.6) were somewhat affected by signal to noise issues (due to the failure of the ALMA chopper), but have provided an independent confirmation that there are no obvious gross surface errors to be found in the Vertex prototype antenna. The upper limit on the weighted rms surface is around 20 microns on scales larger than 3 meters. This is a measurement including both the main reflector and subreflector. No OOF measurements have been made on the AEC prototype due to problems with the evaluation receiver.

Based on the antenna prototype performances indicated by the new datasets and analyses we can modify the vendor bid error budgets to estimate what the production antenna surface performances might be: this is show in Table D2. In this table, the following modifications from the vendor estimates have been made (changed quantities are indicated by ** in Table D2):

- The "Gravity (ideal)" and "Gravity (non-ideal)" entries for both antenna designs have been replaced by a single 10 microns (this being an upper limit on the measured total gravity deformation term for both antennas, based on the photogrammetry results).
- For the Vertex antenna, the thermal deformations ("Temperature Gradient") term has been set to 10 microns (upper limits from photogrammetry); other limits can be derived from the holography data, however it is less clear how to assign those estimates across multiple parameters.
- For the Vertex antenna, an additional 16% has been added to the wind component "Wind" to account for the BUS softness suggested by the QD and Focus as a function of elevation results.

Inserting the upper limits determined from our JATG measurements (involving several techniques over the full range of elevations) provides a robust conservative estimate of the surface performance. Table D2 indicates that both antennas can be expected to meet the 25 microns ALMA surface specification over the full range of elevation.

The Vertex surface was also examined via holography during times when thermal regulation control of the cabin walls was on and off; no difference in surface accuracy was seen above the noise of the holographic measuring system over the range of temperatures encountered during the tests.

	Vertex-bid + mods		AEM-bid + mods	
Panels				
Manufacture	8.0		4.5	
Aging	2.0		2.0	
Gravity	2.4		6.9	
Wind	1.1		1.1	
Abs Temperature	0.6		0.9	
Temperature Gradient	2.7		2.6	
Total		9.1		9.0
Backing Structure				
Gravity (ideal)	10.0	**	10.0	**
Gravity (non-ideal)				
Wind	9.7	**	0.7	
Abs Temperature	5.4		5.9	
Temperature Grad	10.0	**	2.1	
Aging	0.0		3.0	
Total		18.0		12.2
Panel Mounting				
Abs Temperature	0.6		2.0	
Temperature Gradient	0.0		2.0	
Panel location in plane	2.0		3.0	
Panel adjustment parallel to plane	3.0		3.0	
Gravity	0.0		0.0	
Wind	0.0		0.0	
Total		3.7		5.1
Secondary Mirror				
Manufacturing	2.0		5.8	
Gravity	2.0		0.4	
Wind	1.0		0.0	
Abs Temperature	1.0		4.5	
Temperature Gradient	2.0		3.0	
Aging	3.0		2.0	
Alignment	3.0		1.7	
Total		5.7		8.4
Holography				
Holography measurement error	10.0	10.0	10.0	10.0
Other errors	2.0	2.0	2.0	2.0
Total surface performance (including JATG estimates)		**23.6**		**20.7**

Table D2: Prod. antenna surface error budgets, modified by JATG upper-limit estimates (**)

Pointing

Optical pointing measurements were carried out on the AEC antenna to address issues raised by the AEG measurements of the AEC all-sky pointing performance (ALMA specification is 2"). Alignment of the feet of the antenna during late 2004 significantly improved the AEC pointing performance; during JATG testing the AEC all-sky pointing performance reached the 2" specification in a majority of cases (Sect. 2.7.2). The ALMA specification for both all-sky and absolute pointing performance obviously refer to radio pointing performance at the Chajnantor site; any impacts of optical seeing at the ATF site need to be carefully subtracted from the antenna prototype testing results. This was not done in previous AEG evaluations of prototype or offset pointing performance. The JATG supports an interpretation of the pointing specifications where an estimate of the seeing at the VLA site would be subtracted from the historical and recent datasets (typically ~1-1.5", based on 20-sec repeated frames taken by the JATG in January 2005; in the AEG optical pointing report seeing as bad as 4" was quoted). Applying this correction to the all-sky pointing specification (e.g. subtracting 1" in quadrature) would lead to both prototypes easily meeting the ALMA specifications.

The JATG did not conduct further testing of the offset pointing performance of the antenna prototypes, but reviewed the existing AEG information and discussed the specifications. Considering (a) the measurement accuracy of all data available on this subject (including the AEG offset pointing observations and accelerometer data), (b) different opinions about the detailed relationship between the specification and the AEG evaluation datasets, (c) the likely impact of removing an estimate of the ATF seeing contribution from the existing results, and (d)(most importantly) the improvements that might be expected from active metrology systems, the consensus view was that the production antennas designs should meet this specification. A key point to note is that neither vendor produced a working metrology system for the prototypes; therefore evaluating the ability of production designs with metrology to meet the offset pointing antenna specifications is difficult and model-dependent. The fact that the measured performance of both prototype antennas without metrology systems was close to the specification implies that only simple metrology will be required on the production antennas. It is also likely that basic metrology systems on the antennas will be necessary to meet the specifications on path delay errors under the full range of conditions on the ALMA site.

Summary

Based on all available data and the ATF testing done by the AEG and the JATG, it is the consensus view of the JATG that both prototype antennas meet the ALMA antenna specifications under direct consideration (surface accuracy at all elevations, all-sky absolute pointing performance) under the environmental conditions encountered during the testing, and that the production antennas based on either design can also be expected to meet these specifications.

4 Acknowledgements

The dedication and hard work of the people who worked at the ATF site cannot be overstated; we are very grateful to Nick Emerson, Pascale Martinez, Eric Pangole, Jack Meadows, Jeff Mangum, Fritz Stauffer, Ralph Marson, Robert Lucas, Dick Sramek, George Reiland and the large crew of Socorro staff who supported the FS tests (day and night) for their extraordinary efforts over the past few months.